REAL-TIME MEASUREMENT OF THREE-DIMENSIONAL MULTIPLE RIGID BODY MOTION

by

FRANK C. CONATI

B.S.M.E., University of North Dakota
(1973)

SUBMITTED IN PARTIAL FULFILLMENT
OF THE REQUIREMENTS FOR THE
DEGREE OF

MASTER OF SCIENCE

at the

MASSACHUSETTS INSTITUTE OF TECHNOLOGY

June, 1977

Signature of Author . . . . . .
Department of Mechanical Engineering, June 22, 1977

Certified by . . . . . .
Thesis Supervisor

and . . . . . .
Thesis Supervisor

Accepted by . . . . . .
Chairman, Department Committee on Graduate Students

REAL-TIME MEASUREMENT OF THREE-DIMENSIONAL MULTIPLE RIGID BODY MOTION

by

FRANK C. CONATI

Submitted to the Department of Mechanical Engineering on June 22, 1977, in partial fulfillment of the requirements for the Degree of Master of Science.

ABSTRACT

A general-purpose system for measuring three-dimensional multiple-body motion patterns has been developed. The system is capable of discretely tracking a maximum of ten bodies in a minimally-invasive fashion throughout a volume space approximately 2 meters cubed. The main components are the Selspot (Position Measuring) System, a laboratory minicomputer and a user-oriented software package. Time-limited storage-based data acquisition and computation has been implemented, and a real-time processing capability has been demonstrated. An analysis of the system is presented. Under suitable conditions, positional parameters can be resolved to one millimeter and orientative parameters to one degree. Position-related accuracy error is shown to be less than ±2% for distance measurements, and orientative accuracy error is shown to be less than ±0.14% over the 360° range. A design is introduced for effectively expanding the tracking volume to approximately 10 meters by 20 meters by 2 meters.

Thesis Supervisors:

Robert W. Mann
Uncas A. Whitaker Professor of
Biomedical Engineering

Derek Rowell
Assistant Professor of
Mechanical Engineering

ACKNOWLEDGMENTS

I am grateful to Professor Robert W. Mann for providing the research environment which allowed the effective execution of this thesis project. I am indebted to him for contributing a visionary research perspective and for exhibiting a personal concern during my academic tenure. I am thankful to Professor Derek Rowell for his continued advice and counsel throughout all phases of the project.

Sincere appreciation is expressed to the National Institute of General Medical Science (NIGMS), the M.I.T. NIGMS Committee and the Whitaker Fund for providing financial support, academic and research.

I wish to acknowledge many Institute friends, fellow graduate students and support staff, and especially my office colleagues, Paul, John, Dave and the Dons. The stimulating mixture of sane and insane wisdom was a constant source of uplift, and shall not be forgotten.

Finally, I am grateful to my parents for their enduring support and encouragement throughout the years.

TABLE OF CONTENTS

PAGE

LIST OF FIGURES

LIST OF TABLES

Chapter 1

INTRODUCTION

1.1 STATEMENT OF THE PROBLEM

With the advent of the high-speed yet low-cost laboratory minicomputer, medically-related research is slowly evolving from an observing, qualitative discipline to one of quantitative precision. This is a particularly difficult endeavour in the case of human experimentation since the involvement of a human subject brings with it very unique problems of accommodation. As a result, the bulk of human-related, biomedical data is gathered under very controlled conditions and is often of a very incomplete nature. The lack of reliable and complete quantitative information is a serious impediment to human-related biomedical research. As an example, in the area of human gait research and analysis, one finds a dearth of complete three-dimensional kinematic data for the lower torso. Instead, studies are invariably limited to planar analyses or are observations of only a few body segments.

The Human Mobility Laboratory at M.I.T. is committed to the task of investigating the nature of human mobility in the broadest sense, and contributing to the rehabilitation of humans with mobility-related afflictions. To fruitfully engage in this type of research, it is of paramount importance that an effective means of gathering data relating to human mobility be available. It is readily apparent that each project undertaken by the Mobility Laboratory will have its own unique goals and needs.

Many of these goals carry with them very specific needs in terms of quantitative measurements, while others by their very nature do not lend themselves to clear definition. The majority of the data requirements fall under four general categories: 1) kinematic data acquisition; 2) force measurement (internally at joints and at extremities); 3) electromyographic activity measurement; and 4) control parameter measurement and feedback.

This thesis is concerned with the design and first-stage implementation of a means to meet the kinematic data requirements of the Mobility Laboratory and to demonstrate the procedure for carrying out motion-related parameter feedback. In consideration of the variety of research goals envisioned by the Mobility Laboratory the following overall problem statement was formulated:

> Needed: A means to monitor in real-time the three-dimensional motion patterns of multiple human body segments throughout a mobility space of dimension approximately 20 meters by 10 meters by 2 meters.

It is this overall problem which is the subject of this thesis.

Most projects carried out under the auspices of the Human Mobility Laboratory would not need nearly the capabilities proposed in the problem statement. In fact, there is no project presently planned which would require all the capabilities in the strict sense. Such a conceptual construct was, however, deemed fruitful so as to encompass the overall system requirements. A design approach cognizant of this total problem would guarantee reasonable versatility in terms of system capabilities.

In order to more effectively understand the background premise of the problem statement, a cursory description of two projects proposed by the Laboratory will be presented. These two projects are introduced to indicate the diverse research interests of the Laboratory and the demands to be put upon a kinematic monitoring system.

The first involves the acquisition of 3-dimensional gait-related motion parameters. Such information is needed to guide and verify the development of dynamic models of the body segmental linkage of the lower torso. These models are invaluable in predicting and understanding the nature of muscle recruitment, the dynamics of human gait, and the forces present in the body joints. In order to effectively generate such models, complete 3-dimensional kinematic data of all the body-segments of the lower torso in normal walking conditions is needed. Thus, it is required that seven body-segments (hip, thighs, calves, feet) be monitored throughout a gait cycle.

The next project to be discussed concerns the development of a facility whose purpose would be the systematic design and evaluation of blind mobility aids. Such a facility was proposed by Professor Robert W. Mann in 1965 and an early sketch of his conception of such a facility is given in Figure 1. In its most fundamental sense, the facility would have the capability to control and investigate most of the design variables of a mobility aid. With such a facility, researchers would be able to study blind mobility, evaluate available blind mobility aids, and then synthesize this knowledge with the techniques of interactive simulation to develop better mobility-aid designs. These designs could then be subjected to immediate testing and modification.

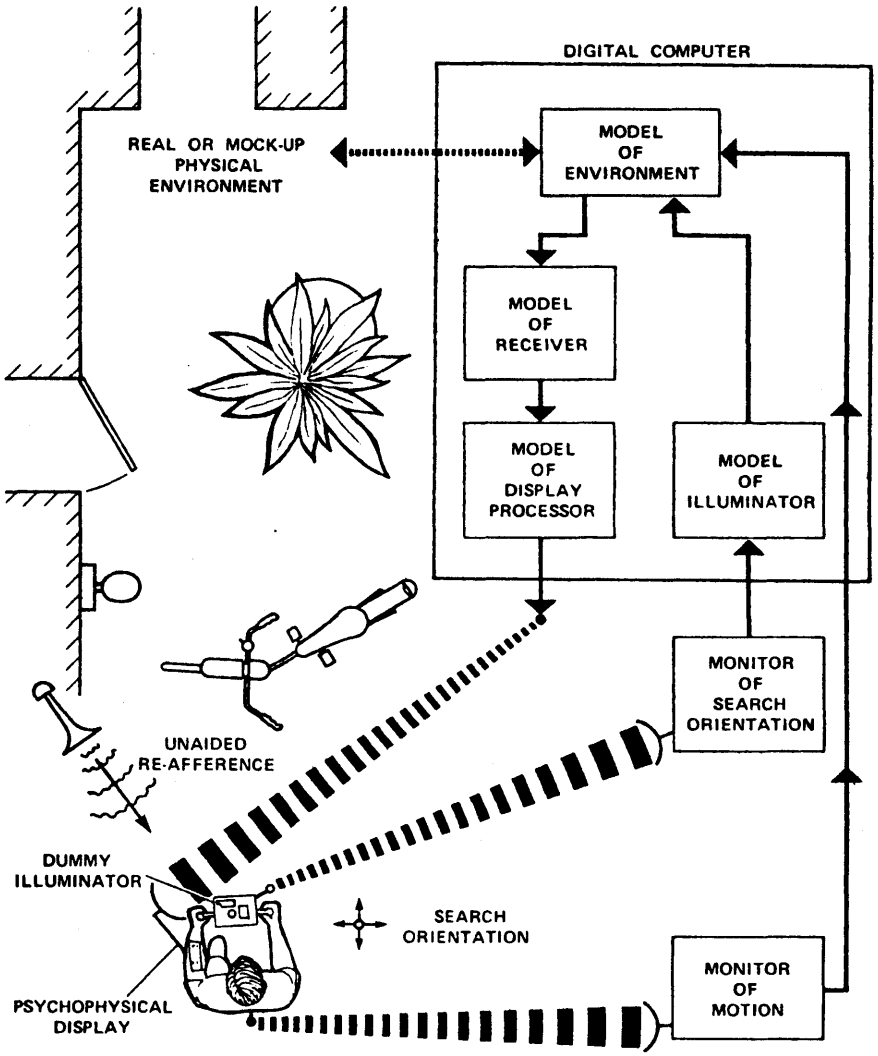

Figure 1. Sketch of a mobility-aid simulator.

Two essential demands of this project from a kinematic monitoring point-of-view are: 1) real-time data acquisition and processing, and 2) absolute 3-dimensional tracking throughout a mobility space. In the case of a mobility-aid simulation, reliable real-time monitoring of the position and orientation of the body in question (head, chest, etc.) is necessary and the data itself must be known with respect to some fixed reference system. To effectively carry out the experiments, monitoring throughout an extensive mobility space is necessary, and the present dimension of the mobility laboratory (20 meters by 10 meters) is considered to be a minimum working space.

To summarize more generally the nature of the two projects, it can be seen that the first one is concerned with multiple body-segment monitoring but not the rigors of real-time processing. The interest is data acquisition and then subsequent data analysis. In the second case, the monitoring equipment is an integral part of a real-time processing loop with rigorous timing constraints. Also coming into play is the necessity to track in real-time the unpredictable movements of a freely mobile person in the large mobility space. In contrast, it can be seen that the data acquisition requirements in this case are minimal, since there is really concern for only a single body-segment.

There is a more general reason other than simple description for elaborating on these two specific Mobility Laboratory projects. They were introduced to show that the design of the kinematic-monitoring system should not be overly geared to specific projects because of the diversified research

scope of the laboratory. Any such attempt would result in undue system constraint and design rigidity. Rather, it is felt that a better approach would be a more generalized conceptual framework, such that many combinations and permutations of the structure can be realized. In this way, by being removed from the prejudicial consideration of a specific problem, a facility can be realized which can be flexibly tailored to the specific projects at hand and more easily respond to future project activity. In this vein, an attempt has been made to consolidate the known applications of the proposed kinematic-acquisition system into an overall problem statement, as introduced earlier. In this way, a system can be designed in view of a single encompassing statement of the problem. It is, of course, capricious to believe that the overall solution need be achieved in the strict sense, nor that a design implementation can be achieved in a single step. The development must proceed in small, modular steps. It is believed, however, that the goal can most effectively be achieved through a conceptual appreciation of the overall purpose of the system, and thus the overall problem and its subcomponents.

1.2 ORGANIZATION OF THE THESIS

The remainder of this chapter is devoted to a survey of several types of kinematic data acquisition systems and a justification for the selection of the system employed. In Chapter 2, the hardware aspects of the computer-based kinematic acquisition system are discussed in detail. Chapter 3 is devoted to a presentation of the technique for calculating 3-dimensional points based on the gathered data and calibration parameters. In Chapter 4,

the analytical technique for computing absolute multiple-body kinematic parameters based on point-coordinate measurement is discussed. Chapters 5 and 6 are concerned with the actual implementation of the system and address experimentally-related issues. A software package has been developed to effectively carry out the processing algorithms and allow general use by experimenters. The general structure and capability of the software system is outlined in Chapter 7. In Chapter 8, an analysis of the performance of the total hardware-software system is presented. In an attempt to illustrate the next major development step of the system, a preliminary conceptual design of a large-volume tracking system is presented in Chapter 9. The final chapter is devoted to a summarial statement of the work achieved and a presentation of recommendations for further development, both in the short-term and the long-term.

1.3 SURVEY OF KINEMATIC ACQUISITION SYSTEMS

In one sense, every kinematic data acquisition system in use is unique in itself and its application to a specific set of problems. However, most approaches fall into a few categories of technique, and three such classifications will be discussed: 1) Image Reduction, 2) Direct Measurement, and 3) Direct Sensing.

Image Reduction. In this category one can consider the hardware aggregate of picture-processing systems, such as photographic, motion-picture, and television. In typical experiments using such systems, human subjects are fitted with highly visible positional markers and the experimental result is a time-division image recording of a movement study.

The recording is then processed frame by frame, and the "positional coordinates" of the landmarks quantified, with a human operator normally an integral part of the processing mechanism. This is typically the case because the human has the required adeptness at recognizing the particular image markers, and when coupled with a precision digitizing instrument, can reduce the data. This is obviously a very slow process and attempts have been made to computerize the entire operation. However, the recognition of the landmark data is not a straightforward procedure and effective yet simple algorithms have not been developed.

In the case of television image analysis, an added problem is the effective handling of data. In order to achieve acceptable resolution, a fine-scaled digital matrix is needed. Typically, a matrix on the order of 256 by 256 (65,536 elements) is employed, and it is readily apparent that each experimental frame constitutes a large data block to be stored, examined and analyzed. Advances have recently been made in intelligently reducing the field to be examined based on knowledge of the particular situation. Although encouraging, the essential pattern recognition and data-handling difficulties still exist and they remain the crux of the problem in terms of the effective implementation of automatic data analysis.

Direct Measurement. The primary measurement device in this category is the goniometer. A goniometer is a potentiometer-based single degree-of-freedom angular rotation sensor. The goniometer can be considered a direct measurement device because it measures a valuable kinematic parameter, relative angular displacement. All the other approaches presented in this section require somewhat elaborate algorithms to determine this particular

kinematic parameter. Goniometers have been extensively used to directly measure such gait parameters as knee angle, hip angle and ankle angle. Unfortunately, in high accuracy situations the goniometric data itself must be "corrected" (Kettelkamp, 1970) to accurately reflect the actual joint angles because of the physical placement of the goniometers on the body segments.

As the degrees of freedom and the number of body segments to be examined simultaneously increases, the goniometer hardware required becomes more and more unwieldy and encumbering to the subject. Because of this problem, their use is normally restricted to the measurement of the relative motion of only two body segments. It should also be pointed out that the goniometer cannot directly measure translational displacements, additional hardware needed to measure such parameters.

The capability of measuring only relative angular and translational displacement is a hinderance in terms of system versatility. This constraint clearly limits the experimental capability and also tends to propagate kinematic errors when one examines a multiple body-segment linkage. Further, since there is no absolute reference frame discernible in the system, calibration of the device to measure accurately the anatomically-defined kinematic angles can be difficult.

Direct Sensing. The direct sensing devices are similar to the image reduction devices in that they in general also rely on the perception of landmark "points" to describe the positional and angular location of a segmental body. There is an important difference in the measurement process, however. The sensing devices do not rely upon scene analysis, but can instead

identify the relevant data points directly. This difference greatly eases the problem of data reduction. Two measurement techniques can be classified under this category: 1) acoustic sensing, and 2) infrared detection.

The approach for acoustic location involves a hardware system consisting of essentially the following components: 1) ultrasonic transmitters (one per positional landmark), 2) ultrasonic receivers (an optimum number strategically placed), and 3) timing circuitry. Ultrasonic pulses are emitted from a transmitter and the time to detection noted when the pulses are received at each sensor. From this information the distance between each transmitter and each receiver can be found. It has been shown (Cuscino, 1976) that by using three sensors the distance information uniquely locates a transmitter in 3-dimensional space. The distance information obtained from the ultrasonic hardware must be operated on by a computational algorithm to determine the absolute three-dimensional positional values.

The approach, although conceptually elegant, has practical difficulties which have retarded wide-spread use of the concept. The transmitters which must be fixed to the human subject tend to be bulky and encumbering. Difficulties have been encountered in clearly detecting the onset of the acoustic wave at the sensor, thus limiting accuracy. The system, in its present state of development, is also subject to misleading results when the path between a sensor and transmitter is obstructed or when the operating distance is large. Because of these practical difficulties, the technique has been

applied in only a few well-controlled experimental situations.

The technique of infrared detection, in terms of concept and implementation, is best manifest in a commercially available position-monitoring system known as the Selspot (Selective Spot Recognition) System. The system is individually fabricated by a Swedish company, SELCOM, Inc., and has the following basic components for three-dimensional point location: 1) two infrared point-detecting cameras; 2) infrared light-emitting diodes (maximum number - 30), and 3) control and processing circuitry. The system employs the principle of time-division multiplexing, regularly pulsing each diode and then transmitting in digital form the image location of the diode as sensed by the cameras. A straightforward trigonometric algorithm can then be employed to determine the three-dimensional spatial coordinates based on the camera-detected directional data and the camera position information.

The system represents a new approach and it has not yet been effectively evaluated in terms of performance and suitability for human experiments. Considering its basic similarity to image reduction approaches, the Selspot System clearly advances the state-of-the-art of data acquisition in terms of speed and simplicity. Certain experimental difficulties such as attachment of the diodes to the body segments, calibration of the system and its capital cost are often noted as the most serious drawbacks.

1.4 SELECTION OF A DATA ACQUISITION TECHNIQUE

Three criteria ranked predominately in the selection of the data acquisition technique: 1) suitability for planned experiments; 2) development

cost, and 3) development time. Immediately, in view of the real-time data acquisition requirements, only the goniometric, acoustic and Selspot systems were considered realistically competitive. The inherent pattern recognition problem associated with television-based systems was not considered to hold promise of being reduced to a level needed in the real-time acquisition and analysis projects.

The acoustic approach suffers in that its data reduction speed can be quite long, a reasonable estimate being on the order of 100 points per minute for current hardware. Considerable development time and expense seemed imminent, both in terms of experimental considerations and in terms of increasing performance. Lastly, the acoustic system would invariably require the acoustic frequency range 40-80 kHz for implementation. This directly conflicts with the frequency range employed by an existing blind mobility aid, the Sonicguide, and would most likely conflict with future designs. Based on these factors, the acoustic approach was not given further consideration.

The goniometer method is capable of meeting the real-time data acquisition requirements and has proven to be an effective means of monitoring simple, well-defined relative motions. However, the design techniques one would employ to monitor the motion of several body segments is unclear, and even further from definition is the means one would employ to infer absolute position and orientation information from a goniometer-based system. Although large-scale mechanical linkages and hardware could be designed, the methodology required to insure non-invasive and effective tracking is an unresolved question.

The Selspot System, being a commercially-available, state-of-the-art piece of hardware appeared to hold the greatest promise. Its data transfer capabilities are unmatched, and data-reduction in real-time appeared to be an attainable goal. The system held the promise that when configured in the appropriate manner and when supported with computational software it could determine absolutely-referenced kinematic parameters. Although the 3-dimensional monitoring range of the available system is limited (approximately 2m x 2m x 2m), it appeared feasible that with the development of moderate amounts of further hardware, the Selspot System could track motion patterns over large volumes.

In view of the system requirements of the Mobility Laboratory's projects, it was felt that the Selspot System held the greatest potential for meeting them in the shortest time and at the lowest total cost. As a result, the Selspot System was acquired as the fundamental data-acquisition system.

Chapter 2

THE SELSPOT-COMPUTER DATA ACQUISITION SYSTEM

The Selspot System is a high-performance point-monitoring and data-transferring device. However, the system must be coupled to a computational and high-speed storage system in order for its 3-dimensional position tracking capabilities to be realized . Because of the high data transfer rate (40 kHz) and the unique configuration of the system, a special interface was needed to enable effective coupled operation with the Mobility Laboratory's minicomputer. The subject of this chapter is a description of the Selspot System, the laboratory minicomputer, and the mediating computer interface.

2.1 THE SELSPOT SYSTEM

The Selspot System components are pictorially depicted in Figure 2. A 3-dimensional camera-based tracking system requires remote sensing from two physically-distinct viewpoints to determine three-dimensionality. The Selspot System consists of the following components: two infrared-detecting cameras, infrared light-emitting diodes (LED), a diode power supply, an LED control unit for pulsing the diodes, and a main system unit responsible for overall timing and signal processing.

The Selspot System has the capability of directly tracking 30 LEDs, time-division multiplexing being employed to detect, process and transfer the camera directional information for each infrared-emitting diode (LED). The system's operation is maintained and controlled by a dual-clock timing arrangement which pulses the LEDs, triggers camera sampling operations,

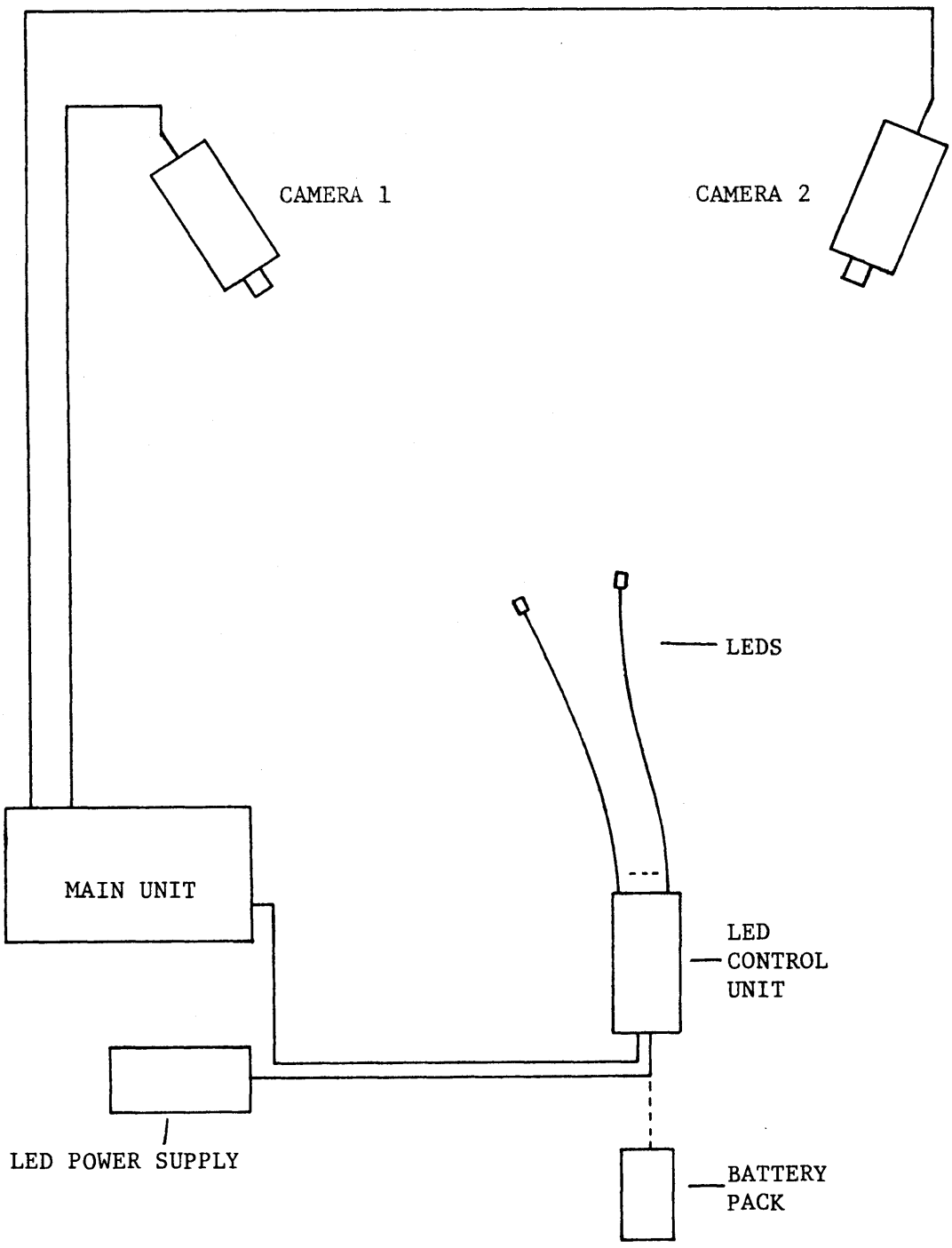

Figure 2a. Block diagram of the Selspot System.

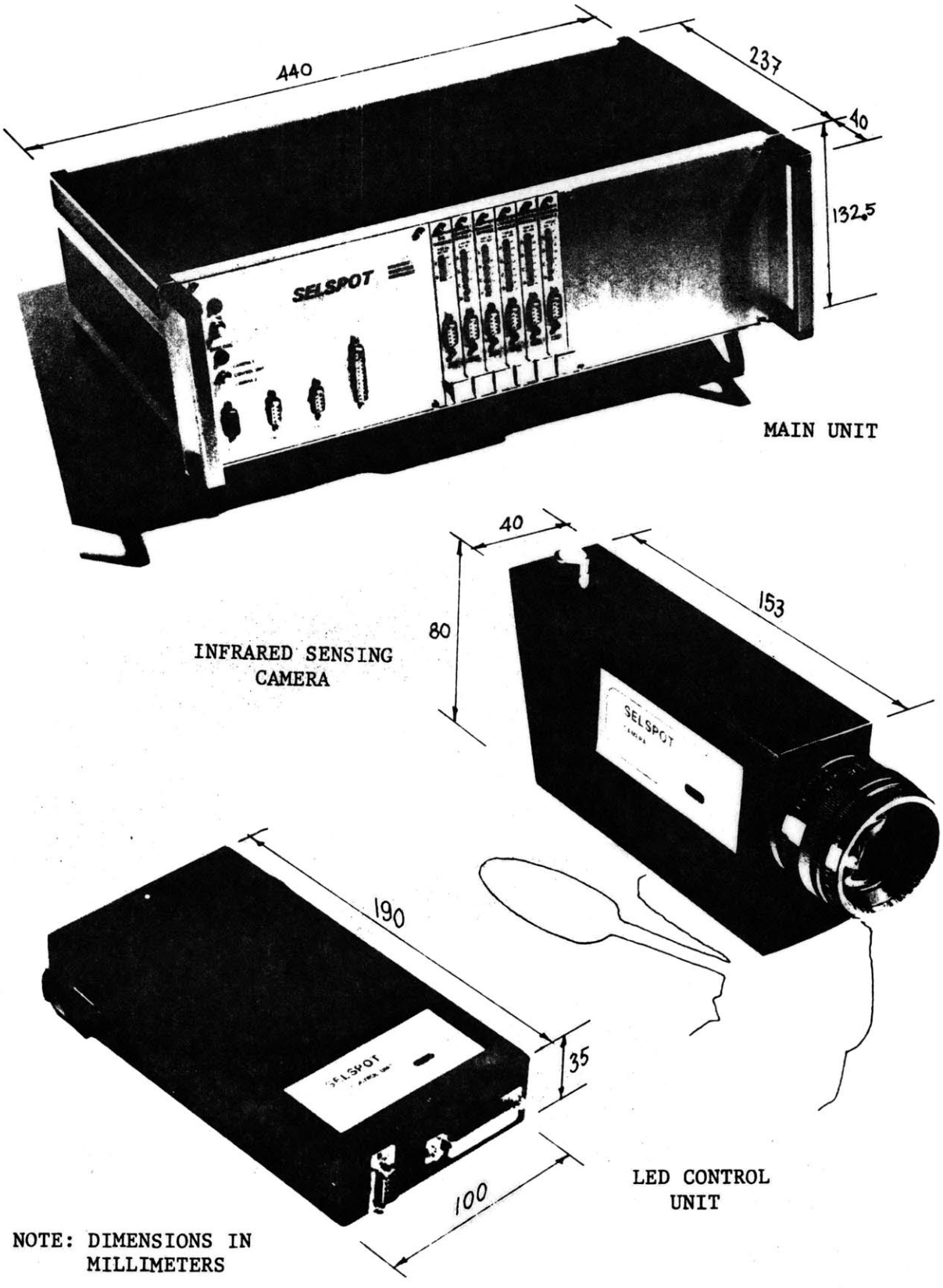

Figure 2b. The Selspot System components.

controls processing of the camera signals, and carries out multiplexing of the system's output onto the data lines. These operations occur in a continuous and cyclical fashion, with a resulting regular sampling rate of 315 Hz for each diode. Before discussing any further the overall system operation, a specific description of two components, the LEDs and the infra-red-detecting cameras, is in order. These two components form the fundamental basis of the system and their operational characteristics will be presented next.

The LEDs and the Camera. The LEDs represent the "points" that will later be analyzed to determine three-dimensional kinematic parameters. The usefulness of the whole technique depends strongly upon the diodes and how well they represent an actual physical situation, and their importance cannot be understated. The infrared light-emitting diodes have special design characteristics both in terms of packaging and performance. The diodes, depicted in Figure 3, are of compact and light-weight (4 grams) design in consideration of experimental applications. Yet their output power, emitted at a wavelength of 9400 nm, is greater than most comparable commercially available components. Because the emission must be detected by two sensors (cameras) at physically disparate locations, the diode's output energy must be geometrically widely distributed. Testing has shown that the detection is adequate up to an angle of 90 degrees measured from the neutral axis of the diode throughout a 360 degree arc about it (see Figure 3). This range of viewability is an important requirement for effective 3-dimensional tracking.

The cameras employed by the Selspot System have two integral components, a lens system for focusing the infrared beam and a detecting plate for sensing its location. The detector plate is the essential measurement mechanism of the Selspot System, and its performance directly determines the characteristic resolution of the system. The detector plate is composed of an analog substrate material which conducts current when activated by a beam of infrared light. An LED beam will induce currents in four conducting leads embedded in the plate with magnitudes proportional to the location of the detection on the plate. One of the functions of the circuitry of the main system unit of the Selspot System is that of processing the four signals from each camera and formulating an X & Y location signal. The data are referenced to a coordinate system on the plate consisting of a set of mutually perpendicular axes positioned as shown in Figure 4. The signals are digitized with 10 bit (1024 units) resolution and as a result, one can view the detector plate as a digital grid with the geometric characteristics depicted in the Figure.

The significance of the X and Y location data from each camera is readily apparent. This data represents a complete geometrically-projected description of the location of the point in space, as shown in Figure 4. With such a "view" of a point (LED) from two directions (cameras), the position of the point in three-dimensional space can be determined. This concept will be covered fully in Chapter 3. Let it suffice in the present discussion that it be stated that the 3-dimensional location of an LED can be found based on the two pieces of data from each camera and various fundamental camera calibration parameters.

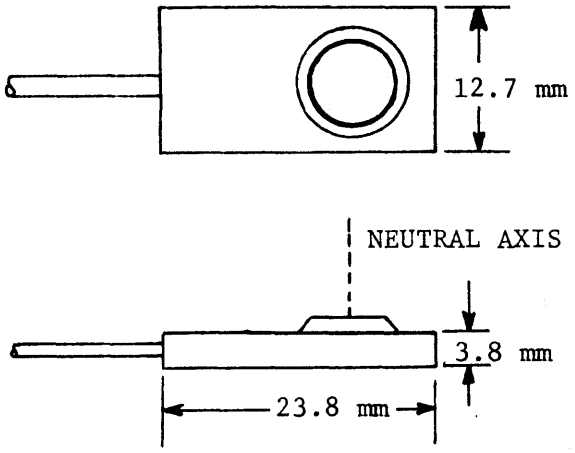

Figure 3. The light-emitting diode (LED).

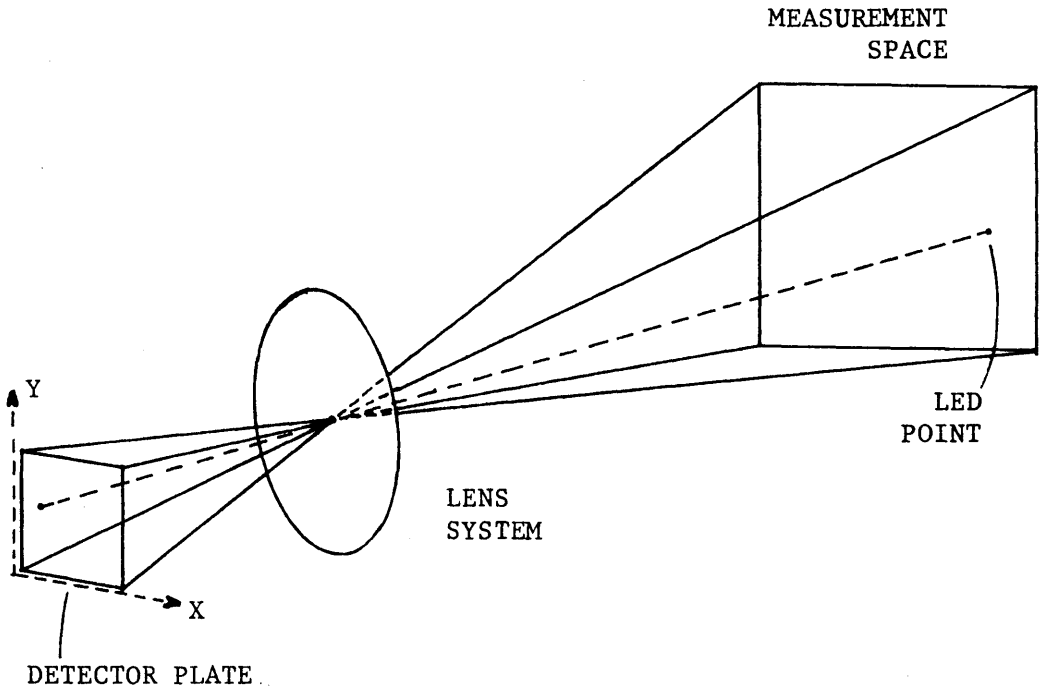

Figure 4. The principle of image-projection detection.

System Architecture. In this section, a brief description of the processing structure of the Selspot System is presented. It is not the intent of this discussion to give a complete and detailed description of the hardware, but rather to point out its salient aspects. A block diagram of the Selspot System hardware is given in Figure 5. It can be seen that the system has several distinct processing modules: 1) camera preamplifiers, 2) pulse shapers, 3) A/D converters, 4) a main control unit, and 5) an LED control unit.

Because the cameras may be physically located a large distance (20 meters) from the main unit, a preamplifier circuit in the camera conditions the data signals for transmission. Detector plate output signals which were on the order of milliamperes are converted and amplified to camera output signal levels on the order of a few volts. In this way, the signals will not be appreciably affected by electromagnetic effects present in the laboratory.

The pulse shaper serves a very critical function. In this module, the 4 detector plate voltages are processed, resulting in 2 output signals which are indicative of the actual X and Y location of the beam hits on the detector plate. In this regard, one important nuance of the detector plate and function of the pulse shaper deserves consideration. In addition to the detector plate currents being affected by the position of the beam on the plate, it can be demonstrated that the energy output (brightness) of the diodes also affects the detector plate currents. Since the diodes will all possess slightly different energy output levels due to manufacturing variance, temperature and powering circuitry, this could

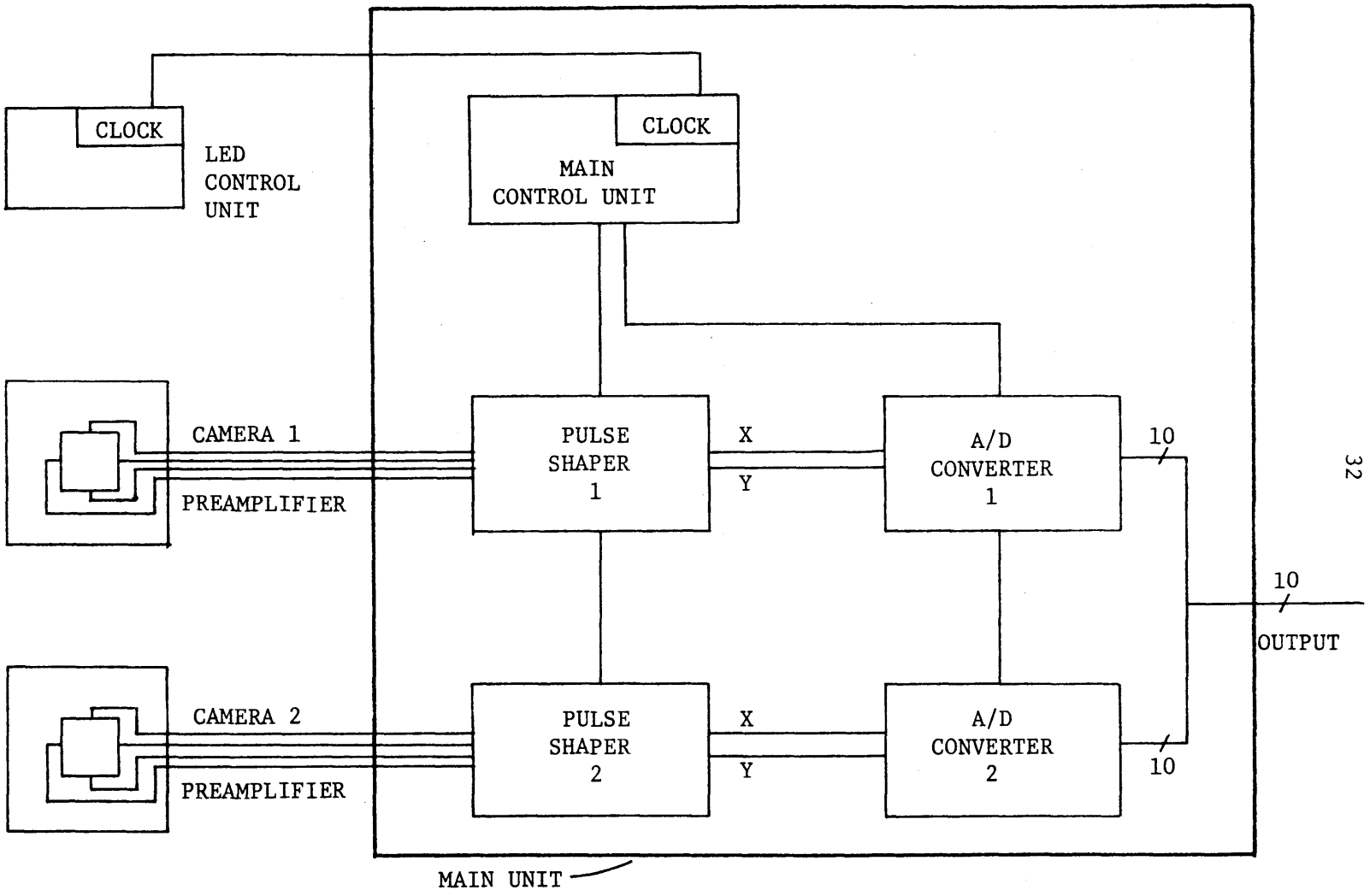

Figure 5. Selspot System processing modules.

pose a severe problem in terms of determining positional location from an analysis of the detector plate signals. In order to eliminate this problem, the LED signal is effectively normalized by dividing it by one-half of the sum of the X and Y signals. In this way, the effect of brightness is neutralized and discarded from the signal. This procedure does, however, couple the X and Y signals. Because of the small inherent performance differences in the hardware components, there may be a small detectable variance between the X and Y gains of any particular camera. Since the signals of the detector plate are coupled, it is futile to attempt to adjust the individual gains for uniformity. In view of the nature of the algorithm for calculating the 3-dimensional position parameters, this small variance must be compensated and the adjustment will be discussed in Chapter 4.

After the X and Y signals have been formed by the pulse shaper, they are then digitized by a successive approximation A/D converter, stored in a register, then subsequently presented to the data lines at regular intervals.

The circuitry of the Selspot System is designed such that when a point location is digitized, the resulting X and Y numbers are the values which represent the location of the center of the beam. This is an important feature because the beam even when focused may fall over several "digital" values, thus causing the possibility of digitizing ambiguity. By digitizing the location of the center of the beam in all cases, a consistent and relevant signal is obtained regardless of focusing and signal power.

It can be seen that the Selspot System has two clocking devices, one in the LED control unit (LCU) and one in the main system unit (Figure 5). In order for the system to perform properly, these two clocks must be synchronized. This can be accomplished in two ways: 1) through the use of a hard-wire connection, or 2) by a technique known as optical syncing. The pulse of the channel 1 LED is configured to be slightly longer (5 microseconds) than the other channels and the Selspot System has circuitry to detect and synchronize based on this detection. However, if channel 1 is not detected by the cameras, then the synchronization fails and the output data will not be meaningful. If one is operating in optical mode and the LED control unit is mounted on the human subject, then the only remaining trailing connection is the one running to the LED power supply (Figure 2). The LED control unit can be configured with an LED power pack which then allows free movement unencumbered by trailing paraphenalia.

System Timing. In the previous paragraphs, the essential sequence of operational events has been described. In simple terms, the timing cycle for a particular LED can be described as: 1) energize the LED, 2) sample the detector plate sensor, 3) turn off the LED, 4) digitize the X and Y signals, 5) transfer the data to the output lines and 6) move on to the next LED. It can be seen from Figure 5 that the processing of the data from each camera is carried out in parallel and then multiplexed onto the data lines.

To illustrate the overall timing structure, a timing diagram of the essential output signals and various operations of the Selspot System is

presented in Figure 6. The system timing is determined solely by the Selspot System hardware and is not alterable by the experimenter. From the Figure, it can be seen that the total time required to sample all the LEDs is approximately 3.2 milliseconds (315 Hz). Within that cycle time, 100 microseconds is allocated for the sampling, processing and transferring of the data for each channel. Figure 6 shows a 200 microsecond gap between channel 1 and channel 2. This time interval, as stated by the manufacturer, is needed to verify the presence of an optical synchronization signal when operating in that mode.

Within the 100 microsecond interval allocated for each channel, a particular LED is pulsed on for 50 microseconds and is then off for the remaining 50 microseconds of its interval and all the other channel intervals. It should be noted that as a result the LED pulsing operates with a 50% duty cycle, and an individual LED operates with a 1/60 duty cycle. Because of the low duty cycle for each particular LED, it can be pulsed with high current, thus enabling the emission of a greater than normal amount of optical power.

As discussed earlier, in a 2-camera situation there will be 4 10-bit pieces of data per channel sample, an X and a Y for each camera. These pieces of data are serially-multiplexed onto the data output lines at regular time spacings during a channel interval and in the following order; 1) X-camera 1, 2) X-camera 2, 3) Y-camera 1, and 4) Y-camera 2. To precisely identify and synchronize with the time interval when a piece of data is available for transmission, a "Data Sync" signal (Figure 6) is provided as a standard output of the Selspot System. Other timing signals

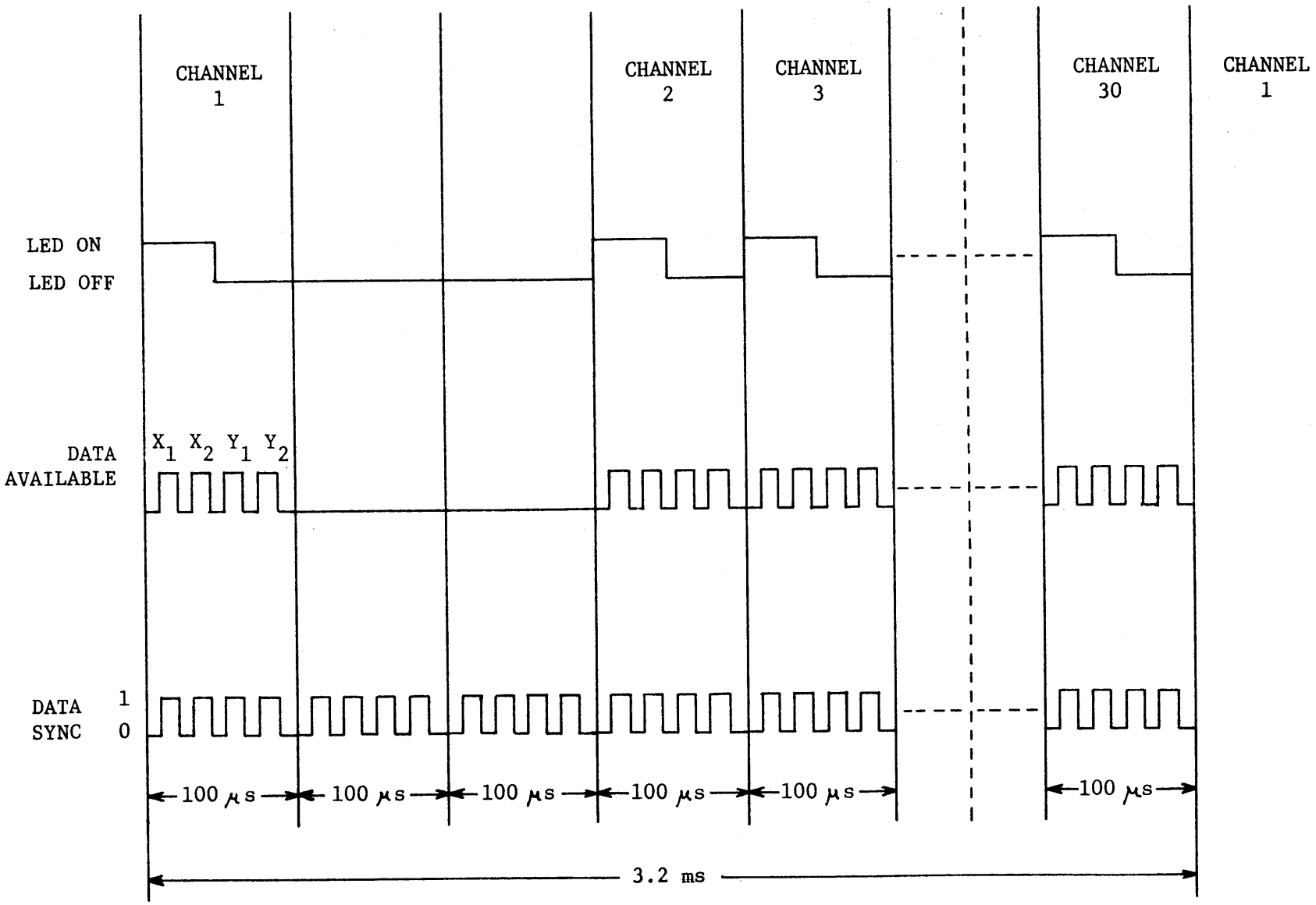

Figure 6. Selspot System timing.

are available and they will be discussed as necessary in the sections concerned with the computer interface.

2.2 THE SELSPOT-PDP 11/40 DIRECT MEMORY ACCESS COMPUTER INTERFACE

The Selspot System is best utilized when used in conjunction with a computer. In order to most effectively transfer data from the Selspot System to the computer, a special interface based on the principle of direct memory access was configured. The design and implementation of the interface is the subject of this section.

The PDP 11/40. The Human Mobility Laboratory is equipped with a multi-purpose Digital Equipment Corporation PDP 11/40 computer, a medium-sized laboratory minicomputer. The system is equipped with 32k core memory, 2 disk-based mass storage devices, a VT11 interactive graphics display, a Gould 5000 printer/plotter and a general interfacing hardware package known as the Laboratory Peripheral System (LPS). The LPS is a general-purpose interface module consisting of a 16-bit digital input/output device, 12-bit A/D and D/A converters, relays and other various devices.

Introduction to the Interface Design. As discussed earlier, an important reason for selecting the Selspot System as the data-acquisition system was its promising real-time capability. Since throughput cycle time is a crucial parameter in such a situation, any design means by which this cycle time can be reduced should be pursued. The design of the interface, then, can take on added importance in view of this perspective.

There are several design goals which can be delineated immediately. In an overall sense, it is desired that the interface carry with it a high

level of operational efficiency. This implies several specific design goals: 1) that a data transfer be carried out quickly with little processor overhead, 2) that the device be of straightforward design, both in terms of reliability and development cost, and 3) that the device be flexible in terms of adaptability to different types of interfacing situations.

The first and foremost requirement of the interface is that it have the capability to effectively transfer the regularly-spaced data stream for a given Selspot sampling cycle. To illustrate the effectiveness of a Direct Memory Access device in this instance, the techniques one would need to employ to utilize the standard digital input module of the Laboratory Peripheral System are presented initially. These procedures can then be compared to the actual implemented system when discussed in the next section.

The data transfer rate (40 kHz) needed in this application is at the extreme reaches of the LPS digital I/O capability. There are essentially only two techniques which could be employed to use this peripheral device for the problem; 1) direct computer control data transfer and 2) interrupt routine data transfer. In the former, the computer directly controls the peripheral device and, since the data transfers are initiated by the Selspot System, must remain dedicated to the device to detect the presence of new data. In this case, it can be appreciated that the central processing unit (CPU) has no opportunity to carry out any other operations because of this need for complete dedication to the data-transferring peripheral device.

An alternate technique is one which enables the computer to be dedicated to the peripheral device only when new data is present and ready to be transferred. In this situation, the peripheral device is "interrupt-enabled"; that is, upon receiving an external trigger at the peripheral device, the computer can be interrupted in its normal processing and commanded to jump to an "Interrupt Service Routine". In this case, the routine would contain the computer instructions necessary to transfer the piece of data to core memory and then reinitialize the peripheral device to receive more data. This technique is clearly more efficient since the computer is free to carry out other processing tasks when data is not being presented to the peripheral device.

As a result of the stringent timing and high-bandwidth nature of the incoming data from the Selspot System, this approach cannot be effectively utilized in this particular hardware configuration. The amount of time needed to switch processing modes (approximately 10 micro-seconds) coupled with the time required to prepare the device to receive each piece of data is large enough that the processor is still "dedicated" to the peripheral device throughout a data transfer sequence.

In view of these complications, it is apparent that a more specialized piece of equipment should be applied to this application. The device which best suited the situation was the DEC-Kit 11-D Direct Memory Access (DMA) Interface, a Digital Equipment Corporation standard product. This device is a high-performance internally-controlled interface which can transfer data words directly from an external device to core memory without CPU

intervention or participation. This approach represents a powerfully efficient means of inputting data to the computer and a closer examination of the device follows.

The DEC-Kit 11-D Direct Memory Access Interface. The DEC-Kit 11-D is a complete interfacing device which attaches directly to the Unibus structure of the PDP 11/40. The device consists of 4 functional registers and other associated digital hardware. The registers are specified as 1) the control status register, 2) the word count register, 3) the bus address register and 4) the data buffer register.

The control status register is the "controller" for the device, with specific bit formulations (see Figure 7) triggering and controlling the execution of certain data-transfer maneuvers. The word count register initially contains the number of data transfers to be made in a given transfer sequence and after each data transfer, the word count register is automatically decremented by 1. The bus address register contains the absolute core memory location where the next data word will be transferred. After each data transfer, the bus address register can be automatically incremented to the next memory location if desired. The data buffer register temporarily holds the last transferred data word until it can be moved to core memory.

In a typical data inputting sequence, the progression of events would be as follows. First, all the registers must be initialized to proper format for operation; 1) the bus address register must be loaded with the beginning core location address where the data is to be put, 2) the word count register must be loaded with the value specifying the

BIT	FUNCTION
00	IN: Read/write bit controls all data input transfers.
01	OUT: Read/write bit controls all data output transfers.
02	FNCT: Read/write bit available at the output cable for use as a function bit.
03	STAT: Read-only bit at the input cable and is used to indicate status.
04	Reserved for Extended Bus Address Bit 16.
05	Reserved for Extended Bus Address Bit 17.
06	ENB: Read/write bit enables DECkit 11-D priority interrupts when set to a 1. Disabled when set to a 0.
07	READY: Read-only bit, when set to a 1, specifies that the DMA is conditioned to accept a command.
08	LAST DIRECTION: Read-only bit specifies the direction of the last transfer: 0=input, 1=output.
09	LAST TRANSFER: Read-only bit is set to a 1 when the final data word is transmitted.
10	INPUT: Set to a 1 by DATA AVAILABLE IN when data is presented to the input. INPUT causes a data transfer when bit 00(IN) is set.
11	DA: DA is set to a 1 when DATA AVAILABLE OUT is asserted and is cleared to 0 when DATA ACCEPTED IN is asserted, signifying acceptance of the data.
12	OF: Set to a 1 upon completion of an input DMA cycle when XOF is held low. OF, when set to a 1, sets bit 15 and causes an interrupt request.
13	INPUT DEMAND: Read-only bit set to a 1 when input data presented but DMA not ready to accept it.
14	NEX: Read-only bit is set when an addressed memory location fails to respond within 20 microseconds.
15	SPECIAL CONDITION: Read-only bit is set to a 1 by NEX, INPUT DEMAND, OF or by word count overflow when bit 06 is zero.

Figure 7. Control Status Register bit functions.

number of data words to be transferred, and 3) the control status register must be loaded with the bit pattern specifying the operation to be carried out. The DMA device will then operate automatically and independently until the data transferring sequence has been completed. When operating in this mode, the device can transfer up to 450,000 pieces of data per second.

The Interface Design Approach. Since the interface device will directly determine the logistics of the data transfers, it is desirable at this point to specify more clearly the types of data transfer functions to be performed. Fundamentally, there are two kinds of processing situations which the interface must effectively deal with and two critical functions which should be controlled by the interface. The two kinds of processing situations which can be delineated are; 1) data acquisition for permanent storage, and 2) real-time processing where data management takes on a cyclic 3-fold form of acquire, process and destroy. In the former case, the interest is that of laying the data sequentially into core or some other fast medium, and then transferring it in bulk to a permanent storage device. In the latter case, the process would follow the lines of specifying a small block of core for the incoming data and then continuously writing over it as the data becomes obsolete after processing.

Concerning functional control, it is desirable to be able to transfer the data for a selectable number of channels at a specified frequency in each processing mode. Because the Selspot System is fixed in its sampling frequency (315 hz) and its channel capacity (30), it presents the possibility

of 37,800 data transfers per second. In most experimental situations, this capability will not be needed. An interface which could exhibit data selection versatility would greatly streamline the data handling problem.

In seeking an interface design which would best meet the performance needs discussed above, it was decided that a hybrid design, involving hardware and software design, offered the greatest benefits and versatility. Not only would the hardware configuration inevitably be simpler and more reliable, but with software control capability there would be programmatic flexibility for substantially changing the operations.

It can be seen that in each Selspot cycle (Figure 6) there is a time interval, 200 microseconds long, during which no data transfers occur. The adopted operational approach of the interface can be stated as follows; 1) "interrupt" the processor at the data gap in every Selspot cycle, 2) exit to an Interrupt Service Routine, 3) assess the present situation, 4) carry out any operational changes, 5) reinitialize the DMA registers, and 6) return to other processing tasks. All the operations just described can be carried out in much less than the 200 microsecond time interval, thus allowing complete control over the operations to be carried out for each Selspot cycle.

In order to facilitate the hardware implementation of the design, the channel "numbering" of the Selspot System was shifted by one channel. This change was accomplished by a pin connection reassignment on the LED control unit and is completely invisible to the user. The effect of this

action is that now the 200 microsecond interval occurs at the beginning of the redefined Selspot cycle.

To more clearly understand the function and the power of the Interrupt Service Routine approach, an examination will be made of the management of two very different yet entirely feasible experimental situations. The first situation involves a straightforward data acquisition problem in which an experimenter wishes to sample the first 10 channels of the Selspot System at 79 Hz and trigger the beginning and the end of the experiment (i.e., a walking gait experiment). In this case, it is desired to sample every fourth cycle (315/4 = 79) of the Selspot System, transfer 40 data words (10 channels * 4 data words per channel) in each sampling cycle, and check a start sampling and stop sampling decision flag. All these functions can be easily carried out through simple decision-making and modification of the DMA registers in the Interrupt Service Routines. A block diagram algorithm for carrying out this situation is given in Figure 8, part b). It can be seen that only the data which is desired will be transferred and all other ignored by the computer.

In the second case, a real-time experimental situation is examined in which a single-sampling of 10 channels is to take place after a processing flag has indicated that the present data has been examined and processed. Such a flag would then allow new data to be written into the temporary data memory block, destroying the previous set of data. The algorithm for accomplishing this is given in Figure 8, part a. It can be seen that in the latter case the bus address register is reinitialized at

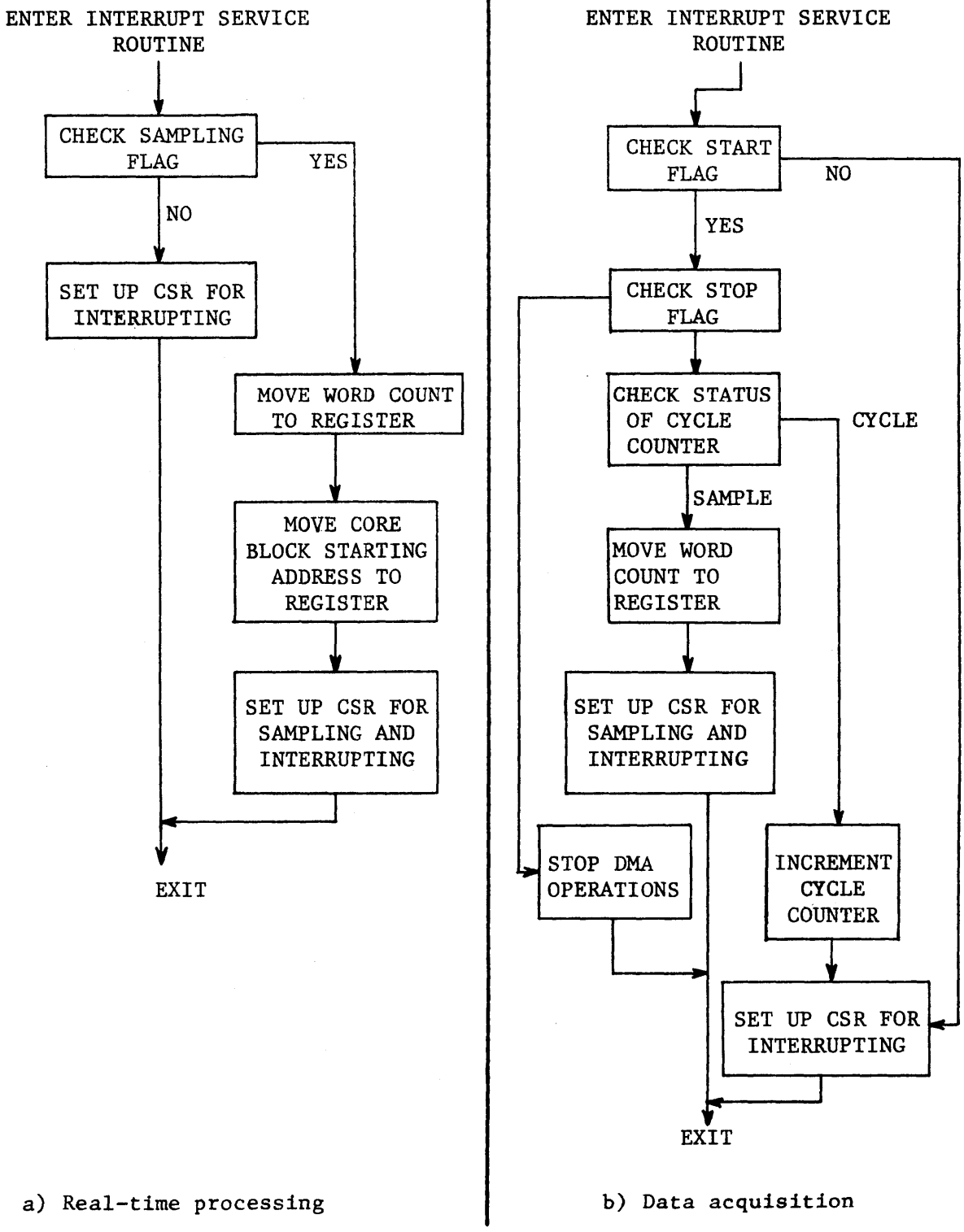

Figure 8. Two DMA data transfer algorithms.

every sampling cycle to the beginning of the data buffer, and that now the frequency of the sampling is determined directly by the processor. Simply by changing a few assembly language statements in the Interrupt Service Routine and the main initialization routine, the functioning of the DMA interface can be drastically modified.

Since the DMA can completely manage itself after its registers have been initialized, the CPU is free to carry out other processing tasks unaware of and independent of the DMA device. Only once per Selspot cycle and for approximately 50 microseconds is the CPU servicing the DMA and thus distracted from its normal processing. Because of the system architecture of the PDP 11/40 and the relative infrequency of the processor interruption, this operation will not seriously affect the overall software processing efficiency. The process of "interrupting" the CPU is efficiently handled by the Operating System in that all work in progress is logically stored away and then retrieved for continued processing after the Interrupt Service Routine has been executed.

Implementation of the Interface Design. An integral aspect of the interface design is the assumed ability to be able to trigger an external interrupt at the beginning of the 200 microsecond interval in each Selspot cycle. It can be seen from the operational description of bit 12 (Figure 7) of the DMA control register that only by holding the XOF signal line low (0 volts) can an external device interrupt the processor. However, the structure of the DMA device does not allow this feature to be functional after the word count register has reached 0. Further information can be obtained from "The DEC Kit 11-D Assembly & Installation Manual." In the

proposed interface design, this is always the situation since all data transfers have been completed before an Interrupt Request is initiated. In order to obtain the feature of triggering an interrupt at any time, a small modification was made to the backplane circuitry of the DEC-Kit 11-D DMA. To utilize this added feature, the FNCT bit (bit 02) of the DMA control status register must be set high. When the FNCT bit is not set, the DMA device performs in the standard manner.

A limited amount of digital processing logic was required between the Selspot System outputs and the DMA signal inputs in order to provide the proper type of signals for carrying out functional tasks. This interfacing logic was configured as a plug-in board which was mounted in the Selspot System main unit. The digital logic circuit is shown in Figure 9.

There are two primary inputs to the DMA device which must be conditioned from several outputs signals of the Selspot System, the Interrupt Request pulse and the Data Transfer pulse. The Selspot System contains a 5-bit counter known as the "channel number counter". During the 200 microsecond interval, the channel number specification is 00001 for the first 100 microseconds and 00010 for the final 100 microseconds. The logic that senses the counter bits generates a high pulse during the 200 microsecond data gap for each Selspot cycle. This signal serves two purposes. The low to high transition at the beginning of the interval triggers a pulse generator which sends a 10 microsecond pulse to the XOF line of the DMA. This pulse is long enough to guarantee a response to the interrupt request, yet is short enough so as not to cause a second interrupt when the system is reinitialized.

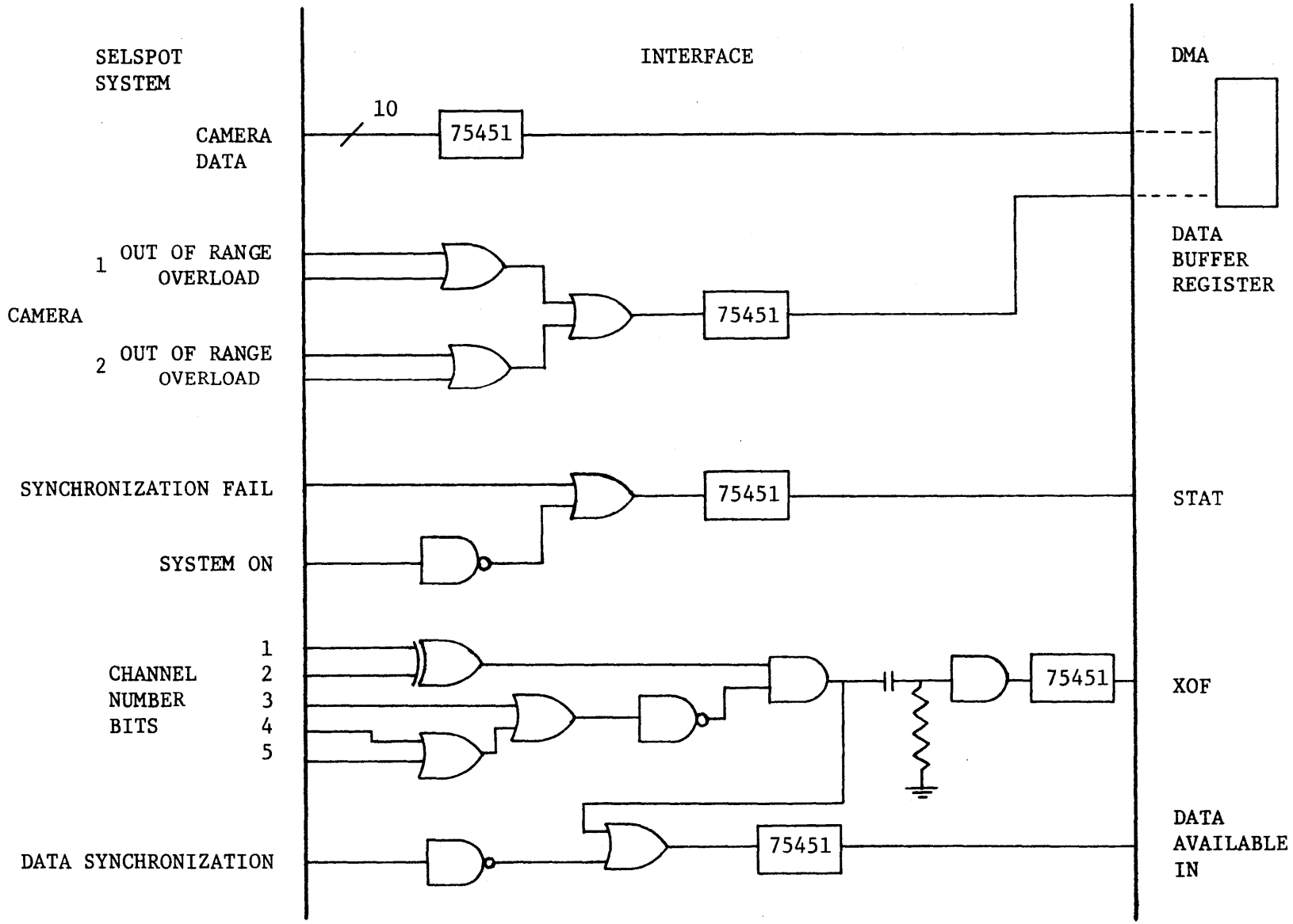

Figure 9. Digital logic of the Selspot-DMA interface.

The second purpose the signal serves is that of masking the Data Sync signal, an output signal of the Selspot System (see Figure 6). The data sync signal is used to initiate each individual DMA data transfer, and it continues to be active during the 200 microsecond interval. By driving it high during this interval, unintended DMA data transfers cannot occur.

One final function served by the digital logic is that of warning the user of bad data. The Selspot System has signal outputs which warn of undetected LEDs due to either too weak or too strong a signal. Whenever such a situation occurs, a high signal is sent to the 14th bit of the DMA data buffer. In this way, irrelevant data can easily be separated from good data since the bad data will contain the number 16384 (2^{14}). Because the highest value normally encountered is 1024, such a data value can be eliminated from any further processing.

DMA Handling Software. An integral aspect of the Selspot-PDP 11/40 interface is the device handling software. The real control of the transfer of data to the PDP 11/40 is embedded in the initialization software and the Interrupt Service Routine software. Several assembly language DMA handling routines have been written to control the DMA in different functional situations. These routines are callable from Fortran, the main user language for all the developed software. An example of a CALL statement to an assembly language subroutine is the following: CALL TKSSM2 (IBUF,NCHN,NFREQ). This particular subroutine represents the format and parameter specification for executing a permanent storage data acquisition sequence. The user need only specify the buffer name where the data should be stored, the number of channels to be sampled, and the frequency of

sampling. This specific routine begins the sampling when a start pulse is asserted to the LPS digital I/O device and terminates the sampling when a stop pulse is received at the same device. The triggering is initiated from a control box located in the experimental area.

In this chapter, a description of the Selspot-PDP 11/40 data acquisition system has been presented. This system, as shown in Figure 10, forms the basic hardware configuration employed for monitoring motion patterns.

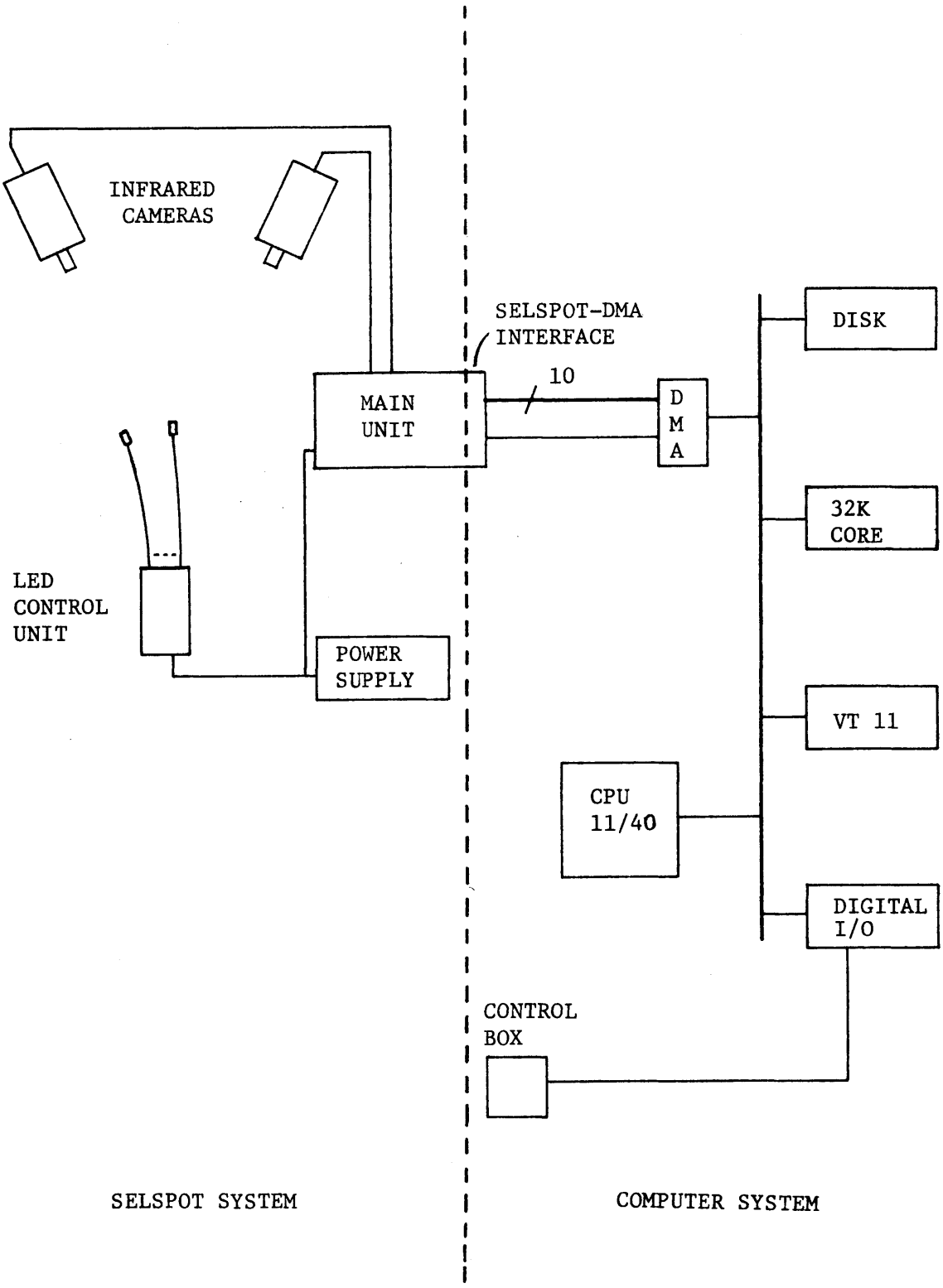

Figure 10. The Selspot-PDP 11/40 data acquisition system.

Chapter 3

DETERMINATION OF ABSOLUTE THREE-DIMENSIONAL COORDINATES USING THE SELSPOT-COMPUTER SYSTEM

3.1 INTRODUCTION

The Selspot System produces image projections of LED points from two views and, in conjunction with certain camera calibration parameters, sufficient information is available to determine absolute three-dimensional coordinates. In this chapter, the technique for finding such coordinates will be discussed.

The analytical approach for determining the three-dimensional kinematic parameters of rigid bodies assumes knowledge of the spatial coordinates of three points on the rigid body. With this information, a unique set of kinematic parameters can be found. Therefore, the ability to find the three-dimensional coordinates of the 30 LED points is of direct significance to the overall kinematic problem which will be fully developed in the next chapter.

The technique employed in this thesis for finding absolute three-dimensional coordinates is a direct approach in the sense that the various procedures and parameters have direct physical significance. This type of approach, albeit more involved than some indirect calibration-mapping approaches (Duda - 1973), was selected because it can be continuously applied through all the development phases of the kinematic-monitoring facility.

Thus far, it has been implicitly assumed that the infrared cameras

are placed in some particular viewing position and then remain statically-placed throughout an experimental phase. In such a situation, an image-view mapping technique appears attractive. However, in order to track human motions over a large spatial volume, as discussed in Chapter 1, it is inevitable that the cameras will need to move in an active tracking fashion. The three-dimensional calculation technique utilized in this thesis can be applied in such a situation without special changes or accommodations. In view of the ease and the computational efficiency with which it can handle the moving camera problem, it was chosen over other techniques at the expense of some calibration efficacy.

In this chapter, a stationary camera situation will be assumed to allow the discussion to remain as straightforward as possible. In Chapter 9, the problem of tracking motion over large spatial volumes is introduced, and the application of the computational technique in such a situation will be discussed at that time.

An outline of the approach of the three-dimensional calculation technique is in order. It can be shown that the image view (X and Y) of each camera plus a third directional parameter, focal distance, is sufficient information to formulate a locally-referenced direction vector pointing in the direction of the pulsed LED. By judicious choice of a camera coordinate system and proper interpretation of the focal distance and the Selspot data, a physcally relevant direction vector for each camera can be specified with respect to its own local coordinate system. The direction numbers of the vector for each camera are then determined with respect to a global reference frame. With this information and the

absolute positional coordinates of the origin of each camera coordinate system, a simple lines-in-space algorithm can be applied to find an intersection point which will be seen to be the absolute three-dimensional location of the LED point.

The line-in-space formula which was utilized (Leithold-1968) can be stated as follows:

> Let L be a line in three-dimensional space such that it contains a given point $P_o(X_o,Y_o,Z_o)$ and is parallel to the representation of a given vector $\underline{R} = (a,b,c)$, where a, b, c are the Cartesian direction numbers of $\underline{R}$.
>
> Then, the equation of the line is

$$\frac{X - X_o}{a} = \frac{Y - Y_o}{b} = \frac{Z - Z_o}{c} \quad .$$

Given two such independent lines in space, each containing the LED point, then the absolute spatial coordinates of the LED point can be found by determining the point of intersection of the two lines.

The equation of the line shows that essentially two types of information are needed to determine it: 1) the XYZ coordinate of a point lying on the line formed by the LED beam; and 2) a set of absolute Cartesian direction numbers for the beam. In Figure 4, a hypothetical LED beam is focused on the detector plate. The behavior of a complex, multiple lens system can be described in terms of the representation shown in the Figure. All the infrared beams must pass through a single point called the focal point, which is located a distance F away from the

detector plate and along the neutral axis of the lense.

In terms of the camera detection system, the focal point is the only point which will always lie on a line formed by an LED beam. Therefore, the absolute XYZ coordinate of the focal point of each camera referenced to a global coordinate system must be found. The procedure for doing this is discussed in Chapter 5, and can be assumed to be available in this presentation. The determination of the second group of parameters, the LED beam direction numbers for each camera, will be examined in this chapter. First, the determination of the parameters in a local camera coordinate system will be introduced and in the following section, the transformation of the parameters to the global reference system as required will be discussed.

3.2 DEFINITION OF THE POINT DIRECTION VECTORS IN THE CAMERA COORDINATE SYSTEM

The data output for each of the Selspot System cameras is a projected view of each LED point in terms of an X and a Y value. This data is referenced with respect to each individual camera but has no globally-referenced significance. In order to define the structure with which to give the Selspot System output a globally-referenced significance, a local camera coordinate system will be defined for each camera, and a global reference system will be defined to which the locally-referenced Selspot data will later be transformed.

This approach is illustrated in Figure 11(a), where for the sake of discussion a global reference system has been defined which has as its

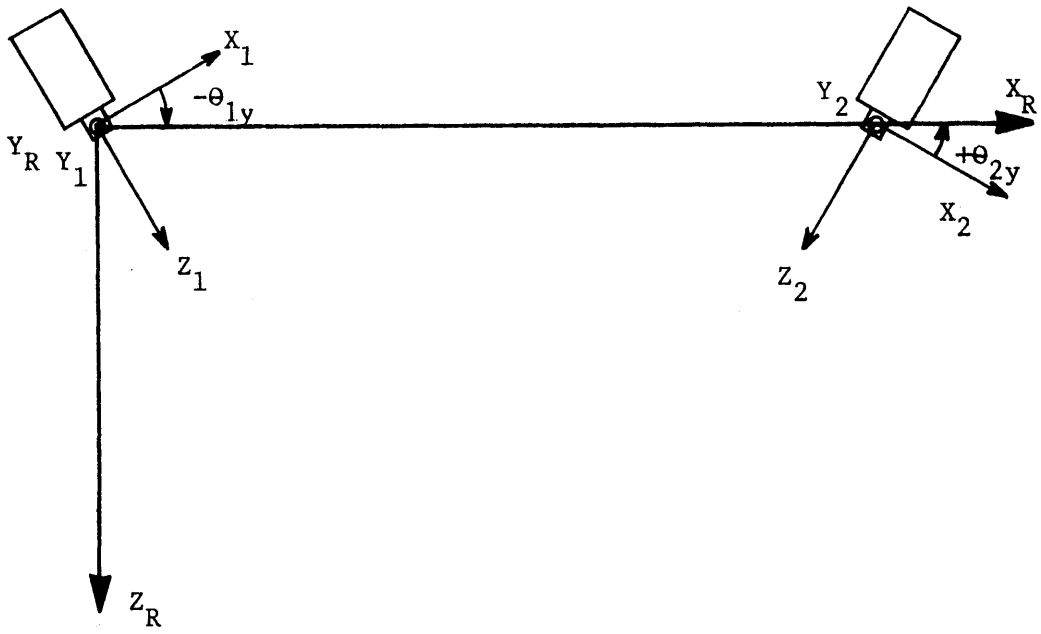

a)

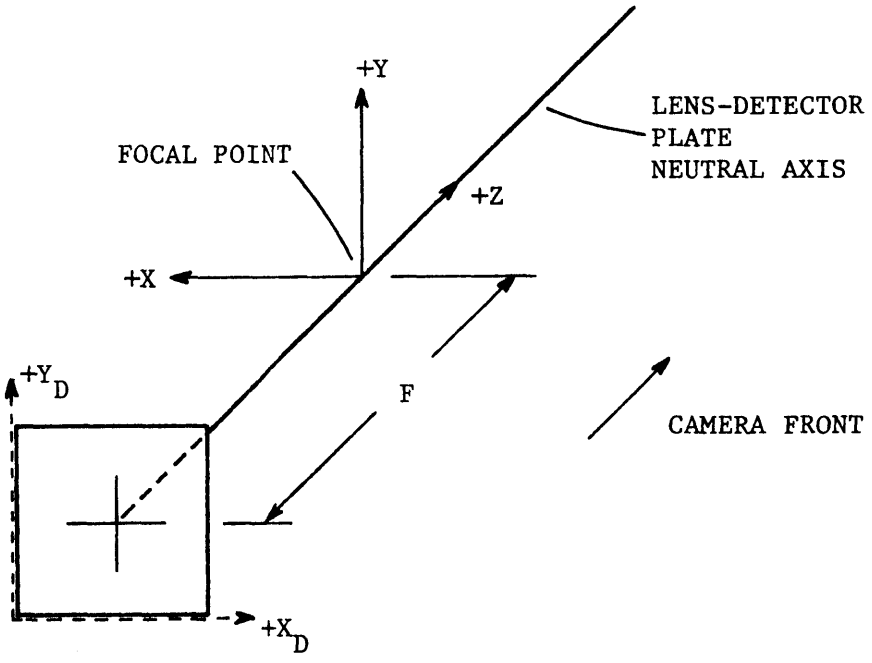

b)

Figure 11. Definition of the reference coordinate system and the camera coordinate system.

origin the focal point of camera 1, and the focal point of camera 2 as a point on its +X axis. The local coordinate systems are defined such that their origin is positioned at the focal point of their respective camera. The orientation is defined such that the X and Y axes of the camera coordinate system and the X and Y axes of the Selspot detector plate are respectively angularly similar, and the +Z axis is directed outward along the detector plate-lens neutral axis. This is illustrated in Figure 11(b).

It is desired that the Selspot data be used to quantify the Cartesian direction numbers of the LED beam with respect to the camera coordinate systems just defined. This can be accomplished by a simple transformation of the Selspot data. The output of the Selspot System is given in terms of 10 bit (1024 units) data words, the values ranging from 0 to 1024. As illustrated in Figure 12, all the incoming Selspot data is transformed to a new detector plate coordinate system (X_T, Y_T) which alters the range of the Selspot System data to that of a -512 to +512 scale and alters the directivity of one axis.

A hypothetical LED beam path has been depicted in the Figure. It can be seen that after this particular data has been transformed to the new detector plate coordinate system, the resulting $+X_T$ and $+Y_T$ digital values are directly analogous to the directional components one would logically infer with respect to the camera coordinate system. It should be noted that this direct applicability is true in all four quadrants of the detector plate. The third component needed to form the direction vector is the focal distance F, and it must be determined from a

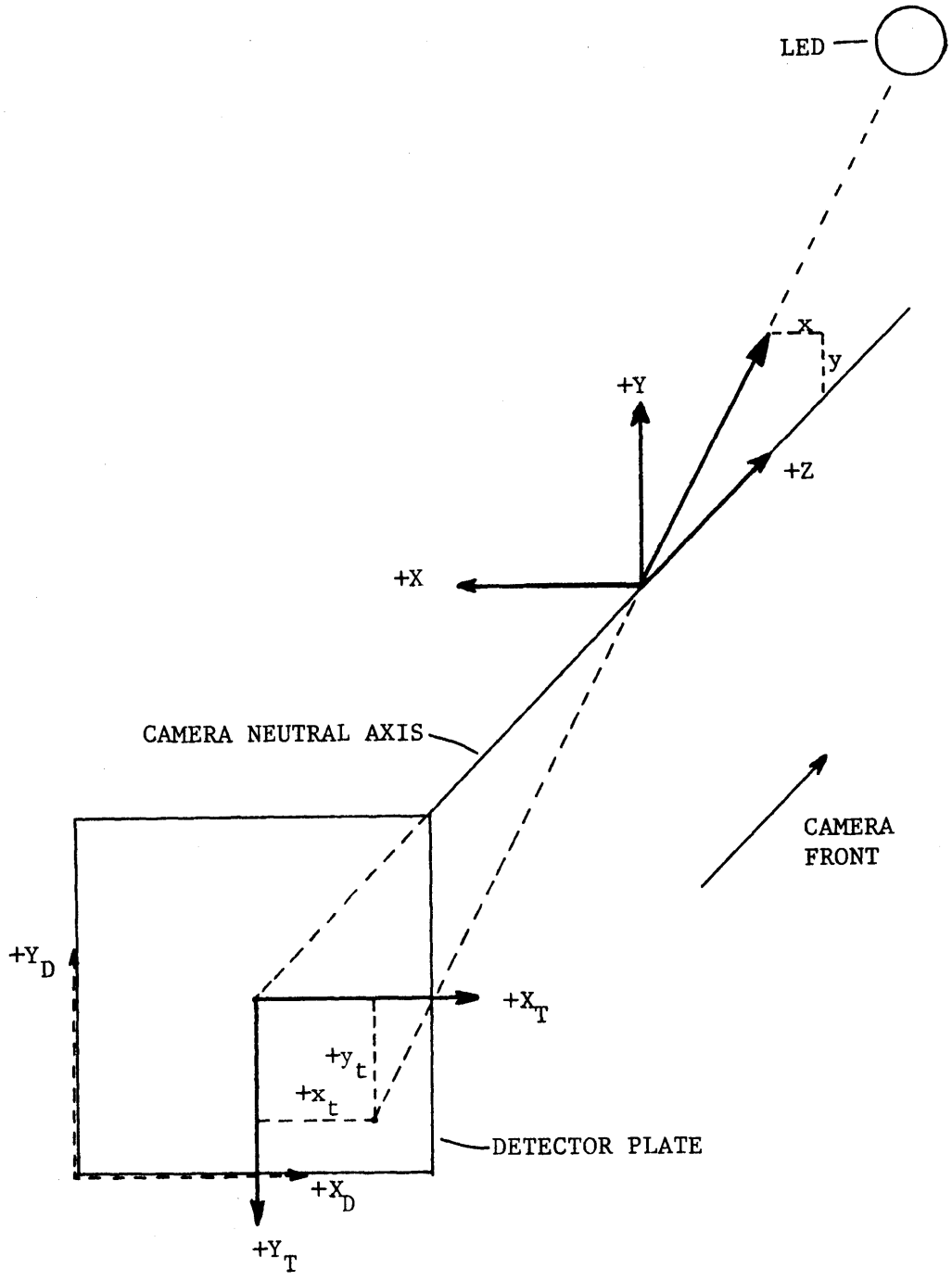

Figure 12. Formation of the camera direction vector.

calibration procedure. Its calculation will be discussed in Chapter 5.

Before the complete direction vector in each camera coordinate system can be formed, the three components must be referenced in the same scale. The actual size of the usable portion of the detector plate is 10 mm by 10 mm, which means that in physical terms there are 102.4 Selspot units per millimeter of physical distance along the detector plate. Since a set of direction numbers is magnitude independent, and in order to minimize computations, the focal distance (specified in millimeters) is scaled up by a factor of 102.4 .

In summary, through the definition of a camera coordinate system, the transformation of the Selspot data, and the introduction of a third directional component, focal distance, a physically relevant set of direction numbers relative to the local camera coordinate systems has been derived. To apply the line-in-space formula, the direction numbers must be transformed to the global reference system.

3.3 ROTATION OF THE CAMERA COORDINATE SYSTEM TO THE REFERENCE COORDINATE SYSTEM

It is required that the direction numbers of a particular LED beam for each camera be expressed in the designated global coordinate system. The most general rotational transformation is that which assumes a disparity of all three Cartesian rotation angles. To simplify both the computational algorithms and the experimental calibration procedures, the decision was made that a limited geometric constraint would be imposed on the experimental camera positioning.

It is assumed in this thesis that in an experimental situation there will be only one axis which must be rotated, and that axis will be the Y axis (θ_y). The type of experimental situation which is assumed is depicted in Figure 11(a). This implies that a calibration adjustment of the cameras can be performed so that there is no angular disparity about the X axis or the Z axis between the camera coordinate systems and the global coordinate system. This procedure is discussed in the calibration section of Chapter 5. This requirement has the important benefit of eliminating the need to measure and specify two other rotation angles for each camera. The two angles, θ_{1_y} and θ_{2_y}, are the only angles which need be determined and the procedure for finding them is also discussed in the calibration section of Chapter 5. Given the two rotation angles, it can be shown that the following rotation formula is applicable:

$$X' = X \cos\theta - Z \sin\theta$$

$$Y' = Y$$

$$Z' = Z \cos\theta + X \sin\theta$$

where X,Y,Z are the point direction number components in the camera coordinate system and X',Y',Z' are the point direction number components in the global reference system, and $\theta = \theta_{i_y}$ $(i = 1,2)$.

3.4 THE MATHEMATICAL ALGORITHM

The line-in-space formula, applied to each camera's data, results in the following two equations.

Redefining the nomenclature to suit the present situation, let

$(P1_i)$ = XYZ positional coordinates of the origin of the camera 1 coordinate system referenced to the global coordinate system, respectively;

$(P2_i)$ = XYZ positional coordinates of the origin of the camera 2 coordinate system reference to the global coordinate system, respectively;

$(V1_i)$ = XYZ LED direction numbers for camera 1 referenced to the global coordinate system, respectively;

$(V2_i)$ = XYZ LED direction numbers for camera 2 referenced to the global coordinate system, respectively,

where (i = 1,3). Therefore,

$$\frac{X - P1_1}{V1_1} = \frac{Y - P1_2}{V1_2} = \frac{Z - P1_3}{V1_3} \qquad \text{(camera 1)}$$

$$\frac{X - P2_1}{V2_1} = \frac{Y - P2_2}{V2_2} = \frac{Z - P2_3}{V2_3} \qquad \text{(camera 2)}$$

The result of the specified operations for a particular LED sample is a set of two linear equations in absolute three-dimensional space, each passing through a camera and referenced to the global coordinate system. The LED point coordinates can be found by solving for the projected point of intersection. A solution of the equations for the XYZ coordinates follows:

$$X = \frac{\frac{P1_3\ V1_3}{V1_1} - \frac{P2_1\ V2_3}{V2_1} + P2_3 - P1_3}{\left[\frac{V1_3}{V1_1} - \frac{V2_3}{V2_1}\right]} \qquad \text{(X-Z plane)}$$

$$Y = \frac{\frac{P1_2\ V1_1}{V1_2} - \frac{P2_2\ V2_1}{V2_2} + P2_1 - P1_1}{\left[\frac{V1_1}{V1_2} - \frac{V2_1}{V2_2}\right]} \qquad \text{(X-Y plane)}$$

$$Z = \frac{\frac{V2_1\ P2_3}{V2_3} - \frac{V1_1\ P1_3}{V1_3} + P1_1 - P2_1}{\left[\frac{V2_1}{V2_3} - \frac{V1_1}{V1_3}\right]} \qquad \text{(Y-Z plane)}$$

It should be noted that several sets of equation solutions exist and the particular set presented here takes into consideration various geometric and computational conditions which tend to enhance the reliability of the solution. This issue will be discussed further in Chapter 5.

Chapter 4

DETERMINATION OF THREE-DIMENSIONAL KINEMATIC PARAMETERS FOR MULTIPLE RIGID BODIES

This chapter is concerned with the problem of determining the kinematic parameters for multiple rigid bodies based on the measurement of three-dimensional coordinates of LED points. In order to effectively carry out such a task, several important kinematic principles need to be applied and a kinematically-based methodological structure must be established.

The first sections of this chapter are designed to introduce the conceptual framework which forms the basis for the definition of the overall kinematic problem to be addressed in this thesis. The final sections then present the analytical and computational algorithms for solving the kinematic problems.

4.1 INTRODUCTION

The fundamental kinematic law which will be applied to the kinematic problem states that if the three-dimensional coordinates of at least three points defined on a rigid body are known, then the body's kinematic configuration, or kinematic "state," is unique and determinable. This basic kinematic principle can easily be demonstrated. It is readily apparent that with only a single point on a rigid body defined in three-dimensional space, the object could be in any of a variety of configurations and not violate the single-point spatial coordinate

constraint. Similarly, with two points on the body completely described, the body is still free to rotate around an axis through the two points and not violate the constraint. However, at the introduction of a spatial description for a third point, a unique configuration or "state" of the body is defined.

It is apparent that by affixing a minimum of three LEDs to a body segment of interest, the means exists to define the unique configurational state of the body throughout a time span. Because the three-dimensional coordinates for 30 LEDs can be found employing the Selspot System, it is thus theoretically possible to track the configurational patterns of ten body segments.

Kinematic configurations can be described in terms of two pure kinematic components, position and orientation. It can be stated that irrespective of the configuration of any two Cartesian coordinate systems, the kinematic relationship between them can always be completely described in terms of 1) a positional (translational) change, and 2) an orientative change. This two-component kinematic description is a convenient conceptual construct and can assist in clarifying and simplifying the general kinematic problem at hand.

A logical way to structure the problem of determining multiple-body kinematic parameters is to define a global, or reference, coordinate system, and a set of body coordinate systems fixed to the set of rigid bodies for which kinematic descriptions are desired. The most straightforward kinematic description employing this structure is a distinct configurational description (positional and orientative) of

the relationship of each body coordinate system with respect to the reference coordinate system. This approach is the fundamental mechanism of kinematic description employed in this thesis. The next sections will deal with the kinematic concepts that have been introduced in greater detail.

4.2 DESCRIPTION OF KINEMATIC CONFIGURATION

The concept of a configurational description of a rigid body based on positional and orientative components has been introduced as one means of denoting its "kinematic state." In this section, the mathematical description will be presented and then a more rigorous examination of the concept will be carried out.

Mathematical Description. Initially, a consistent coordinate system nomenclature will be designated. The nomenclature of Kane is applied (Kane-1968) since it is well-suited for the systematic description of multiple coordinate systems. Referring to Figure 13, R_i (i = 1,3) and B_i^n (i = 1,3) are defined as right-handed Cartesian coordinate systems with the X axis designated by i=1, the Y axis by i=2, and the Z axis by i=3. The reference coordinate system $\underline{R}$ is fixed in three-dimensional space, and the body coordinate systems, $\underline{B}^n$, are fixed in their respective body. The lower-case notation, r_i (i = 1,3) and b_i^n (i = 1,3) denotes unit vector definition. Further, the orientation of a body $\underline{B}$ with respect to the reference system $\underline{R}$ can be specified in terms of

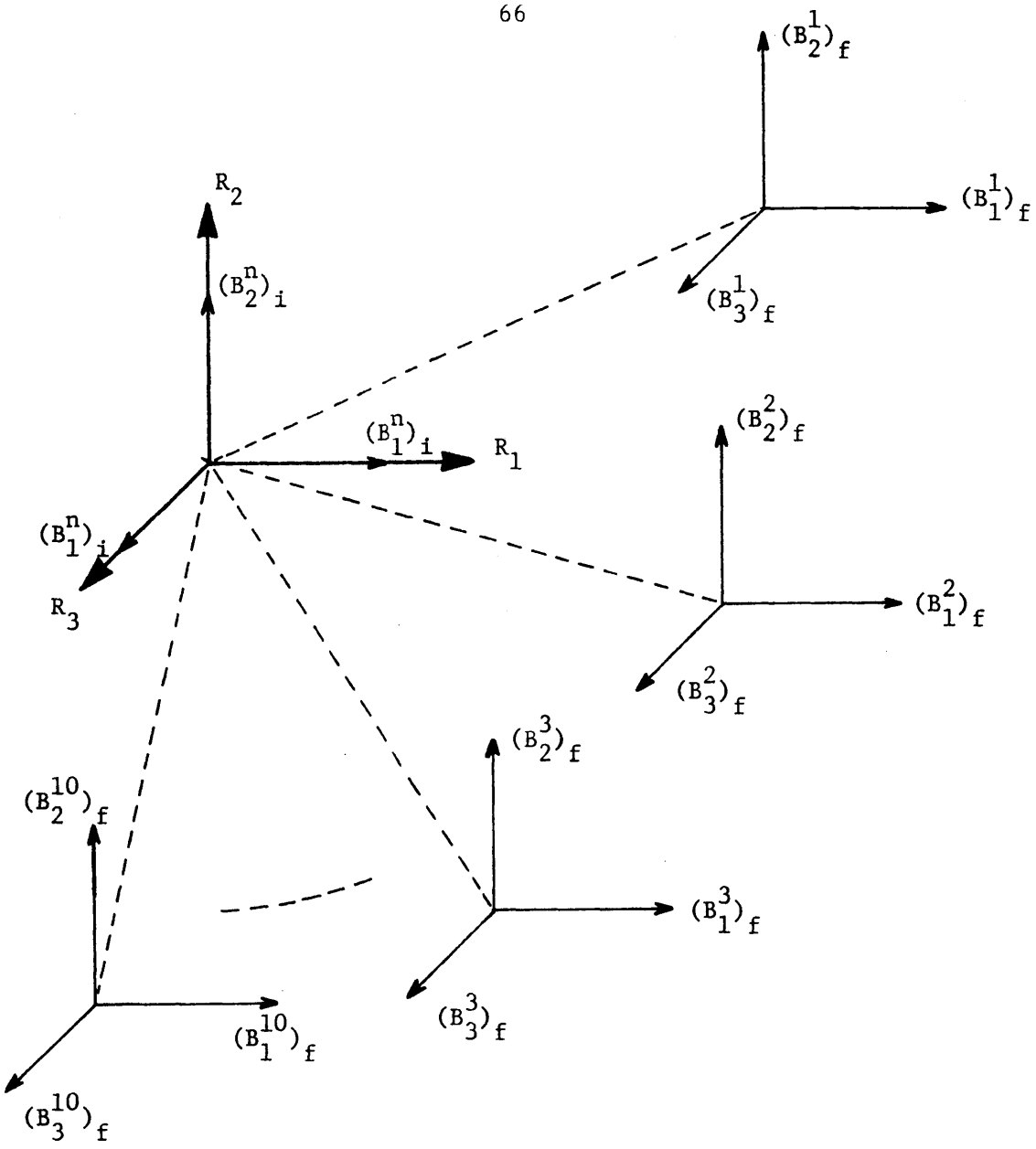

NOTE: NOTATION $(\ )_i$ DENOTES INITIAL STATE
NOTATION $(\ )_f^i$ DENOTES FINAL STATE

n = 1, 10

Figure 13. The kinematic formulation for a particular time step.

three successive rotations, θ_1, θ_2, and θ_3. These rotations can be illustrated in the following manner if a description of the orientation of an arbitrarily-located $\underline{B}$ with respect to the reference system is desired. By aligning $\underline{B}_i$ with $\underline{R}_i$ and then performing three successive right-handed rotations of $\underline{B}$, of amount θ_1 about B_1, θ_2 about B_2, and θ_3 about B_3, the final orientation is duplicated. Having specified θ_i $(i = 1,3)$ in this manner, a unique orientation of a body $\underline{B}$ in $\underline{R}$ is determined for all rotation combinations $(\theta_1, \theta_2, \theta_3)$ in the range $0 \leq \theta_1 < 2\pi$, $0 \leq \theta_3 < 2\pi$, and $-\pi/2 < \theta_2 < \pi/2$. This orientation angle sequence is best denoted as the modified Euler angle three-body axis orientation scheme.

The following statement can now be made about the orientative relationship between a body coordinate system and the reference coordinate system:

$$\begin{bmatrix} b_1 & b_2 & b_3 \end{bmatrix} = \begin{bmatrix} r_1 & r_2 & r_3 \end{bmatrix} R$$

and

$$\begin{bmatrix} b_1 \\ b_2 \\ b_3 \end{bmatrix} = R^T \begin{bmatrix} r_1 \\ r_2 \\ r_3 \end{bmatrix}$$

where $\underline{R}$ is the 3×3 orthogonal rotation matrix, and $\underline{R}^T$ is its transpose.

The rotation matrix is defined in terms of the nine direction cosines (the nine vector dot products between the orthogonal sets of unit vectors fixed in the body and the reference frame). It can also be presented in terms of the three rotations θ_1, θ_2, and θ_3 about the body

coordinate system (Lenox-1976). Therefore,

$$R = \begin{bmatrix} r_{11}' & r_{12}' & r_{13}' \\ r_{21}' & r_{22}' & r_{23}' \\ r_{31}' & r_{32}' & r_{33}' \end{bmatrix} \quad \text{and} \quad R^T = \begin{bmatrix} r_{11}' & r_{21}' & r_{31}' \\ r_{12}' & r_{22}' & r_{32}' \\ r_{13}' & r_{23}' & r_{33}' \end{bmatrix}$$

where

$$r_{ij}' = r_i \cdot b_j \quad (i,j = 1,2,3)$$

$$r_{11}' = \cos\theta_2 \cos\theta_3$$

$$r_{21}' = \cos\theta_1 \sin\theta_3 + \sin\theta_1 \sin\theta_2 \cos\theta_3$$

$$r_{31}' = \sin\theta_1 \sin\theta_3 - \cos\theta_1 \sin\theta_2 \cos\theta_3$$

$$r_{12}' = -\cos\theta_2 \sin\theta_3$$

$$r_{22}' = \cos\theta_1 \cos\theta_3 - \sin\theta_1 \sin\theta_2 \sin\theta_3$$

$$r_{32}' = \sin\theta_1 \cos\theta_3 + \cos\theta_1 \sin\theta_2 \sin\theta_3$$

$$r_{13}' = \sin\theta_2$$

$$r_{23}' = -\sin\theta_1 \cos\theta_2$$

$$r_{33}' = \cos\theta_1 \cos\theta_2$$

In conclusion, it is readily apparent that the complete configurational relationship between two Cartesian coordinate systems can be mathematically described through the use of a three-component vector which expresses a positional relationship between the coordinate system origins and a 3×3 rotation matrix which expresses an orientative relationship.

The Underlying Concept. An important concept to be understood when discussing a kinematic description of a rigid body is that there is no single kinematic statement which can be made. Each point on a rigid body will have a different kinematic description due to the geometric nature of the positional component. Therefore, a kinematic description must be given in terms of a definable point on the body in order to be relevant and meaningful. The entire act of defining a body coordinate system at some point on the object of interest is a recognition of this fact. The definition of a body coordinate system and a reference coordinate system establishes the specific kinematic problem to be solved. The problem is uniquely established as that of finding the positional and orientative relationship of the origin of the body coordinate system with respect to the origin of the reference coordinate system.

It follows from the above statement that given the configurational description of a point on a rigid body and the geometric structure of the body, the configurational description of any other point on the body can be found. In a later section of this chapter, this concept will be applied further and take on added importance. It is apparent that the orientation at every point on a rigid body is the same while the position is not. The straightforward implication is that position is a spatially-dependent parameter while orientation is spatially-independent. The power of such a realization rests in the knowledge that if the orientation is known at a single point on a body, it is known at every point on the body. This is not the case for position since the positional parameter is coupled to spatial geometry and body orientation, and each point on the body is affected in a different manner.

4.3 THE CONCEPTUAL APPROACH TO THE KINEMATIC PROBLEM

A crucial aspect in the design of a kinematic data-acquisition system is the definition of the methodological structure of the data-reduction process. It is readily apparent that several very different approaches to such a general kinematic problem could be applied, all with different computational and logistical characteristics.

It is the intent of this section to give insight into the approach employed in this thesis, define in detail the ensuing kinematic problem, and then delineate the procedures to systematically structure the problem.

The Approach. It has been indicated that the overall problem of determining kinematic parameters for multiple bodies can be approached in several different ways. It is obvious that the particular approach which might be utilized in any given experiment will be directly related to the type of information desired. As an example, in an experimental situation related to motion analysis, the approach might take the following form. First, the initial configurational relationship of the body coordinate systems to the global reference frame are determined, and then incremental configurational changes are determined for each body coordinate system through time. The result is a discrete "frame by frame" approximation of the body motion as described by the incremental relationship of each new configuration with respect to the configuration of the previous time step.

Another experimental situation which could be envisioned might involve the analysis of a multiple-body linkage system. A reasonable kinematic approach in this situation could be that of establishing a hierarchy of body-coordinate systems, each system described relative to its particular higher-level coordinate system (body of attachment). This process continues to the highest-level system which is then referenced to the global reference system. In this way, configurational information is consistently given relative to the body to which it is attached. It is clear that many other experimental situations could be conceived, and each one best approached by a slightly different type of kinematic analysis.

This thesis was concerned with defining a system of configurational description which would be general-purpose in that all other possible descriptions could be derived from it and at the same time straightforward from a conceptual point of view. Although transformations to different kinematic descriptions will increase the computational load in some cases, it can be argued that this drawback is negligible when compared to the total experimental capability and flexibility resulting from a general-purpose approach.

The conceptual approach which was adopted can be stated as follows: for each time step of data gathering, the kinematic problem is formulated as that of determining the position and orientation of each body coordinate system being considered with respect to the reference coordinate system. This is illustrated in Figure 13, and it can be considered to be the most general description since at each time step the kinematic

parameters for each body coordinate system are expressed in completely absolute and independent terms. It can be realized that once this type of description has been obtained, a myriad of other relationships can be derived, among them the two discussed earlier, incremental motion and relative motion of linkage components.

The approach has the added advantage that each body coordinate system configurational problem can be treated independently, and without special regard for the actual physical situation. If a solution algorithm can be found for the single body coordinate system problem, then it is clear that the multiple-body problem can be solved provided there is a suitable data-reduction structure.

The formal kinematic problem was structured in the following manner. For a particular time step, as illustrated in Figure 13, each body coordinate system under consideration is "conceptually" superimposed [$\underline{B}_i^j = \underline{R}_i$ $(i = 1,3;\ j = 1,n)$] on the reference coordinate system in an initial state. Then, after a measurement sequence, the specific kinematic problem to be solved is that of finding the configurational relationship between the initial (conceptual) state and the final (actual) state. With such an approach, the absolute positional and orientative parameters for each body coordinate system can be systematically found at each time step with respect to the reference coordinate system.

Configuration Description: Definition of the Body Coordinate System. Thus far, it has been tacitly assumed that a body coordinate system has been established on the body of interest. As discussed earlier, this

implies that a tangible point associated with the body has been designated at which a configurational description is desired. Clearly, such a designation should be made by the experimenter with complete freedom. Thus, an approach for defining and locating a particular desired point for kinematic description based on the measured LEDs needs to be established.

Recalling the situation during a measurement sequence, the sole information which is available concerning the nature of a body is the spatial coordinates of the LED points. Although it would seem logical to use an actual LED point as the identifier for the location of a kinematic description, this would be an unwieldy procedure and a restrictive one since it would not allow the description of internal points of body segments, a clear desirability.

An approach has been formulated which allows the designation of any point for examination. The technique also inherently fulfills the necessity of specifying the initial state of the body coordinate system in terms of spatial coordinates, as discussed in the previous section. The procedure, although requiring some pre-experimental direct measurements, is of a general and straightforward nature. In Chapter 5, some methods for streamlining the direct measurements will be discussed.

The entire process of definition reduces to the problem of specifying the spatial coordinates of the LED points affixed on a particular body with respect to the desired definition of the particular body coordinate system. The procedure is illustrated in Figure 14. In part (a), a rigid body containing LED points is depicted. A body coordinate system

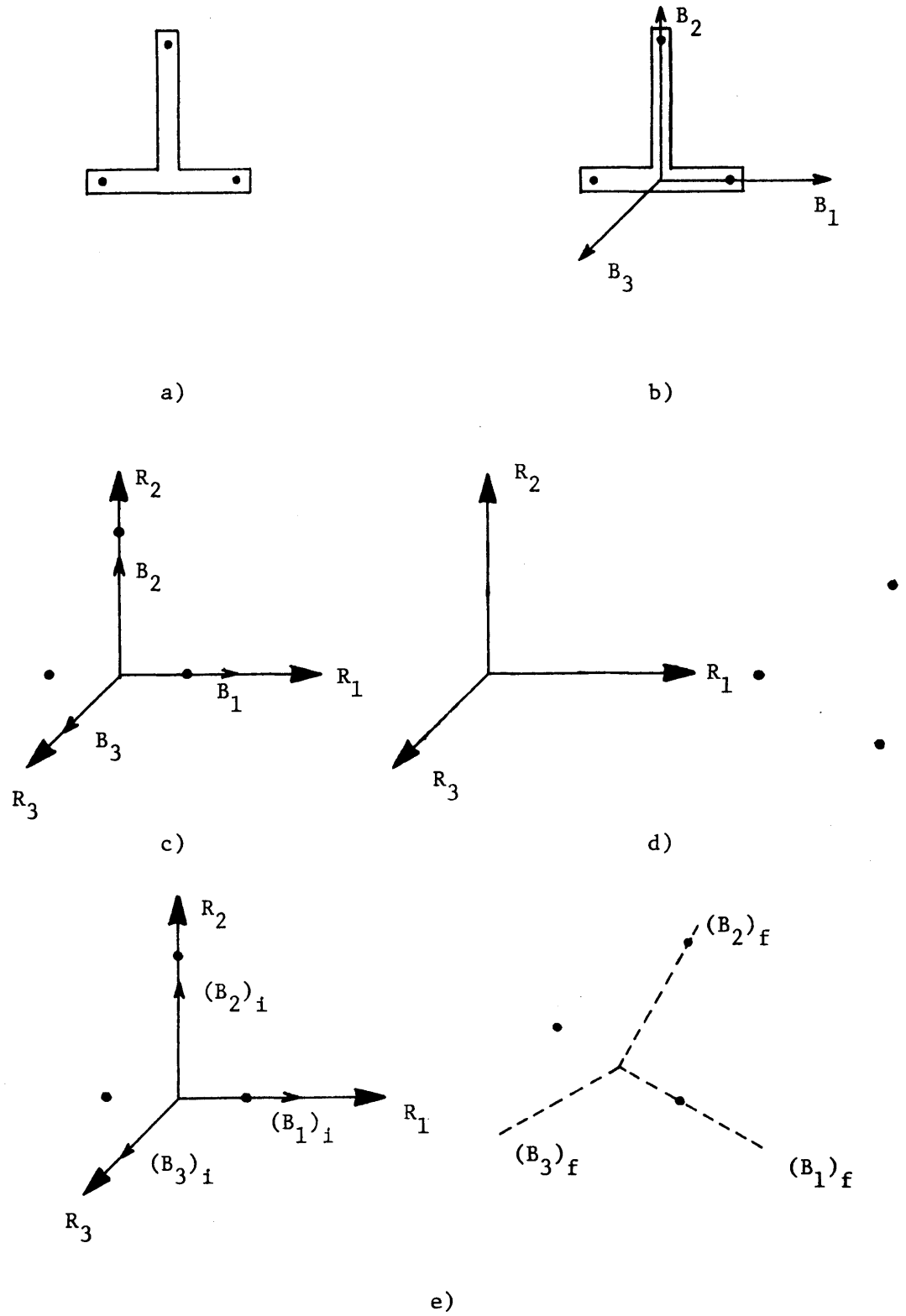

Figure 14. Correlation between the LED points and the body coordinate system.

is then designated in part (b), and is defined when the spatial coordinates of the LEDs are specified with respect to the coordinate system, part (c). In part (d), the actual kinematic information measured at a particular time step is displayed. Finally, in part (e), all the information available at a particular time step is brought together and the specific kinematic problem is thus formulated. The initial state is defined by "conceptually" placing the body coordinate system and the LED coordinates at the reference system R . The final state is "depicted" by locating the body coordinate system based on the measured LED points. The coordinate system is shown in dotted-line form because its configuration is the essential unknown for which a solution is sought.

4.4 CALCULATION OF THE CONFIGURATION PARAMETERS

As depicted in Figure 15, it is desired to find the configurational parameters at a particular time step which relate the initial condition, the hypothetical location of the LED points (body coordinate system), to the final condition, the actual LED point measurement. The problem will be examined in two parts: 1) the determination of the positional component and 2) the determination of the orientative component. Initially, a few issues need be introduced and the procedures delineated for resolving them.

Definition of a Mean Point for Calculation. In almost all cases as introduced earlier, the point at which a kinematic description is

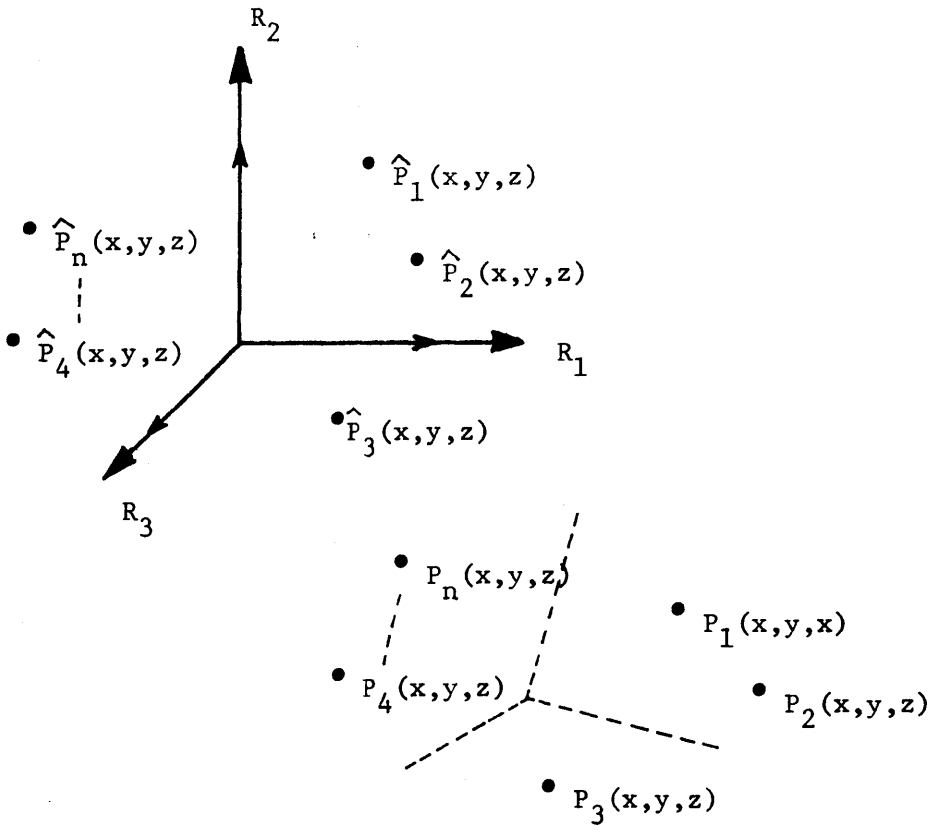

Figure 15. Depiction of the point-oriented kinematic problem (for a particular body and a single time step).

desired, the body coordinate system origin, will be a completely "fictitious" point and it can be seen that the parameters must be found indirectly. Therefore, the complete information about the body is dependent upon the measurement and manipulation of as few as three LED points.

The Selspot System, like any measurement system, is subject to measurement errors due to the inherent limitation of the device as well as to noise effects present in the system. In view of this fact, it would be reasonable to attempt to find a time-step to time-step reference point, or calculation point, which would be as accurate as possible based on the LED points. It can be stated (Lenox-1976) that the most accurate point (although fictitious) which can be determined on the rigid body based solely on the LED point coordinates is the three-dimensional mean point of the measured three-dimensional points. Therefore, a point which will be designated $\underline{Q}$ is defined as

$$\underline{Q} = Q_x r_1 + Q_y r_2 + Q_z r_3$$

where

$$Q_x = \sum_{I=1}^{n} \frac{X_I}{n}$$

$$Q_y = \sum_{I=1}^{n} \frac{Y_I}{n}$$

$$Q_z = \sum_{I=1}^{n} \frac{Z_I}{n}$$

and X_I, Y_I, Z_I, are the measured coordinate magnitudes of the ith point.

The point Q is the most accurate because the error in fixing the mean point will in general be 1/n (where n = number of points considered) times the average error in fixing any of the actual measured points. Since this point is the most reliably determined point based on the measurement data, the position and orientation shall be determined at this point.

From the point of view of the orientative calculation, this presents no problem since orientation parameters are the same at every point on the body. However, it will be seen that a slightly indirect procedure must be utilized to determine the positional parameters of the origin of the body coordinate system if it and the mean point Q are not synonomous.

In conclusion, because the mean of the measured points is the most reliable and reproducible point throughout a time span, calculations will always be carried out at this point initially and then the parameters derived for the actual point of interest, the origin of the body coordinate system.

Calculation of Position. The procedure for calculating the position of the origin of a body coordinate system is based upon the calculation of the position of the mean point Q and the application of the principle discussed earlier concerning the configurational description of points on a rigid body. It can be stated as follows (Panjabi-1971): given the six-component description (P_x, P_y, P_z, θ_1, θ_2, θ_3) at a point on a rigid body, then the configurational description at any other point

can be found given the Cartesian spatial relationship between the two points.

The initial position point coordinates carry with them the means to establish the Cartesian spatial relationship between $\underline{Q}$ and the body coordinate system origin, designated $\underline{O}$.

The following definition shall be made:

$$\hat{\underline{Q}} = \hat{Q}_x r_1 + \hat{Q}_y r_2 + \hat{Q}_z r_3$$

where

$$\hat{Q}_x = \sum_{I=1}^{n} \frac{\hat{X}_I}{n}$$

$$\hat{Q}_y = \sum_{I=1}^{n} \frac{\hat{Y}_I}{n}$$

$$\hat{Q}_z = \sum_{I=1}^{n} \frac{\hat{Z}_I}{n}$$

and $\hat{X}_I$, $\hat{Y}_I$, $\hat{Z}_I$ are the initial coordinate magnitudes of the ith point. It can be seen that the components of $\hat{\underline{Q}}$, then, define the spatial relationship between $\underline{Q}$ and $\underline{O}$.

The determination of the position of the body coordinate system origin, $\underline{O}$, given the six-component configuration of $\underline{Q}$, requires a back calculation where first the positional effects on $\underline{Q}$ of an orientative change at the origin are "subtracted away," and then the spatial relationship

between $\hat{\underline{Q}}$ and the origin, $\underline{O}$, subtracted. The resulting position is then the actual position of the defined body coordinate system origin.

The calculation can be written as follows:

$$\underline{O} = \underline{Q} - \hat{\underline{Q}} - \underline{R}\hat{\underline{Q}}$$

where $\underline{R}$ = 3×3 rotation matrix.

Calculation of Orientation. There are a limited number of techniques which can be applied to find the orientative parameters that are desired based on point coordinate measurement. It has been chosen to apply the Schut algorithm (Schut-1960/61, Lenox-1976), which is based on the Rodrigues formulation of rotation. The next section is devoted to a discussion of the Rodrigues' formulation of rotation and following that, the Schut computational algorithm for finding the necessary parameters is presented.

The main desire in this analysis is to find the orientative parameters, θ_1, θ_2, θ_3, and the rotation matrix. The Schut algorithm, based on the orientation equations of the Rodrigues formulation, can be used to determine the rotation matrix directly based on the initial state and final state three-dimensional point coordinates of points on the body. Then, secondarily, the θ_1, θ_2, and θ_3 parameters can be found from the rotation matrix.

The Rodrigues Formulation. The Rodrigues formula for rotation stems from Euler's Theorem (Beer-1972) which states: "The most general displacement of a rigid body with a fixed point $\underline{O}$ is equivalent to rotation

of the body about an axis through $\underline{Q}$." The term "fixed point $\underline{Q}$" implies that there is a pure orientation change taking place about $\underline{Q}$, since only under that condition would the point remain fixed. This equivalent formulation is pictorially compared with the three-axis rotation in Figure 16. It can be shown that the two descriptions are equivalent and consistent with the situation that has been structured in this analysis. Positional change and orientative change are being treated separately; therefore, Euler's theorem is applicable since there will be a fixed point in this part of the analysis, namely the mean point of calculation $\underline{Q}$. Recalling the premise that configuration is always calculated at the point $\underline{Q}$, it can be seen that the positional component of the point has been accounted for in the previous section, and that only the orientation at the point remains to be determined.

In Figure 16, $\underline{\lambda}$ is defined as the unit direction vector of the Euler axis and θ is defined as the amount of rotation about the axis (Lenox-1976). It can be written that

$$\underline{\lambda} = \lambda_1 r_1 + \lambda_2 r_2 + \lambda_3 r_3$$

The Rodrigues vector, $\underline{\rho}$, is to be defined as

$$\underline{\rho} = \tan\left(\frac{\theta}{2}\right) \underline{\lambda} , \quad 0 \leq \theta \leq 180°$$

If $\underline{\rho}$ is known, then

$$\underline{\lambda} = \frac{\underline{\rho}}{|\underline{\rho}|}$$

and

$$\theta = 2 \tan^{-1} |\underline{\rho}|$$

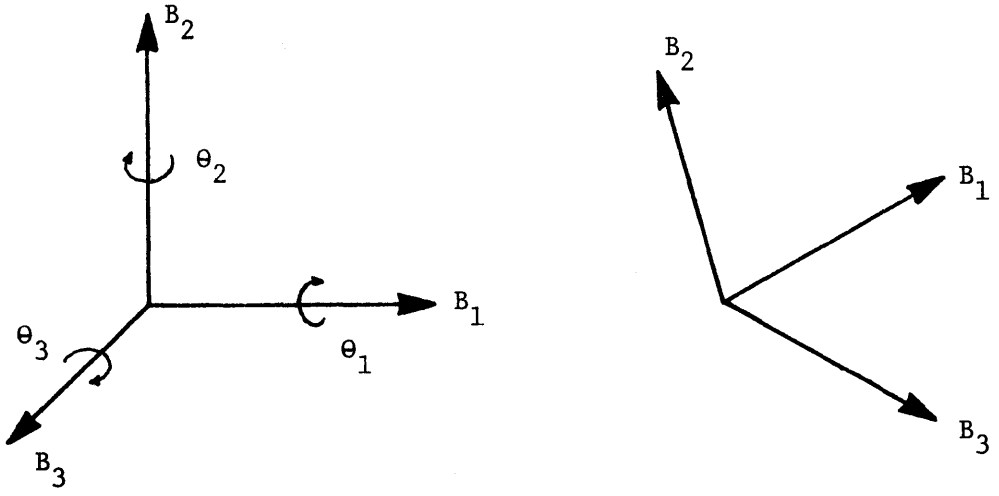

INITIAL FINAL

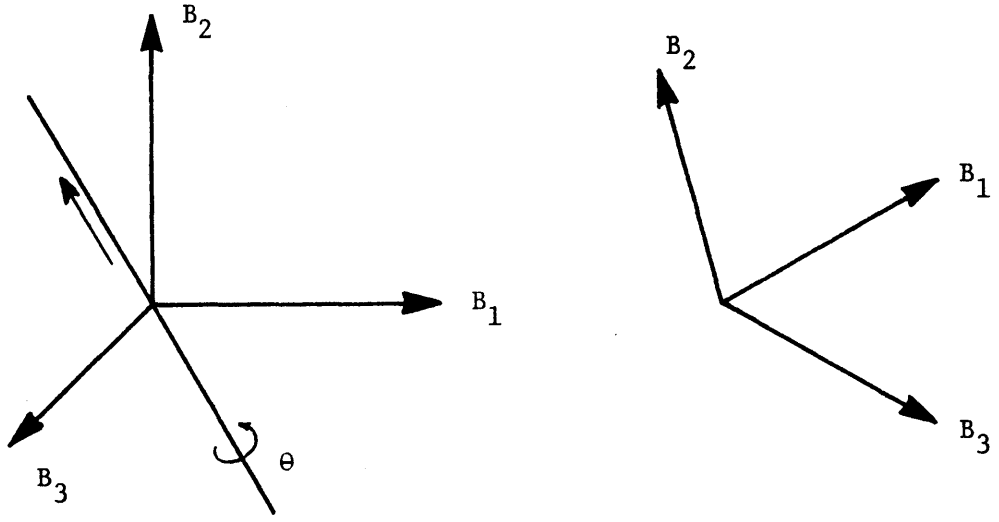

INITIAL FINAL

Figure 16. Equivalent orientative description--
3-axis and Rodrigues axis.

It can be seen that one Rodrigues vector, $\underline{\rho}$, completely characterizes an equivalent change of orientation of a rigid body. The vector is further defined as

$$\underline{\rho} = \rho_1 r_1 + \rho_2 r_2 + \rho_3 r_3$$

Since the rotation matrix and the right-handed rotations are being sought in this analysis, it can be shown, as derived in Appendix 1, that the rotation matrix can be expressed entirely in terms of the Rodrigues parameters, ρ_i (i = 1,3):

$$\underline{R} = \frac{\begin{bmatrix} 1 + \rho_1^2 - \rho_2^2 - \rho_3^2 & 2(\rho_1\rho_2 - \rho_3) & 2(\rho_3\rho_1 + \rho_2) \\ 2(\rho_1\rho_2 + \rho_3) & 1 + \rho_2^2 - \rho_3^2 - \rho_1^2 & 2(\rho_2\rho_3 - \rho_1) \\ 2(\rho_3\rho_1 - \rho_2) & 2(\rho_2\rho_3 + \rho_1) & 1 + \rho_3^2 - \rho_1^2 - \rho_2^2 \end{bmatrix}}{1 + \rho_1^2 + \rho_2^2 + \rho_3^2}$$

The three Cartesian rotations can then be easily expressed in terms of the Rodrigues parameters as follows:

$$\theta_2 = \sin^{-1}\left[\frac{2(\rho_3\rho_1 + \rho_2)}{1 + \rho_1^2 + \rho_2^2 + \rho_3^2}\right]$$

$$\theta_1 = \sin^{-1}\left[\frac{-2(\rho_2\rho_3 - \rho_1)}{1 + \rho_1^2 + \rho_2^2 + \rho_3^2 \quad \cos\theta_2}\right]$$

$$\theta_3 = \sin^{-1}\left[\frac{-2(\rho_1\rho_2 - \rho_3)}{1 + \rho_1^2 + \rho_2^2 + \rho_3^2 \cos\theta_2}\right]$$

It can be seen that if the Rodrigues vector can be calculated, based on point coordinates, then the means will exist to describe orientative change either in terms of an equivalent rotation axis or in terms of Cartesian rotations. The Schut algorithm serves the purpose of finding the Rodrigues vector.

The Schut Algorithm. In view of the previous discussion, it is desired to find the Rodrigues vector which describes orientative change based on an initial state and final state set of point coordinates on thebody. In order to satisfy Euler's law and designate the mean point $\underline{Q}$ as the fixed point of orientative description, the initial state coordinates are expressed with respect to $\hat{\underline{Q}}$, and the final state coordinates with respect to $\underline{Q}$. Therefore, the following definitions are made (Lenox-1976):

The initial state coordinates are defined as

$$\hat{\underline{P}}_I = \hat{X}_I r_1 + \hat{Y}_I r_2 + \hat{Z}_I r_3 \quad \text{where I = ith point.}$$

The initial state coordinates with respect to $\hat{\underline{Q}}$ can be expressed as

$$\hat{\underline{P}}_{I/\hat{Q}} = \left(\hat{X}_I - \hat{X}_Q\right) r_1 + \left(\hat{Y}_I - \hat{Y}_Q\right) r_2 + \left(\hat{Z}_I - \hat{Z}_Q\right) r_3$$

The final state coordinates are defined as

$$\underline{P}_I = X_I r_1 + Y_I r_2 + Z_I r_3$$

The final state coordinates with respect to $\underline{Q}$ are

$$\underline{P}_{I/Q} = (X_I - X_Q)r_1 + (Y_I - Y_Q)r_2 + (Z_I - Z_Q)r_3$$

Finally, the following variable redefinitions are made:

$$\hat{X}_I = \hat{X}_I - \hat{X}_Q \; ; \quad \hat{Y}_I = \hat{Y}_I - \hat{Y}_Q \; ; \quad \hat{Z}_I = \hat{Z}_I - \hat{Z}_Q$$

$$X_I = X_I - X_Q \; ; \quad Y_I = Y_I - Y_Q \; ; \quad Z_I = Z_I - Z_Q$$

In equation form, then, the resulting problem which Schut (1960) addressed and derived a solution for was the following:

$$\underline{\hat{P}}_{I/\hat{Q}} = \underline{T}\underline{P}_{I/Q}$$

where $\underline{\hat{P}}_{I/\hat{Q}} = \begin{bmatrix} \hat{X}_I \\ \hat{Y}_I \\ \hat{Z}_I \end{bmatrix}$ and $\underline{P}_{I/Q} = \begin{bmatrix} X_I \\ Y_I \\ Z_I \end{bmatrix}$

and $\underline{T}$ is the unknown transformation matrix.

It can be seen that the problem which Schut examined defines a transformation from the final state to the initial state, which is the reverse of the transformation sought in this analysis. However, Lenox (1976) showed that this difference can be taken into account by a simple

sign reversal of the Rodrigues parameter results of the Schut algorithm, and that change is incorporated in this presentation.

Schut, by taking particular notice of the form of the rotation matrix which is desired, was able to apply a modified form of the Cayley Transformation (Mirzebruck-1971) to the problem.

Defining a skew-symmetric matrix, $\underline{S}$, where

$$\underline{S} = \begin{bmatrix} 0 & -c & b \\ c & 0 & -a \\ -b & a & 0 \end{bmatrix}$$

and choosing a fourth parameter, d , the Cayley Transformation of the matrix $\underline{S}$ can be written

$$\underline{T} = (d\underline{I} - \underline{S})^{-1} (d\underline{I} + \underline{S})$$

where $\underline{I}$ is the identity matrix. If this operation is carried out as indicated, T is found to be

$$\underline{T} = \frac{\begin{bmatrix} d^2 + a^2 - b^2 - c^2 & 2ab - 2cd & 2ac + 2bd \\ 2ab + 2cd & d^2 - a^2 + b^2 - c^2 & 2bc - 2ad \\ 2ac - 2bd & 2bc + 2ad & d^2 - a^2 - b^2 + c^2 \end{bmatrix}}{d^2 + a^2 + b^2 + c^2}$$

It can be seen that if the assignment $a = \rho_1$, $b = \rho_2$, $c = \rho_3$, and $d = 1$ is made, then the matrix $\underline{T}$ is exactly equal to the rotation matrix, $\underline{R}$. By making the variable assignment and continuing with

the solution as Schut did, it can be seen that

$$\underline{\hat{P}}_{I/\hat{Q}} = (d\underline{I} - \underline{S})^{-1} (d\underline{I} + \underline{S})\underline{P}_{I/Q}$$

$$(dI - \underline{S})\underline{\hat{P}}_{I/\hat{Q}} = (d\underline{I} + \underline{S})\underline{P}_{I/Q}$$

Carrying out the indicated operations and collecting terms, the following equations are obtained:

$$\begin{aligned}
-(\hat{Z}_I + Z_I)\rho_2 + (\hat{Y}_I + Y_I)\rho_3 + (\hat{X}_I - X_I) &= 0 \\
(\hat{Z}_I + Z_I)\rho_1 - (\hat{X}_I + X_I)\rho_3 + (\hat{Y}_I - Y_I) &= 0 \\
-(\hat{Y}_I + Y_I)\rho_1 + (\hat{X}_I + X_I)\rho_2 + (\hat{Z}_I - Z_I) &= 0
\end{aligned}$$

$$(I = 1,2, \ldots, n)$$

Schut then derived a fourth equation to complete the set. It can be shown (Bisshopp-1969) that the projection on the Euler axis of the magnitude of an initial point coordinate vector equals the projection of the final point coordinate vector. Therefore,

$$|\underline{P}_{I/\hat{Q}}| = |\underline{P}_{I/\hat{Q}}|$$

$$|\underline{\hat{P}}_{I/\hat{Q}}| \cdot \underline{\rho} = |\underline{P}_{I/Q}| \cdot \underline{\rho}$$

$$\hat{X}_I\rho_1 + \hat{Y}_I\rho_2 + \hat{Z}_I\rho_3 = X_I\rho_1 + Y_I\rho_2 + Z_I\rho_3$$

$$(\hat{X}_I - X_I)\rho_1 + (\hat{Y}_I - Y_I)\rho_2 + (\hat{Z}_I - Z_I)\rho_3 = 0$$

The following four equations are obtained, and this is the basic equation set for which Schut sought a solution:

$$(\hat{X}_I - X_I)\rho_1 + (\hat{Y}_I - Y_I)\rho_2 + (\hat{Z}_I - Z_I)\rho_3 = 0$$

$$- (\hat{Z}_I + Z_I)\rho_2 + (\hat{Y}_I + Y_I)\rho_3 + (\hat{X}_I - X_I) = 0$$

$$(\hat{Z}_I + Z_I)\rho_1 - (\hat{X}_I + X_I)\rho_3 + (\hat{Y}_I - Y_I) = 0$$

$$-(\hat{Y}_I + Y_I)\rho_1 + (\hat{X}_I + X_I)\rho_2 + (\hat{Z}_I - Z_I) = 0$$

$$(I = 1,2, \ldots, n)$$

It can be seen that there is a set of four linear equations for each point on the body which has a set of initial and final coordinates. The very nature of the equation solution which Schut employed allows an over-redundant system to be effectively utilized in a statistical manner. An over-redundant system can be considered to be one which contains more than six independent Cartesian coordinate parameters in the initial and final state, or in this analysis any system with more than three observed points. In view of the measurement error present in any experimental situation, this feature is inviting for then the possibility exists to increase the

reliability of the calculations through the use of more than three LED points on a rigid body of interest.

The solution (Lenox-1976) of the sets of equations, where n is the number of points observed on the body, is handled by first normalizing the $\hat{\underline{P}}_{I/\hat{Q}}$ and $\underline{P}_{I/Q}$ position vectors so that each point will have an equally weighted effect. Then, a least square fit of the $n \times 4$ sets of linear equations is carried out, resulting in a single set of four linear equations which are then solved.

In previous discussions, a relevant calculation was shown to require the observation of three points. Because this may not seem consistent in view of the present set of equations available for each point, a simple thought experiment is in order. If only one point on the body was observed, then the mean $\underline{Q}$ and the observed point would be the same point, and $\hat{\underline{P}}_{I/Q} = 0$ and $\underline{P}_{I/Q} = 0$. There is no solution in this case. If only two points are observed, then it can be seen that the mean $\underline{Q}$ will be collinear with the two data points in both states, and a rotation around the line defined by the collinear points would not be detected. Therefore, again it is clear than three points are needed to calculate a mean $\underline{Q}$ which used with the point coordinates will lead to a unique solution.

The actual solution procedure is given next. Initially, the normalization of the point coordinates is carried out, each Cartesian component of each point being divided by the total magnitude. In this discussion, the original notation is retained through the rest of the presentation although it can be assumed that the points have been normalized.

Schut, in carrying out the solution, defines and n×4 matrix, $\underline{A}$, where

$$\underline{A} = \begin{bmatrix}
(\hat{X}_1 - X_1) & (\hat{Y}_1 - Y_1) & (\hat{Z}_1 - Z_1) & 0 \\
0 & -(\hat{Z}_1 + Z_1) & (\hat{Y}_1 + Y_1) & (\hat{X}_1 - X_1) \\
(\hat{Z}_1 + Z_1) & 0 & -(\hat{X}_1 + X_1) & (\hat{Y}_1 - Y_1) \\
-(\hat{Y}_1 + Y_1) & (\hat{X}_1 + X_1) & 0 & (\hat{Z}_1 - Z_1) \\
\hline
(\hat{X}_2 - X_2) & (\hat{Y}_2 - Y_2) & (\hat{Z}_2 - Z_2) & 0 \\
0 & -(\hat{Z}_2 + Z_2) & (\hat{Y}_2 + Y_2) & (\hat{X}_2 - X_2) \\
(\hat{Z}_2 + Z_2) & 0 & -(\hat{X}_2 + X_2) & (\hat{Y}_2 - Y_2) \\
-(\hat{Y}_2 + Y_2) & (\hat{X}_2 + X_2) & 0 & (\hat{Z}_2 - Z_2) \\
\hline
\vdots & \vdots & \vdots & \vdots \\
\hline
(\hat{X}_n - X_n) & (\hat{Y}_n - Y_n) & (\hat{Z}_n - Z_n) & 0 \\
0 & -(\hat{Z}_n + Z\ ) & (\hat{Y}_n + Y_n) & (\hat{X}_n - X_n) \\
(\hat{Z}_n + Z_n) & 0 & -(\hat{X}_n + X_n) & (\hat{Y}_n - Y_n) \\
-(\hat{Y}_n + Y_n) & (\hat{X}_n + X_n) & 0 & (\hat{Z}_n - Z_n)
\end{bmatrix}$$

Therefore,

$$\underline{A} \begin{bmatrix} \rho_1 \\ \rho_2 \\ \rho_3 \\ 1 \end{bmatrix} = 0$$

The least square adjustment fit is accomplished by pre-multiplying $\underline{A}$ by $\underline{A}^T$, obtaining

$$\underline{S} \begin{bmatrix} \rho_1 \\ \rho_2 \\ \rho_3 \\ 1 \end{bmatrix} = 0$$

where

$$\underline{S} = \underline{A}^T \underline{A} = [s_{ij}] \qquad (i,j = 1,2,3,4)$$

where

$$s_{11} = \left[(\hat{X}_I - X_I)^2 + (\hat{Y}_I + Y_I)^2 + (\hat{Z}_I + Z_I)^2\right]$$

$$s_{22} = \left[(\hat{X}_I + X_I)^2 + (\hat{Y}_I - Y_I)^2 + (\hat{Z}_I + Z_I)^2\right]$$

$$s_{33} = \left[(\hat{X}_I + X_I)^2 + (\hat{Y}_I + Y_I)^2 + (\hat{Z}_I - Z_I)^2\right]$$

$$s_{44} = \left[(\hat{X}_I - X_I)^2 + (\hat{Y}_I - Y_I)^2 + (\hat{Z}_I - Z_I)^2\right]$$

$$s_{12} = -2\left[Y_I\hat{X}_I + \hat{Y}_I X_I\right] = s_{21}$$

$$s_{13} = -2\left[X_I\hat{Z}_I + \hat{X}_I Z_I\right] = s_{31}$$

$$s_{23} = -2\left[Z_I\hat{Y}_I + \hat{Z}_I Y_I\right] = s_{32}$$

$$s_{14} = 2\left[Z_I\hat{Y}_I - \hat{Z}_I Y_I\right] = s_{41}$$

$$s_{24} = 2\left[X_I\hat{Z}_I - \hat{X}_I Z_I\right] = s_{42}$$

$$s_{34} = 2\left[Y_I\hat{X}_I - \hat{Y}_I X_I\right] = s_{43}$$

where the brackets imply summation over (I = 1,2, ..., n).

The algorithm Schut developed for finding ρ_1, ρ_2, and ρ_3 is as follows (Lenox-1976):

$$s'_{22} = s_{22} - \frac{s_{12}s_{12}}{s_{11}}$$

$$s'_{23} = s_{23} - \frac{s_{13}s_{12}}{s_{11}}$$

$$s'_{24} = s_{24} - \frac{s_{14}s_{12}}{s_{11}}$$

$$s'_{33} = s_{33} - \frac{s_{13}\,s_{13}}{s_{11}} - \frac{s'_{23}\,s'_{23}}{s'_{22}}$$

$$s'_{34} = s_{34} - \frac{s_{14}s_{13}}{s_{11}} - \frac{s'_{24}\,s'_{23}}{s'_{22}}$$

$$s'_{44} = s_{44} - \frac{s_{14}s_{14}}{s_{11}} - \frac{s'_{24}\, s'_{24}}{s'_{22}}$$

$$\rho_3 = \frac{s'_{34}}{s'_{33}}$$

$$\rho_2 = \frac{(s'_{24} - s'_{23}\rho_3)}{s'_{22}}$$

$$\rho_1 = \frac{(s_{14} - s_{13}\rho_3 - s_{12}\rho_2)}{s_{11}}$$

Lenox indicates that the employment of 4n equations, and not 3n, has two advantages: 1) it is not necessary to select independent equations from the available ones, and 2) the coefficients of the resulting normal equations ($\underline{S}$ matrix) become very simple functions of the initial and final state scalar coordinates when sets of four equations are employed in the indicated repetition sequence.

Having determined a procedure for finding the Rodrigues vector from initial state and final state point coordinates, the rotation matrix and the Cartesian rotation parameters for a particular time step can be found by appropriate substitution of the Rodrigues parameters into the equations presented earlier. Since orientation is the same at every point on a rigid body, no further calculations are required.

Discussion of the Method. In the previous sections, a technique and computational algorithm for finding position and orientation at a designated point on a rigid body based on initial and final state point

coordinates has been presented. A few closing remarks concerning the technique are in order.

A paramount consideration in selecting an analytical technique is its sensitivity to measurement error in the data. Most techniques perform quite admirably when given exact theoretical input data, but become severely error-prone when subjected to inaccurate data. This is particularly true when calculating the orientative parameters, which are understandably vulnerable to point-placement error.

Roth (1966) has investigated a vector-based solution technique which also finds the Rodrigues parameters. He found this technique to be very sensitive to the data accuracy and noted that small variations in the coordinates had a profound effect on the parameters. Lenox (1976) attempted to apply statistical techniques to the Rodrigues vector employed by Roth. Although some improvement was perceived, the calculations became very complicated and unwieldy. Lenox then applied the Schut algorithm and found that its performance far surpassed the vector technique when tested with error-prone data. Importantly, the better performance was achieved by applying a substantially simpler and more computationally-efficient algorithm.

The Schut algorithm seems to derive its reliability from the simple and efficient operation of reducing an overdetermined system to a "best" calculation. The vector equation formulation is not geared for calculation with an overdetermined system, and therefore is directly dependent upon the accuracy of only a few coordinates. The Schut algorithm smooths the data through a least-squares fit before the calculation, thus enhancing

the possibility that the resulting solution will be a reliable one for the given data structure. It should be noted that difference performance characteristics could be obtained with other types of "smoothing" operations and point weighting functions. Further work is needed to determine if the performance can be improved.

In view of the fact that the Schut algorithm is a statistically-based trigonometrically-exact technique, and can effectively handle an overdetermined system, it appeared to be most appropriate for the application presented in this thesis. The precision of the Selspot System is such that a high-performance yet reliable technique is a necessity, and it was felt that the Schut algorithm met this criterion.

Implementation of Multiple-Body Computations. As discussed earlier, because of the kinematic structure which has been chosen, it is possible to treat each rigid body as an independent calculation problem. The main obstacle to be overcome is simply a logistical one. It is clear that an assignment procedure is needed through which LED channels can be assigned to particular rigid bodies, and a bookkeeping procedure required to insure that a particular rigid body calculation is based only on its assigned and affixed LEDs.

Such a structure has been implemented and allows complete freedom of channel assignment ($\geq$ 3 LEDs per body) to any number of bodies ($\leq$ 10 bodies). For each time step, a looping set of computations is carried out, each loop carrying out a complete calculation for a designated rigid body. Further details are presented in Chapter 7, where the system software package is discussed.

Chapter 5

CALIBRATION OF THE SELSPOT SYSTEM FOR ABSOLUTE MEASUREMENT

In Chapter 2 it was introduced that a small scaling difference could exist between the X and Y output of the Selspot System cameras because of small variations in the hardware components. The elimination of this problem by software correction is discussed in this chapter. In initial evaluation experiments using the Selspot System, it was observed that there existed a noticeable problem with measurement nonlinearities due to lens aberrations. A discussion of the problem and a preliminary correction technique is presented. In earlier discussions concerning the calculation of three-dimensional LED point coordinates based on the Selspot System camera data, several independent calibration parameters were needed and assumed available. The determination of these parameters, the camera focal distances, and the camera position quantities are discussed in this chapter.

Many of the parameters which will be discussed presently were obtained through calibration tests with a specially-configured experimental set-up. A 30 LED grid mounting panel was constructed, designed such that it had 3 inch (76.2 mm) spacing [$\pm$ < .02 inch ($\pm$ 5 mm)] of LEDs and could be mounted directly on a 1.5 m by 1.5 m wall-mounted pegboard sheet at arbitrary locations. The pegboard was precisely positioned at a 90° angle with respect to the leveling reference to which the cameras were positioned. The error in positioning the LED grid as desired on the

pegboard was found to be consistently equal to or less than the resolution of the Selspot System at the testing distance. In all experiments, an effective origin was defined on the pegboard sheet and the camera's lens-detector plate neutral axis was bore-sighted to this location while being maintained in a parallel plane to the pegboard.

5.1 DETERMINATION OF THE CAMERA SCALE FACTORS

The discrepancy between X and Y digitation in terms of scaling is an error which must be corrected before any further camera calibration is attempted. The reasoning for this statement is based upon the assumption that the camera focal distance and lens nonlinearity is independent of the X and Y nature of the detector plate in a physical sense, but dependent in a computational sense. That is, in determining the nature of these parameters, X and Y camera-sampled data points will be employed. If the scaling difference has not been corrected before these experiments, then the calculated parameters could have an "averaged" quality which would not represent the physical situation.

A reasonable approach to the scaling discrepancy problem is to compare the X and Y digitation of equal distances in the two directions. From these measurements, a correction factor based on the ratio of one axis' values to the other can be found and then applied to all the data of that axis in subsequent measurements. It should be pointed out that it makes no difference which axis is corrected to which, since the subsequent determination of the focal distance parameter will truly calibrate

the system to the physical world. If one chose to correct the opposite axis of that selected here, the end result would be a small change in the focal distance numerical values.

In order to achieve statistical significance, a logical approach is to carry out the distance comparison using the LED grid panel and to calculate many combinations of distances. Care must be taken, however, to guarantee that the comparisons are independent of a potential lens nonlinearity. It is assumed, as justified later, that the nonlinearity effect is constant throughout a circular rotation at any arbitrary radius measured from the center of the lens. Thus, a comparison of an equal X and Y distance whose midpoint is the center point of the lens should be equally effected by any lens nonlinearity (same radial distance) and thereby cancelled when the ratio is calculated. With a single experimental test, then, many combinations of distances can be examined, and the statistical average found.

The experimental test was arranged such that the grid board would be moved to four different locations (see Figure 18a), and a 5 LED by 5 LED grid of data points sampled at each location. The result of a data gathering sequence was a stored data file of digitized X and Y values for a 10 by 10 equidistant LED point matrix centered at the lens neutral axis (Figure 17). All the possible combinational calculations which met the above criterion were carried out and then an averaged scale factor Y/X was found. The experiment was performed two times for both cameras at two different testing distances. Based on this data, the following Y/X scale factors were defined: for camera 1, .99, and for camera 2, 1.00 .

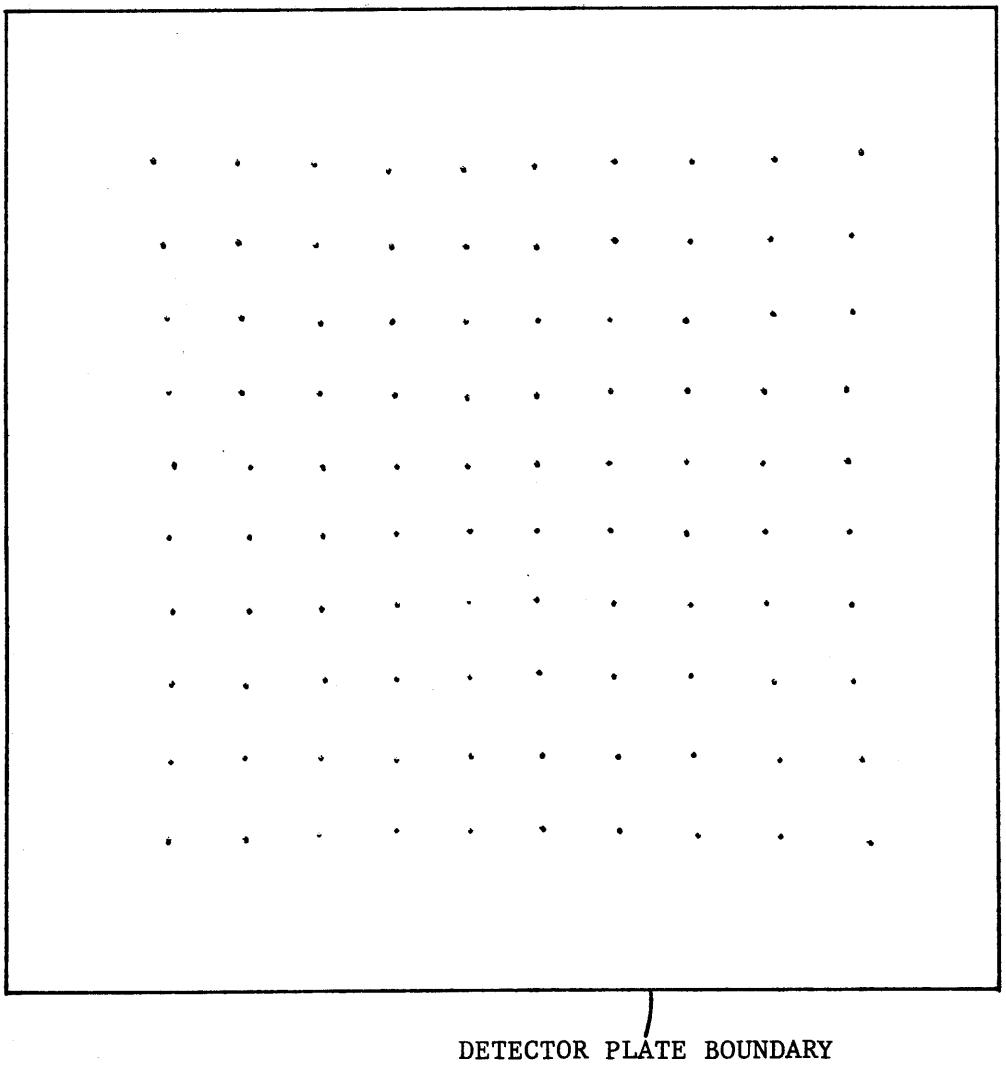

Figure 17. A typical LED grid plot.

These scale factors were used in all subsequent calculations and experiments.

It is valid to ask how often, if ever, such an experiment should be repeated. This is unclear since the scale factors should remain constant if the electronic hardware maintains a stable performance condition. However, a periodic recalculation would seem prudent if for no other reason than to prove that the factors have not changed.

5.2 CORRECTION OF LENS NONLINEARITY

Based on a series of LED grid experiments, it was evident that measurement nonlinearities existed in the system. In Figure 17, a typical grid plot is illustrated. It appears that there are at least two types of nonlinearities present: 1) a consistent location aberration which can be attributed to the lens; and 2) local aberrations due to detector plate sensing idiosyncrasies.

The Selspot System manufacturer has supplied linearity plots of tests conducted for both cameras without lenses, and when examined closely they appear to have similar kinds of local aberration, but not the overall nonlinearity pattern. This evidence quite conclusively points to a severe nonlinearity effect introduced by the camera lens.

It was believed that the lens nonlinearity, since it is based upon physical laws, should exhibit a pattern which could be corrected in a relatively straightforward manner. Since the local aberrations are not based upon a consistent physical law, their correction would undoubtedly be very empirical in nature. In view of this observation and the fact

that the actual effect of the local aberrations on experimental results is not clearly known at this time, corrective mechanisms were examined for the lens nonlinearity problem only. As discussed in the next chapter, several data conditioning and error detection algorithms are applied to all the experimental data as it is being processed, and thus the effect of the local aberrations is minimized if not possibly eliminated.

In attempting to conceptualize the lens aberration nonlinearity in a simple manner, the following hypothesis was formulated. The assumption was made that the aberration is dependent solely on the distance between the beam and the neutral axis of the lens, and that the aberration is the same at any angular location at a given radius. It is assumed that the greater the distance of the LED beam from the neutral axis, the greater is the aberration error. A reexamination of the grid plot in Figure 17 appears to support this nonlinearity conceptual model, and it was employed as the basis for determining a correction algorithm. It was desirable that a correction algorithm be completely independent of any other parameters, in particular focal distance. Therefore, since the focal distance parameter is in essence the "actual transformation factor" between the physical situation and an image view in terms of Selspot units, the implication is that only the nonlinearity pattern itself can be studied. An analysis based on physically relevant quantified data cannot be carried out directly.

In order to quantify the nature of the nonlinearity pattern and at the same time maintain independency of the focal distance parameter, the

following procedure was developed. First, an arbitrary base unit distance in the physical world was defined. Next, a direct conversion factor taking the form of Selspot units/base unit distance was determined at locations near the neutral axis of the lens ("linear" range). Finally, actual measurements were made at various locations away from the neutral axis and compared to a predicted value based on the "linear range" conversion factor. As a result, a set of error values was established.

Several experiments were carried out so as to determine the nature of the linearity pattern. The experimental distance was approximately 6 ft (2 m), and selected on the basis of that which afforded the best overall LED grid coverage of the detector plate sensor. The regular LED grid distance (3 inches - 76.2 mm) was established as the base unit distance. Referring to Figure 18(a), to insure statistical relevance, an average Selspot units/base distance factor was determined based on the 16 distance measurements depicted. Since all 16 LED's are clustered quite close to the neutral axis of the lens, this conversion factor should be a suitable representation of an error-free image projection.

Selspot unit distance measurements were made at five different radial distances, four samples at each distance, as shown in Figure 18(b). An equivalent "expected" Selspot unit distance for a linear situation can be easily determined for the same physical distances. By multiplying the physical distance (in terms of base distance units) between the bore sight location (lens neutral axis) and the measurement point by the linear Selspot unit conversion factor, an "expected" Selspot unit value can

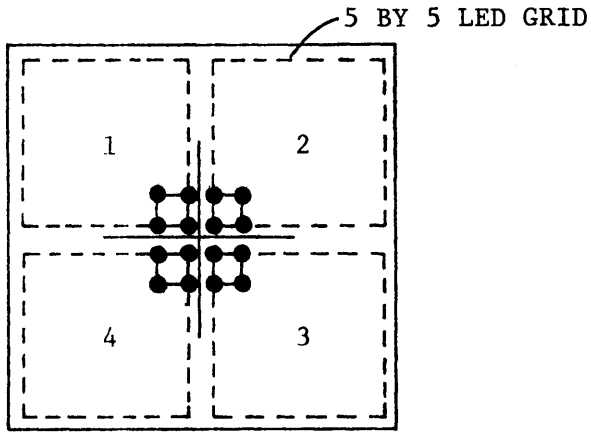

a) Linear base distances

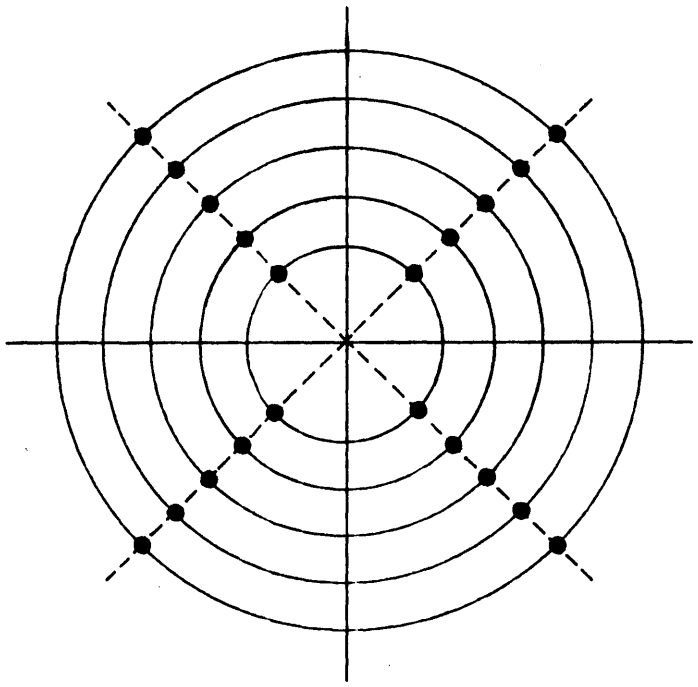

b) LED test points of lens nonlinearity

Figure 18. Measurement aspects of the lens nonlinearity analysis.

be found. The four measurements at each radial distance were averaged, and the error determined by taking the difference of the averaged value and the calculated expected value. In Table 1, several experimental results are compiled which depict the Selspot unit error at the particular Selspot unit distance from the defined origin, the center of the plate.

It would be expected that the lens nonlinearity would manifest itself as a functional which would increase the apparent distance of a measurement from the lens neutral axis (and center of the detector plate) along a radial line. It is desired to find a simple equation formulation which would estimate the error as a function of Selspot unit distance from the plate center. In line with the assumption of the nature of the error, an algorithm is then needed to adjust the location of the point inward along the radial line by the error distance.

A simple function of the nature shown below was formulated:

$$E = fS^2$$

where E = error (in Selspot units)

f = empirical factor

S = distance in Selspot units between the point location and the lens-detector plate origin.

This form was found to be a suitable function for this preliminary investigation. Based on a sequence of experimental tests and the procedure discussed above, the empirical factor which gave a reasonable approximation for the amount of nonlinearity error was found to be .000225 for

Table 1

LENS NONLINEARITY CORRECTION RESULTS

EXPERIMENT	LOCATION	MEASURED DISTANCE (SELSPOT)	ACTUAL DISTANCE (LINEAR)	ERROR	ESTIMATED DISTANCE (CORRECTION)	ESTIMATE ERROR
Camera 1 Test 1	1	49.68	49.66	+ .02	49.12	- .56
	2	156.18	148.99	+ 7.19	150.69	+ 1.70
	3	263.46	248.32	+15.14	247.84	- .48
	4	384.05	347.65	+36.40	350.86	+ 3.21
	5	508.11	446.98	+61.13	450.02	+ 3.04
Camera 1 Test 2	1	49.75	49.73	+ .02	49.19	- .54
	2	156.25	149.19	+ 7.06	150.75	+ 1.56
	3	263.45	248.65	+14.80	247.83	- .82
	4	384.18	348.11	+36.07	350.97	+ 2.86
	5	508.05	447.57	+60.48	449.97	+ 2.40
Camera 2 Test 1	1	50.04	50.02	+ .02	49.55	- .47
	2	155.33	150.06	+ 5.27	150.60	+ .54
	3	263.14	250.10	+13.04	249.56	- .56
	4	382.09	350.14	+31.95	353.47	+ 3.33
	5	501.71	450.19	+51.52	452.37	+ 2.18
Camera 2 Test 2	1	50.01	49.99	+ .03	49.53	- .47
	2	155.31	149.98	+ 5.34	150.59	+ .61
	3	263.10	249.98	+13.14	249.53	- .42
	4	382.10	349.95	+32.15	353.48	+ 3.53
	5	501.73	449.94	+51.79	452.39	+ 2.45

camera 1 and .000196 for camera 2. As shown in Table 1, the estimated error using the above equation and applying the measured distances has been used to correct the data point distances. The results can be compared to the distances which would be expected if the lens was linear. It can be seen that errors which were as high as 60 Selspot units have been reduced to that of a few units.

As an illustration of the effect of the overall correction algorithm, a typical raw and then corrected LED grid plot is given in Figure 19. It can be observed that the correction algorithm substantially improves the nature of the perceived image so as to better reflect reality. However, the problem deserves further investigation and different algorithms should be formulated and tested for better performance.

5.3 DETERMINATION OF THE CAMERA FOCAL DISTANCES

It was shown in Chapter 3 that in order to form the Z component of the LED direction vector, a number which reflected the distance from the detector plate to the focal point was needed. In a physical sense, if the two cameras were alike, then this distance would have to be equal for both cameras, and camera measurements should reflect this similarity. However, tacitly assumed in such a belief is that the "gain" of the system is the same for each camera.

Experiments have shown that this is not the case. Given equal settings and locations of the cameras, the numerical values from the Selspot System exhibit a noticeable difference in gain. The meaning of this phenomenon is that the assumed 102.4 Selspot units/millimeter of detector

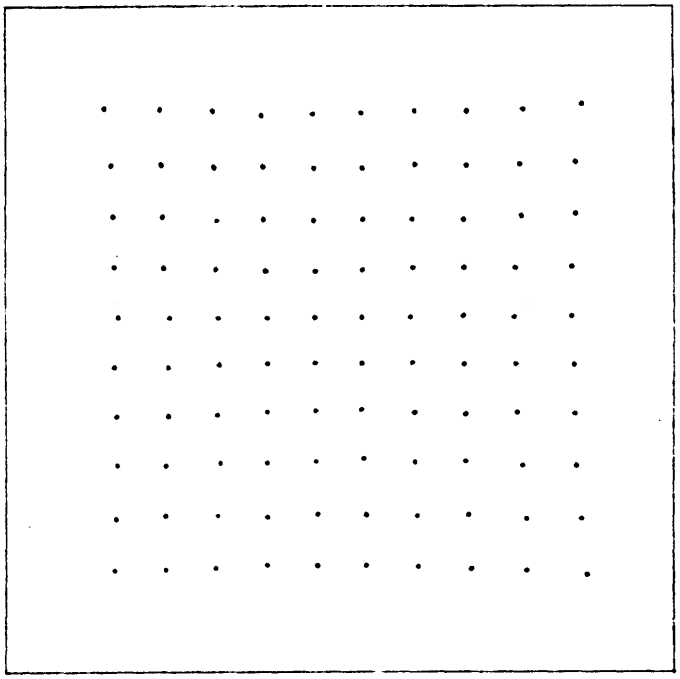

a) Raw data LED grid plot

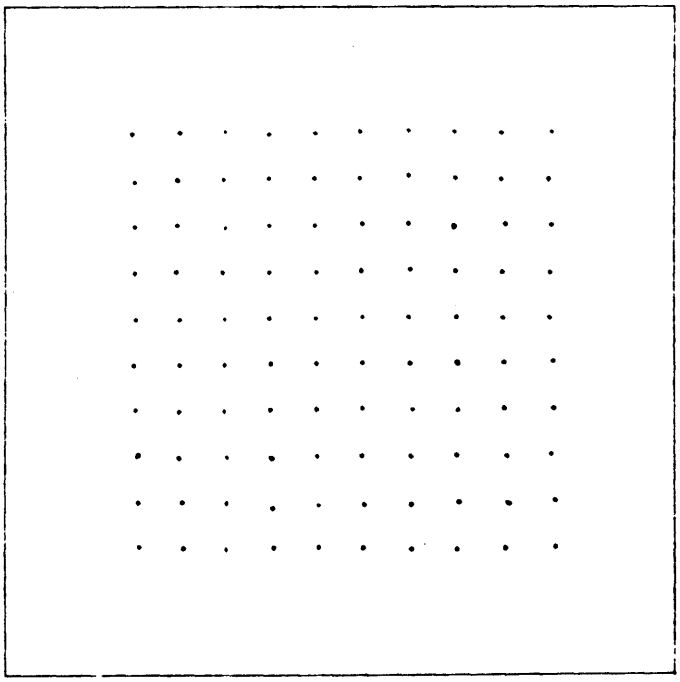

b) Corrected LED grid plot

Figure 19. Result of the nonlinearity correction algorithm.

plate (10 mm by 10 mm plate) is not true for both cameras, if either camera. Since it would be quite difficult to effectively determine the actual number of Selspot units/millimeter of detector plate, and then correct the difference in software, a different approach to the entire focal distance determination problem was enlisted.

It was assumed that the camera and the processing circuitry is a "black box," and a simple image law experiment was performed to determine a focal distance number which in essence equalizes both cameras by finding a true physically-relevant focal distance parameter for each. It is apparent that because the two numbers will encompass the overall gain factors of each camera's processing circuitry, different focal distance numbers are to be expected for equal settings of the cameras. The calculation in effect scales the Z component of the direction vector so that contrary to gain anomalies in the system, a suitable direction vector is obtained which has physical significance.

The image-ratio law was applied, and it can be stated for this application as follows:

$$\frac{f}{d} = \frac{R}{D}$$

where f = focal distance (mm)

d = image distnace (mm)

D = object distance

R = object range

} any consistent unit

Since the image distance is measured in Selspot units, this measurement must be converted to millimeters by applying the factor (102.4 units per millimeter). Therefore,

$$d = \frac{d_m}{102.4}$$

where d_m is the distance measured in Selspot units.

It is prudent, as before, that a procedure be formulated which will give a statistically relevant result. Therefore, a calculation algorithm of the same approach as that for the X-Y scale factors was applied. Because the X-Y scale factor and the nonlinearity correction can be assumed to be incorporated into this analysis, several more usable combinations of distance measurements could be utilized as there are no longer any restrictions.

Since there will be different focal distance factors at every focus setting of the lens, all calculations in this thesis were carried out with the infrared focus setting at 15 ft (4.56 m), the desired setting in view of subsequent system evaluation experiments which were carried out. It should be evident that whenever the focus setting of the cameras is changed, the focal distance calibration experiments must be repeated.

Four experiments were carried out for each camera and the results are summarized in Table 2. For the experiments, two object distances were tested: 1) approximately 6 ft (2 m) since this provided a large coverage of the plate sensor, and 2) 15 ft (4.56 m), since this was the experimental and focus setting distance. Employing the gathered data, which formed a 10 by 10 LED equidistant matrix stored in a data file, 100 different combinations of image law tests were averaged to find a single focal distance parameter. Based on the experiments for the particular focus setting the focal distance parameter was selected to be 15.5 mm for camera 1

Table 2

FOCAL DISTANCE DETERMINATION RESULTS

TEST	DISTANCE (Ft)	CAMERA 1 (mm)	CAMERA 2 (mm)
1	6.	15.525	18.042
2	6.	15.521	18.042
3	15.	15.494	17.960
4	15.	15.480	18.020
		Ave. = 15.505	Ave. = 18.016

and 18.0 mm for camera 2.

5.4 DETERMINATION OF CAMERA POSITION PARAMETERS

In order to calculate three-dimensional points based on the Selspot System camera data, the position and orientation of the camera coordinate systems with respect to the reference coordinate system must be specified. In the general case, three position parameters (P_x, P_y, P_z) and three rotation parameters (θ_x, θ_y, θ_z) must be determined for each camera. As justified in Chapter 3, several set-up assumptions were made in order to reduce the number of calibration parameters required and to streamline the computations (see Figure 11). The following coordinate system protocol is employed in this thesis.

First, it is assumed that $P_{1_x} = P_{1_z} = 0$, which in effect means that the Y-axis of the reference coordinate system contains the camera 1 focal point. Since $P_{2_z} = 0$ was also assumed, the X-Y axis plane of the reference coordinate system contains the focal point of camera 2. Thus, when the cameras are physically placed in the laboratory room, the basic location of the reference coordinate system is also inherently defined. Further, in order to simplify the camera data transformations, it was delineated that the X-Z plane of the reference coordinate system is defined in a globally-level sense, and it is required that a leveling of the camera bodies be carried out. This assures that there will be no angular disparity between the camera coordinate systems and the reference coordinate system in X and Z ($\theta_{1_x} = \theta_{2_x} = \theta_{1_z} = \theta_{2_z} = 0$).

For lack of any better location, a reasonable definition concerning the reference coordinate system location is that it be "placed" in the laboratory floor, which will be assumed to be a level plane. Thus, in this thesis, the X and Z axes of the reference coordinate system lie in the plane of the laboratory floor. In this situation, R_{1_y} and R_{2_y} will be the height of the neutral axis (assumed to be level and containing the focal point) of the camera lens-detector plate above the floor. The numerical values can be easily determined by direct measurement.

The three other parameters remaining to be accounted for, P_{2_x}, θ_{1_y} and θ_{2_y} are not as easily determined, and a procedure to find them will now be presented. In this procedure, the determination of P_{2_x} is dependent upon the availability of the angles θ_{1_y} and θ_{2_y}. Therefore, its calculation will be presented secondly.

In considering possible procedures to determine the angular parameters, direct measurement by precision instruments was discounted at this preliminary stage because of the monetary investment and their questionable effectiveness in this particular application. It was felt that a somewhat more elaborate procedure in terms of total steps but which could be carried out at no additional monetary cost was a worthwhile preliminary step. Since in all probability an experimental configuration may not be changed for some time, the procedure may continue to be useful as the system enters into experimental usage.

The procedure for finding the angles θ_{1_y} and θ_{2_y} is depicted in Figure 20 and can be stated as follows. By placing an LED at precisely a distance B along the perpendicular bisector to the length D

established between the camera tripod rotation axes, and then centering the camera detector plate Y_T axis on the diode beam, the following relationships hold:

$$\theta_{1_y} = -(90° - \theta)$$

$$\theta_{2_y} = (90° - \theta)$$

where

$$\theta = \tan^{-1}\left(\frac{B}{D/2}\right)$$

It can be seen that a completely symmetrical camera configuration is established, and that the nature of the configuration is determined by the magnitude of the distances B and D.

The procedure, although somewhat primitive in concept, is nonetheless able to consistently determine the desired angles to 0.1° . A plumb bob locates the rotation axis point of the camera tripod on the laboratory floor. The distance D between these two points is measured. The bisector point of D is then located and a perpendicular direction specified. The LED is then placed at the desired B distance on this direction vector line. A computer program can be executed which allows real-time remote meter readout of the Selspot System data output for the positioned LED. By employing this configuration, the real-time deviation of the LED from the Y_T axis of a particular camera can be obtained in terms of the X_T axis data. Each camera can then be individually tested and rotated until the deviation is nullified, and then locked in position. Knowing B and D, the angles θ_{1_y} and θ_{2_y}, which will be equal in

magnitude, can be found.

At this point, the complete physical camera configuration has been established and only the parameter P_{2_x} remains to be found to completely define the camera positions. It can be seen from Figure 20 that although D is known, it is not the correct distance since P_{2_x} must be somewhat less. However, it can be seen that if the distance from the camera rotation axis to the focal point for each camera was known, then the projected delta distance in each case could be subtracted from D to find the correct P_{2_x} (Figure 21). This is the procedure which was employed.

The tripod axis to focal point distance to be determined for each camera can be seen to be the sum of the particular focal distance parameter and the distance from the rotation axis to the detector plate, defined as C . The length C has been measured and was found to be 9.5 mm for each camera. Assuming that the two focal distances are known, then a ΔD_1 for camera 1 and a ΔD_2 for camera 2 can be found. In equation form,

$$\Delta D_1 = \frac{(F_1 - C) \cos \theta}{1000}$$

$$\Delta D_2 = \frac{(F_2 + C) \cos \theta}{1000}$$

where F_1 = focal distance (mm) for camera 1

F_2 = focal distance (mm) for camera 2

and ΔD_1 and ΔD_2 are specified in meters. Therefore,

$$P_{2_x} = D - \Delta D_1 - \Delta D_2$$

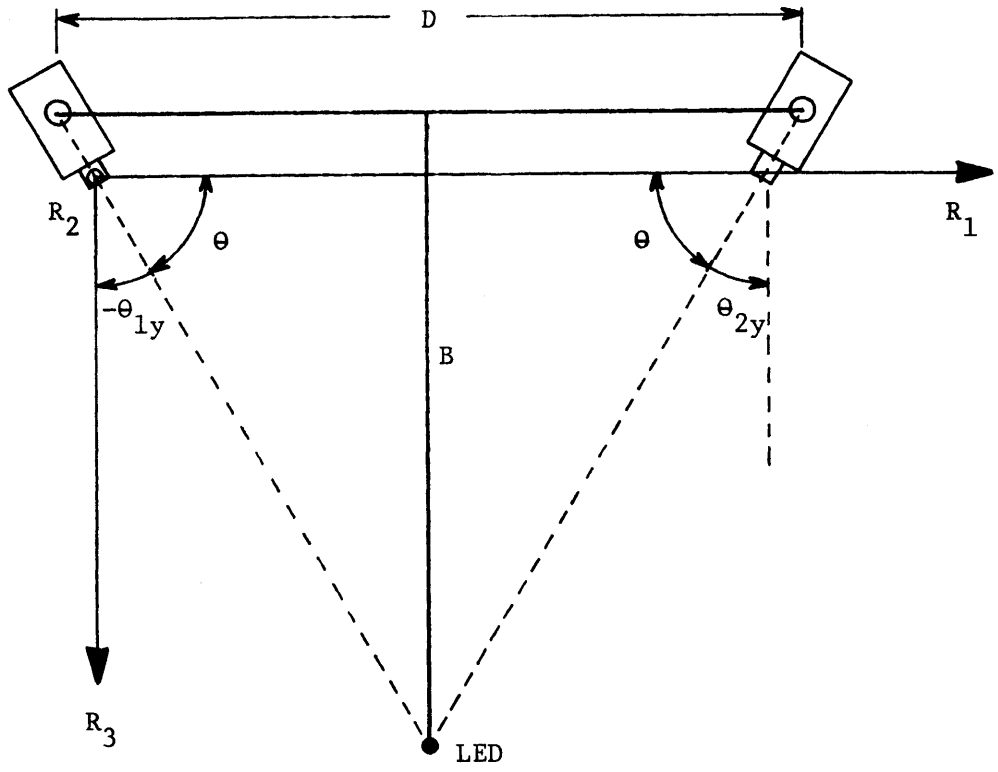

Figure 20. Camera angle determination.

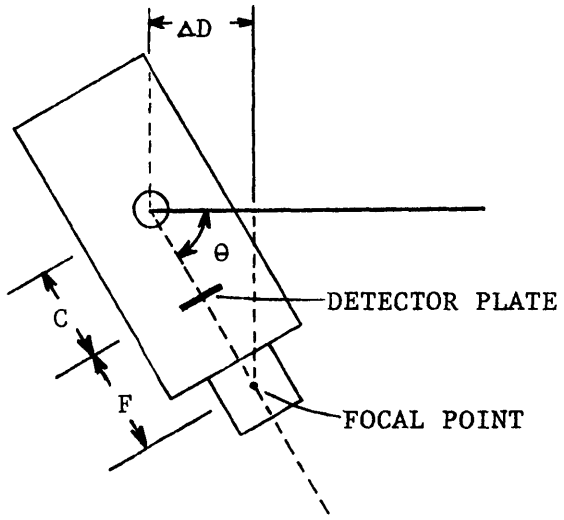

Figure 21. Determination of the distance, ΔD.

where D is the camera tripod axes distance (meters).

A small inherent error involved in the procedure should be pointed out. Since the calculated focal distance for each camera is slightly different, the line P_{2_x} is not exactly parallel to the line D, thus implying that the measured camera angle θ will not exactly equal the actual angles present. However, it can be shown that in a typical configuration the angular error is less than .02° and was therefore assumed to be sufficiently small so as not to be of relevant concern. This error could be eliminated through further computations if necessary.

It is readily apparent that the determination of the camera position parameters is an aggravating measurement problem. Further examination is needed to evaluate this procedure's effectiveness, and an exploration of other possible techniques is needed. An important consideration, however, is the cost of improved accuracy and convenience as weighted against the overall improvement of system performance.

Chapter 6

EXPERIMENTAL CONSIDERATIONS

Having presented various descriptions of the kinematic-acquisition system in terms of hardware configuration and analytical technique, this chapter will be concerned with issues relating to experimental implementation. Of particular concern are practical issues relating to the physical configuration of the Selspot System LEDs and cameras in an experimental situation, and the detection and elimination of data errors.

In any actual experiment, there will be measurement error involved in the data acquisition process, and several techniques are presented in this chapter to recognize and eliminate, or at least minimize, the errors at various stages of the overall processing stream.

6.1 HARDWARE CONFIGURATION CONSIDERATIONS

In this section, several experimental issues relating to LED attachment, camera positioning and lens settings will be presented. Much of the discussion will be concerned with "experimental protocol" in the sense that procedures and methods have been delineated which are based primarily on common sense and observational induction.

Attachment of the LEDs. As discussed in earlier chapters, a minimum of three LEDs must be mounted on each body segment for which three-dimensional configurational parameters are desired. This immediately

raises the question of what constitutes a desirable mounting procedure. Two overall categories of technique can be seriously considered: 1) that which dictates the mounting of each LED directly on the skin tissue of the particular body segment, and 2) that which calls for the mounting of the LEDs on a rigid support structure and then attaching the complete structure to the body segment. For a number of reasons which will be presently discussed, the second approach has been adopted in this thesis and it will be seen that this decision has several ramifications in terms of system implementation and computational algorithm design.

There are four major reasons for adopting the approach of an LED structure: 1) ease of experimental attachment, 2) integrity of rigid body calculations, 3) straightforward specification of the initial state position coordinates and 4) application to error detection algorithms. Each will be discussed in greater detail.

The effectiveness with which an experimental subject can be configured for kinematic monitoring is of paramount importance. It is crucial that the set-up time be minimized and the procedures be simple in nature. In the extreme case where several body segments might be monitored, all thirty LEDs of the Selspot System may need to be utilized. If each LED were to be dealt with individually, the set-up time could be quite long, and there would undoubtedly be major difficulties encountered in the determination of the initial state position coordinates. On the other hand, the logistics associated with attaching a single yet complete structure for each body segment would be substantially less. In this case, there is only one attachment which needs to be carried out for each body segment. A

double-strapping compact type of structure of the form depicted in Figure 22 would allow quick and efficient experimental set-up. An LED structure would also have the important advantage of allowing optimal LED placement in terms of viewability and computational reliability.

An important assumption in the overall analytical technique employed in this thesis is that the LED points are part of a rigid body structure. If the LEDs were mounted on the skin tissue individually, there is a strong possibility that there would be interspatial LED movement during an experiment due to muscular activity and slippage. The rigid body assumption would no longer hold and, in a computational sense, this violation would greatly reduce the reliability of the calculations. When the LEDs are mounted on a rigid structure, this important condition is always satisfied and the overall rigid body problem takes on a different and manageable nature. That is, the problem now becomes one of minimizing any movement between the LED structure and the body segment. Clearly, any kind of slipping or tissue-LED structure vibration will also give misleading results. However, since a complete LED structure can be quite compact and will weigh on the order of tens of grams, movement based on dynamic inertial effects should be minimal. In addition, is is anticipated that strapping techniques can be developed which will reduce the "mobile" nature of flesh and tissue without putting stress on the subject. At the very least, however, it can be speculated that slippage or vibration of the structure would manifest itself as a distinctive high-frequency motion pattern which could be recognized and eliminated, if desired.

The analytical technique for calculating position and orientation has been discussed, and it can be recalled that at each time step a calculation is made based on a "conceptualized" initial state and an actual measured final state. The problem of specifying the initial state, the positional coordinates of the LEDs with respect to their particular body coordinate system, can be substantially minimized when an LED structure is employed.

To illustrate a possible specification methodology, a realistic body coordinate system - LED structure configuration is depicted in Figure 22. In this example, it is desired to determine configurational parameters at a point along the neutral axis of the body segment bone. By employing an LED fixture, the spatial interrelationship of the LEDs is fixed for all time and their positional coordinates can be accurately measured with respect to some arbitrary LED structure coordinate system as shown in Figure 22(a). It is evident that a direct precision measurement need be carried out only once for each LED structure, and the coordinates can then be permanently stored in a data file. In part (b) of Figure 22, the LED structure is shown strapped to the body segment, and the desired body coordinate system is depicted. The LED structure, through proper alignment, can be attached in a way that the LED-structure coordinates need only be translated by an amount r so as to be specified with respect to the desired body coordinate system. The circumference of the body segment can be easily measured after the structure is affixed, and then the radius r estimated. With this single parameter, computational algorithms can then atuomatically specify the correct initial state

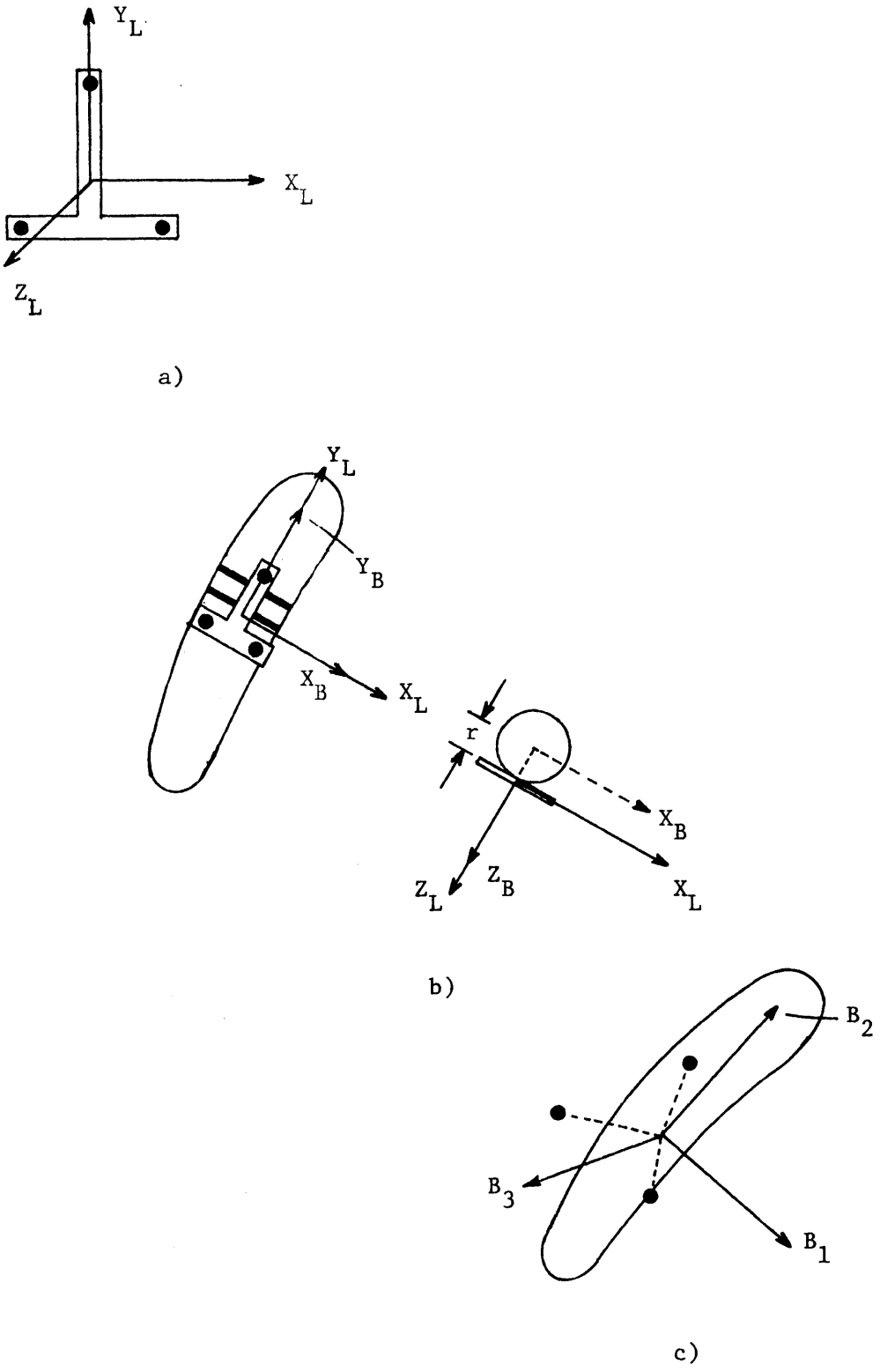

Figure 22. An approach for body coordinate definition in an experimental situation.

positional coordinates based on the predefined LED-structure data file. In its basic form, this procedure would allow quick attachment of LED structures and easy specification of the body coordinate system via the initial state coordinates [Figure 22(c)].

A further advantage of the LED structure approach is its applicability in terms of error detection. Algorithms have been developed which detect and eliminate poorly-measured point coordinates. The LED spatial relationships which were accurately measured for each structure and which formed the basis for subsequent definition of the initial state, are used as a "standard" with which to compare the nature of the actual computed coordinates using the Selspot System. Thus, at each time step the measured data can be compared to the "standard" and the quality of the measurement assessed. The specific technique will be presented later in this chapter. If the LEDs were mounted separately on the skin, this entire error detection concept could not be justified since any interspatial LED movement during experimentation would completely nullify the validity of the approach.

Geometric Considerations-Camera Placement. There are several considerations to be taken into account when determining the placement of the cameras for an experiment: 1) the detectability of the LEDs by both cameras, 2) the geometric nature of the three-dimensional point calculation, and 3) the LED-camera operating distance.

The LEDs which are employed as part of the Selspot System are high-powered, wide-angle dispersion diodes. However, the greatest emitted

intensity occurs at the neutral axis, and the best digitization of the diode image projection will result if the two cameras are located in the line-of-sight of the diode neutral axis. The concern pertaining to the effect of camera placement on the three-dimensional point calculation stems from straightforward geometric considerations. Since the calculation is based on two direction vectors, both subject to small deviation errors, it can be shown that the effect of the error is a minimum when the two direction vectors intersect at 90°.

It is apparent in view of the above discussion that camera placement geometry is primarily a compromising process between two oppositely-working forces, LED detectability and direction vector geometry. In most cases, a knowledge of the capability desired for a particular experimental situation applied in consort with a consideration of the discussed issues will readily lead to a suitable camera geometry.

Having delineated a camera placement geometry, it can be seen that in a symmetrical configuration the distance between the cameras will determine the total volume and range characteristics involved. It is readily apparent, as shown in Figure 23, that the greater the distance between the two cameras, the greater will be the volume of viewability. However, with greater separation at a given set of camera angles is a concomitant increase in the operating distance from an LED to each camera. The LEDs presently employed will maintain full system resolution up to a distance of approximately 5 meters. As the distance increases, the signal/noise ratio decreases, and system resolution capability is sacrificed. Under normal circumstances, the LED signal cannot be reliably

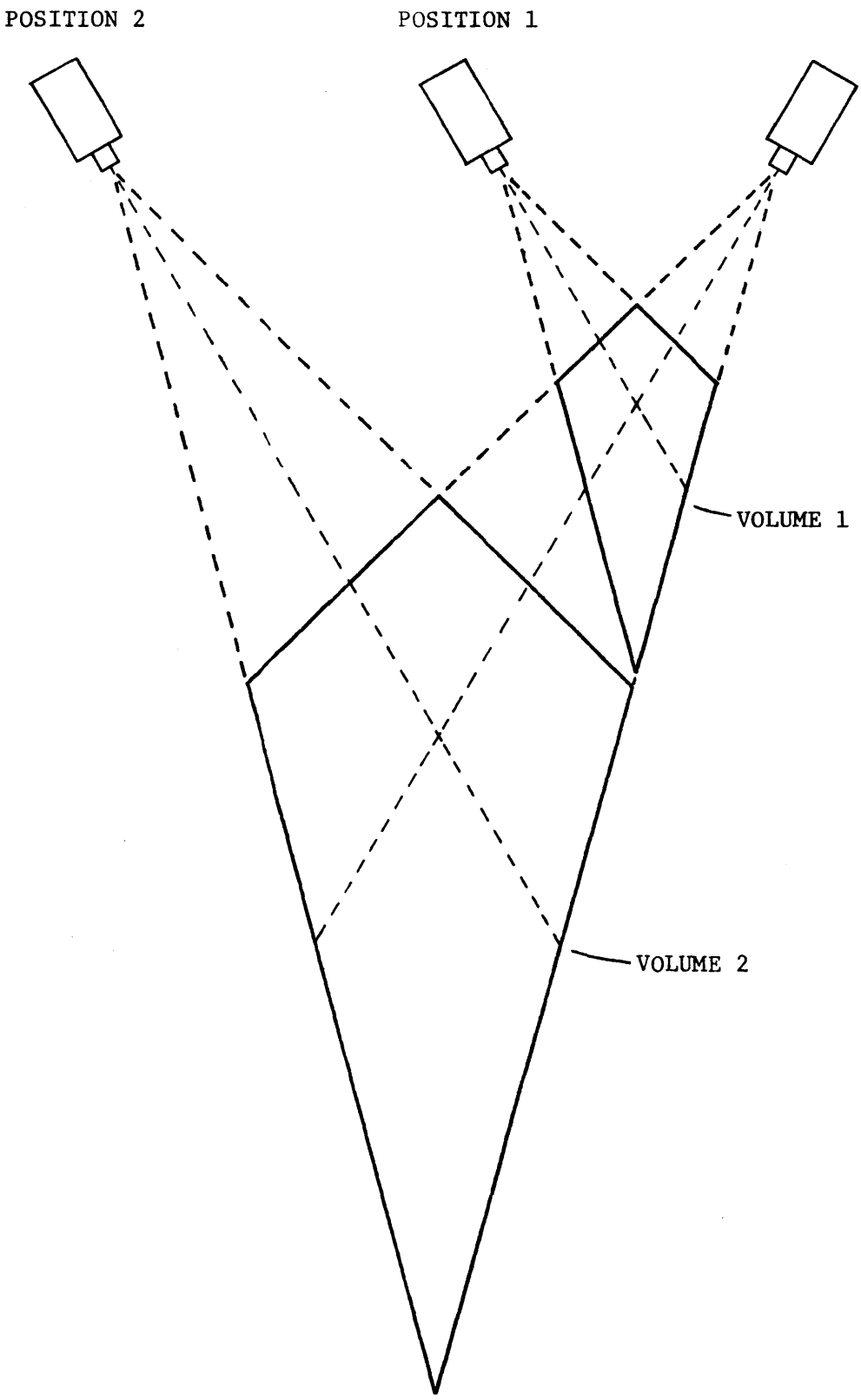

Figure 23. Volume characteristics of camera placement.

detected when the distance reaches approximately 10 meters.

Optical Noise Considerations. The LED infrared signal detection process can be adversely affected by primarily the following two means: 1) focus and aperture settings of the camera lens and 2) infrared reflection noise from floors and other surfaces.

The detector plates of the infrared cameras have a finite optical energy range throughout which a successful digitization of the LED signal will occur. Because of the desire to use a given set of diodes at a number of different distance ranges, a lens with a large range of aperture settings is supplied. After the experimenter has determined the approximate range at which the diodes will be operated, the lowest aperture setting before signal overload occurs should be found since this guarantees the best signal/noise ratio. Increasing the aperture setting above this point will decrease the signal/noise ratio and the performance of the system.

As introduced in an earlier chapter, the operating principle of the Selspot System is such that the focusing of the LED beam is not a crucial consideration. The processing circuitry automatically digitizes the location on the detector plate which is perceived as the "center" of the beam. In this way, an unfocused LED signal will still be digitized with consistent accuracy. However, some loss in resolution capability will be perceived at the extremes of focusing error. Therefore, adjustment of the focus of the camera lens to the approximate operating distance of the diodes is a recommended procedure.

If an LED optical signal is reflected from a floor or wall surface with sufficient strength and a correct directivity so as to be detected by a Selspot camera, a serious error in the digitization of the LED signal will result. Normally, a single infrared beam is detected and the "centered" location of the beam on the detector plate is the digitized output. If, however, this primary beam is complemented with a secondary beam due to reflection, then two beams will activate the plate. The resulting digitized signal in such a case will be the location on the plate which is the "optical energy average" of the two beams. It can be expected that in most cases the secondary beam will be much less powerful than the primary one, thus causing an averaging error which may not be easily detectable through subjective observation of the results.

To guard against multiple-beam detection, surfaces in the experimental room should be as non-reflective as possible, and in certain experiments, deflecting shields strategically placed in the room or on the cameras should be considered. Experimental situations calling for special consideration are normally those in which the range is quite large or the diodes are positioned less than a foot from the floor. Both types of situations are geometrically susceptible to a floor reflection problem, which is the most prevalent.

6.2 DETECTION OF LED MEASUREMENT ERRORS

It has been pointed out in earlier discussions that the Selspot System is subject to measurement errors, and that these errors can be of

sufficient magnitude so as to give misleading results. Several factors can affect its performance in terms of potential resolution and accuracy. Some important ones are the following: 1) low signal/noise ratios occurring at poor LED detection angles or large measurement distances; 2) the presence of detector plate sensing irregularities (local nonlinearities); 3) location digitization errors due to a reflection problem (multiple-beam averaging); and 4) the presence of Gaussian noise effects during signal measurement.

These kinds of errors are subtle and often times cannot be directly ascertained. An objective criterion is needed to rationally detect such types of measurement error and eliminate error-prone data points from the computational algorithms.

It has been discussed in Chapter 4 that the analytical technique for calculating body segment configuration can easily handle an overdetermined system and take advantage of the extra information to make a more reliable compuation. This opens up the possibility of assigning more than the required three points to a body segment so as to increase accuracy and maintain calculational integrity in the face of measurement error or undetected and obscured LEDs. If only three points are used per body segment and if at any time one of the LEDs goes undetected or is eliminated because of measurement error, then the calculation cannot be carried out. With more than three points, however, the chances are of course greater that a calculation can always be made and in most cases, made more reliably.

In this section, an algorithm to detect three-dimensional point

coordinate error is presented. Two types of error-handling problems will be discussed: 1) the accommodation of unmeasured LEDs and 2) the testing of measured LEDs and the elimination of those which have inaccuracies.

Elimination of Undetected LEDs. When an LED is undetected due to obscuration, overloading or signal weakness, a potentially valid data signal, although erroneous in this situation, is still placed on the Selspot System data output lines. As discussed in Chapter 2, provision was made for the 14th bit of the Direct Memory Access data buffer register to be set high when such a condition occurred. All the Selspot System raw data which is to be processed is examined for the occurrence of this anomaly, and if perceived, the data is modified in order to distinctively identify it. Provisions have been established so that the particular LED point is not applied in any further calculations and compensating action is taken considering its absence.

Detection and Elimination of Points with Accuracy Errors. More difficult to detect is an absolute error in measurement. The data in many respect appears normal, thus enhancing the need for a technique to judge its accuracy and validity. By adopting the premise that all the LEDs assigned to a certain body segment will be attached to a rigid support structure which is then mounted on the body segment, a criterion for judging point coordinate quality can be formulated.

A significant aspect of having an accurate set of initial state

position coordinates available is that this constitutes a physically-based pattern "standard" which can be compared to the pattern measured and calculated using the Selspot System. It has been discussed that the mean of the measured LED points for each body segment, designated $\underline{Q}$ (along with its counterpart, $\hat{\underline{Q}}$), should have less positional error than any particular individual LED point. As introduced by Lenox (1976) and modified for this application, it is suggested that an error criterion can be established by comparing the mean $\hat{\underline{Q}}$ to point distance for the "standard" coordinates and the mean $\underline{Q}$ to point distance for the measured coordinates. In this way, a distance specification for each initial state point can be individually compared to a distance specification for each measured LED point. A large variation between an initial state "standard" distance and a final state "measured" distance for a particular LED point would imply some sort of measurement error. The following definitions are made:

$$\hat{D}_I = \sqrt{(\hat{X}_Q - \hat{X}_I)^2 + (\hat{Y}_Q - \hat{Y}_I)^2 + (\hat{Z}_Q - \hat{Z}_I)^2}$$

and

$$D_I = \sqrt{(X_Q - X_I)^2 + (Y_Q - Y_I)^2 + (Z_Q - Z_I)^2}$$

where I = ith point.

The algorithm has been implemented in such a manner that the experimenter can specify a percent distance variation cutoff, and any data points failing to meet the limit of the variation are eliminated from further consideration. The percent distance variation specification

takes the form

$$\Delta D_I = \left| \frac{D_I - \hat{D}_I}{D_I + \hat{D}_I} \right| \times 100$$

In normal situations, most of the error-inducing factors introduced at the beginning of this section will cause a fairly large increase in the percent length variation for a particular point. Experiments have shown that percent length variation increases on the order of 5-10% are common when large measurement errors are present. The algorithm just presented is effective at detecting these rather large measurement errors. Some errors, however, do not cause such a large change, and as a result, the specification of the variation cutoff takes on added importance. A very relaxed criterion will not effectively eliminate data points which have only moderate measurement error. Yet at the same time, too stringent a criterion could of course cause the elimination of all points, since there will always be some length variation (presently 1-2%) because of the inherent limits of the total system. Further investigation into the specification of an "optimum" distance variation cutoff is needed so as to best utilize the error reduction possibilities.

Since the mean point $\underline{Q}$ is the point for which the configurational description is always initially calculated, and since it is the composite average of all the measured LED points, it would be a prudent exercise to recalculate $\underline{Q}$ if some of the final state LEDs were eliminated by the above algorithm. In this way, the reliability of the point $\underline{Q}$ would be further enhanced since its calculation would then be the mean of only those points which passed the length-variation criterion, and thus met

a certain standard of accuracy. This recalculation feature using only the best-measured points has been implemented as an automatic procedure in the algorithm.

Implementation of the Error Algorithm. The error detection and elimination algorithm presented in the previous two sections cannot be directly implemented as discussed without severe negative ramifications. The problems stem from two difference considerations.

First, when comparing $\underline{Q}$ to LED point distance variations in the initial state and an arbitrary final state, it is crucial that the distance calculations in both cases be based upon a similarly-obtained $\hat{\underline{Q}}$ and $\underline{Q}$. If, for instance, some LED points are not detected at a particular time step, then the calculation of the mean $\underline{Q}$ will be dependent upon a slightly different set of points than the $\hat{\underline{Q}}$. The $\hat{\underline{Q}}$ calculation, in the present conception, would include all the LEDs assigned to a particular body segment while a $\underline{Q}$ calculation could conceivably be based on a smaller number of actually-measured LED points. Clearly, in such a situation, the distance comparisons would have little meaning.

The second major problem relates to the temporal integrity of the body coordinate system origin. It can be recalled, based on discussions in Chapter 4, that the consistent location of the origin of the body coordinate system from time step to time step is directly dependent upon the location of the point $\underline{Q}$. Through time, if the calculation of the point $\underline{Q}$ is based upon a continuously fluctuating set of LED points, then the physically-relevant location of the point $\underline{Q}$ will "migrate" in

a manner dependent on the fluctuation. This implies that the origin of the body coordinate system, and hence the point of configurational description, will not be consistent from time step to time step. For effective configurational description, this problem must be eliminated.

In this section, the procedure employed for guaranteeing correct mean point to LED distance comparisons and for maintaining body coordinate system integrity when confronted with undetected and consciously-eliminated LEDs is presented. The overall process is depicted in flowchart form in Figure 24. In this way, the step-by-step nature of the procedure as it responds to special situations is more clearly evident.

It can be seen that if there are undetected LEDs at a particular time step, then an inner algorithm is executed which recalculates $\hat{Q}$ without the undetected LEDs. A new set of $\hat{Q}$ to point distances is then calculated, and it can be seen that the distance comparison will now be physically correct and meaningful. In order to maintain the integrity of the final state Q location, a correction distance, $\Delta Q'$, is calculated. $\Delta Q'$ is defined as the difference between the original $\hat{Q}$ (all LEDs) and the new $\hat{Q}'$ (detected LED points). The correction distance is subtracted from the final state Q and it can be seen that this procedure will eliminate the "migratory" nature of the Q due to undetected LEDs.

A similar type of process (see Figure 24) occurs if some LED points fail the cutoff of the distance variation comparison at a particular time step. Following the premise of recalculating Q to enhance its reliability, a new Q is calculated, based only on the final state LED points

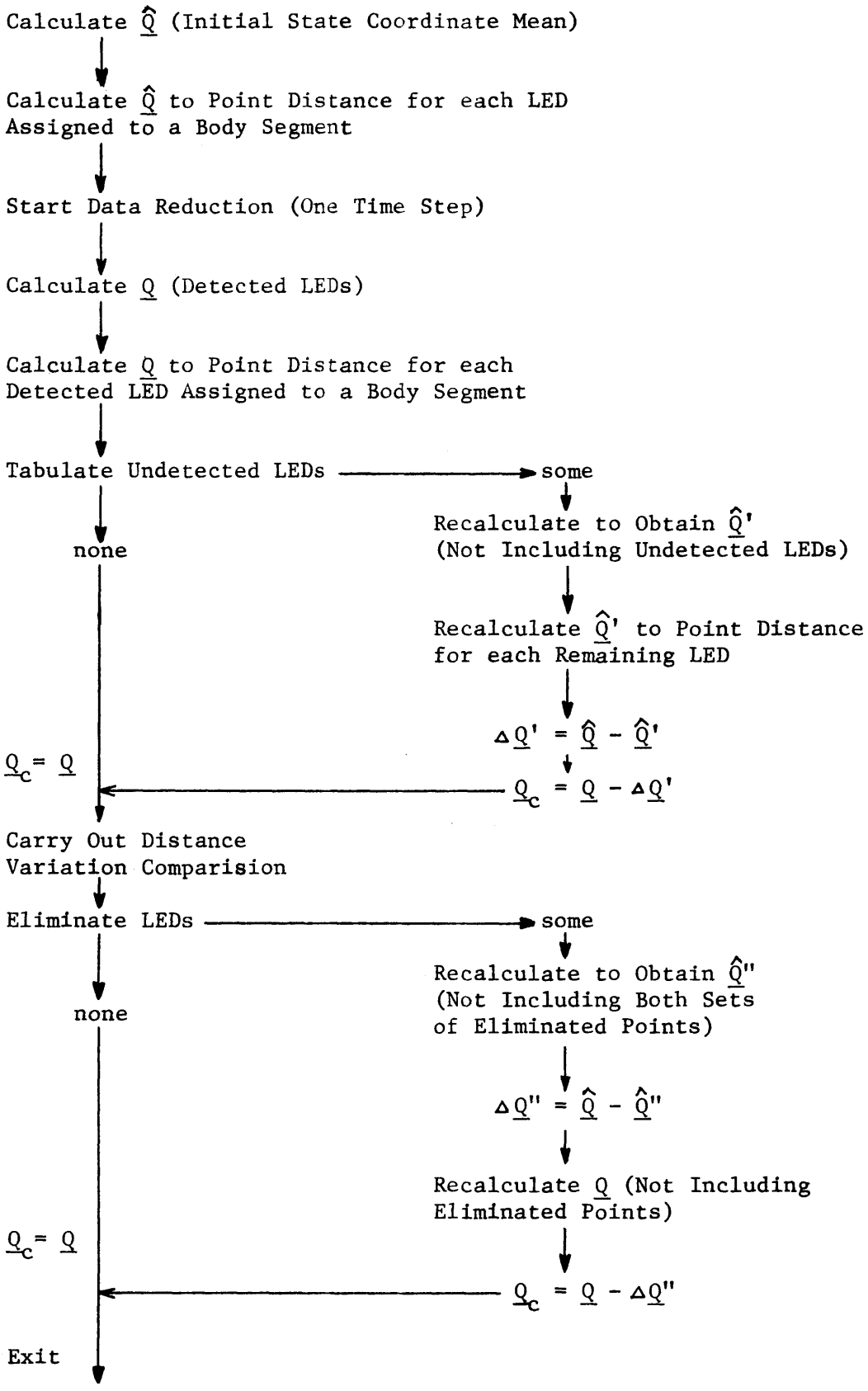

Figure 24. Bad data point elimination flowchart.

which remain. To maintain location integrity, another inner algorithm is executed which recalculates $\hat{\underline{Q}}$, this time without both sets of eliminated LED points, the undetected set and the inaccurate set. A correction factor, designated as $\Delta\underline{Q}''$, is then calculated. $\Delta\underline{Q}''$ is defined as the difference between the present $\hat{\underline{Q}}''$ and the original $\hat{\underline{Q}}$ (all LEDs). The new recalculated $\underline{Q}$ is then corrected by the factor, $\Delta\underline{Q}''$.

After the execution of this algorithm, the configurational calculation is carried out with the point of description designated $\underline{Q}_c$ in Figure 24, and utilizing only the sets of LED points, initial state and final state, which remain.

It is readily apparent that the set of "standard" initial state coordinates is of vital importance in carrying out the algorithm. The initial state coordinates constitute the only completely reliable positional coordinate "picture" of the LED pattern for a particular body segment structure, and they are the only means by which an incompletely-measured LED point pattern can be effectively analyzed. Again, the value of the LED support structure approach is evident.

It is clear that if less than three points are available for the configurational algorithm, then a calculation cannot be carried out. The approach of then assigning more than three LEDs to each body segment, if less than ten bodies are designated, is justified. However, it is speculated that there may be an upper limit in terms of effective experimental implementation. It is suggested that at higher numbers of LEDs per body segment, such as 10-30 LEDs, the accrued benefit may not warrant the experimental problems associated with a bulkier and heavier

LED structure. Based on the performance characteristics of the Selspot System, it is believed that in most cases an assignment of five to seven LEDs per body segment will yield the best data point sets without creating undue experimental problems.

There are, however, certain experimental situations which warrant large assignments of LEDs per body segment. The problem of tracking head movements in blind mobility analysis is a case in point, since the human subject must have complete freedom of movement in all directions. Although the camera tracking problem is discussed later in Chapter 9, it is envisioned that LEDs would need to be attached all around the head in order to maintain reliable viewing of LEDs with the two cameras. A conceivable LED structure in this case might be a specially-configured head-worn helmet, and it can be appreciated that at any particular time step many LEDs will be obscured, and as the subject moves, the visible set of LEDs will dynamically change. It can be seen, however, that the suggested LED configuration applied with the algorithm discussed above will guarantee a consistent and stable description of the three-dimensional positional and orientative parameters at the origin of the body coordinate system, the designated point of description.

6.3 DATA CONDITIONING

In the previous section, a pattern and accuracy recognitive procedure of bad data point elimination was presented. This algorithm is well-suited for pinpointing and eliminating data points with large errors in accuracy. In view of the difficulty in specifying a distance variation

cutoff which will consistently eliminate points with moderately low error, a frequency-dependent filtering procedure is presented in this section for attacking these errors as well as an ever-present sampling-noise error. The sampling noise can be attributed to a digitization error due to small random noise effects present in the Selspot System.

The smoothing procedures, by examining the frequency content of the data, greatly enhance the possibilities for elimination of small-scale measurement errors. The filtering techniques presented in this section, it can be seen, complement the distance variation technique in terms of the particular kinds of measurement errors each is best suited for dealing with, and the detection approach each utilizes.

The smoothing routines discussed in this section are high-order low-pass digital filters with a specified cutoff frequency. In this way, a time-history data point set of a physical parameter can be analyzed and any frequency component which is higher than the specified cutoff frequency eliminated. This is precisely the type of function which is needed since data point measurement errors and the sampling digitization errors will both be manifest as high-frequency signals. It then becomes the task of the experimenter to determine the lowest cutoff frequency which can be specified without affecting the experimental information, since the lower the cutoff frequency, the more minimal the effect of the errors, and thus the more reliable the results.

It would be a straightforward approach to attempt to apply the low-pass filtering to the configurational results and eliminate the frequency components which are thought to be the result of measurement error.

However, it is readily apparent that large amounts of computation can greatly magnify a small measurement error, and this could lead to large errors in the final results which filtering could not easily eliminate. Thus, it would be desirable to carry out the low-pass filtering as early in the processing stream as possible with the belief that the results would then be more reliable. Precomputation filtering, however, must be utilized with great care because it can quite subtly modify or mask the potential configurational results.

In order to provide maximum flexibility in terms of combinational options, both types of filtering have been implemented. The two types of filtering options will be designated as pre-configurational three-dimensional point filtering and post-configurational parameter result filtering. The experimenter has the option of enlisting the use of either or both types of filtering, and can specify independent cutoff frequencies for both.

The same type of digital low-pass filter (Stearns-1975) is used in both filtering situations to be discussed. The filter is a 6th order Butterworth recursive low-pass digital filter, and is implemented as three filter sections in cascade. For a typical 2nd order section of the filter, if f_m is the filter input and g_m is the filter output at time $t = m$, then the filter algorithm utilized in this application can be written as

$$g_m = A(f_m + 2f_{m-1} + f_{m-g}) - B(g_{m-1}) - C(g_{m-2})$$

where A,B,C are coefficients based on the specified cutoff frequency.

In order that a user-specified cutoff frequency can be implemented, a low-pass filter design algorithm is incorporated as part of the package. The filter design routine calculates the correct section coefficients for a particular specified cutoff frequency, and the filtering algorithm automatically utilizes these parameters in the actual filtering routine.

All recursive digital filters have associated with them a phase lag characteristic, and this lag can be quite severe when low cutoff frequencies (< 20 Hz) are specified. It can be proven (Stearns-1975) that a dual-filtering scheme, first a filtering forward in time and then a filtering of that result backward in time, will eliminate the phase lag. This procedure is a standard part of the filtering algorithm.

Pre-Configurational Three-Dimensional Point Filtering. The earlier that filtering can be employed in the calculation sequence the more reduced will be the errors in the final results. Since the calculation of body-segment orientation is known to be sensitive to the data measurement errors, some filtering should be attempted before this juncture. Two obvious places where filtering could take place is at the raw Selspot data stage (camera data) and at the post three-dimensional point calculation stage. Operating at the camera data level appeared to have some uncertainty in terms of the effect that filtering a set of image projections would have in absolute terms. Therefore, it was decided that a more reliable course of action would be to filter at the post three-dimensional calculation level in view of the direct physical relevance. Although more noise is conceivably introduced by this calculation phase,

the probable effects of a specified filtering plan can be more easily understood.

In considering the filtering procedure to be employed, it should be pointed out that at this stage of the calculation sequence, there exists a time history of the path of each assigned LED point, described in terms of X, Y, and Z sets of coordinates. The simplest and perhaps most effective way to filter this overall signal is to filter the time history of each coordinate axis, X, Y, and Z, independently. Although treating each coordinate of the time history independently does have certain ramifications, it can be seen that this procedure will not misinterpret the frequency content of the total signal, which is the most important consideration. In view of these considerations, it was adopted as the filtering procedure.

In consideration of the actual implementation of the filtering procedure, there is one important experimental problem which must be resolved. As the first phase of signal analysis and error detection, the bad data elimination algorithm for undetected and poorly-measured LED points is applied. During a typical experiment it is possible that an LED point may be obscured or otherwise eliminated throughout small sections of the experiment, thus leaving an incomplete trace as the signal to be filtered. A signal of this sort cannot be filtered because of the lack of data points in various sections of the data set. Because of the possible deleterious effects of attempting to generate suitable data through interpolation, a procedure has been formulated to handle this unique filtering situation. An algorithm has been implemented which examines each coordinate time-

history data set and then treats each intact data segment as an independent signal for filtering. The data array is effectively divided into the number of intact data segments, filtered segment by segment, and then synthesized back into a final data array, all the data gaps and the data values maintained in their original time positions. In this way, the true nature of the data measurement is maintained through to the result phase while at the same time carrying out a valuable filtering process.

Post-Configurational Parameter Result Filtering. This low-pass filtering phase is the final filtering sequence and it operates on the configurational results, the positional and orientative body segment parameters. This filtering can be seen to serve three functions: 1) it further smooths the measurement noise, 2) it smooths the computational noise induced by finite precision arithmetic and 3) it can be used to eliminate any other unwanted higher frequency components than that contained in the experimental information.

Many of the experiments performed in the Mobility Laboratory will be concerned with low-frequency phenomena (< 5 Hz). This is particularly true for gait analysis when the main concern is the overall motion pattern. As will be illustrated in Chapter 8, a low-pass filtering operation at such a level of frequency cutoff is a valuable means of eliminating errors of the type delineated earlier.

In normal situations, as further discussed in the next chapter, the configurational parameter results are stored in a permanent data file. In view of the availability of the raw parameter results and based on the

realization that this phase in the final data conditioning, prior to filtering, all data gaps in the results are linearly interpolated based on each gap's endpoints. The conditioned data array is then filtered at the specified cutoff frequency, and stored as another permanent data file. It can be seen that based on this structure, the raw result data can be filtered any number of times, if for instance different sets of cutoff frequency filtered results are desired.

Chapter 7

THE SOFTWARE SYSTEM

In the previous chapters, the fundamental hardware configuration for monitoring kinematic data has been delineated and the basic analytical algorithms for calculating the absolute kinematic parameters of rigid bodies have been presented. A user-oriented software system, based in the programming language FORTRAN, has been developed to control the data gathering and perform the necessary computations as well as to provide other fundamental data-handling and accessory functions. The purpose of this chapter is to present a general description of the software system package; its structure, capabilities and user-oriented features. More specific software issues relating to user procedures, program functions and computer program statements are discussed in an accessory document, "The TRACK System User's Guide". The general-purpose hardware-software system, as discussed in Chapter 2 and in this chapter, forms the complete kinematic-monitoring and analysis system for experimental use.

7.1 INTRODUCTION TO THE SOFTWARE SYSTEM

In Chapter 1, two applications of the kinematic-monitoring system were discussed, one concerned with the monitoring and analysis of gait kinematics, and the other concerned with the real-time processing of kinematic parameters. These two projects represent the fundamental extremes of system application. They also present a formidable challenge in terms of computational technique.

Given the amount of computation which must be carried out at each time step, it was soon readily apparent that a real-time processing mode would not be able to handle high data-sampling rates, a requirement in the gait-related project. Therefore, a slightly different processing sequence was needed, one which would carry out data gathering, but not begin any further processing until the experiment was completed. Also, a means was needed to handle the data-storage problems throughout the processing which were inherent with this approach.

In order to effectively make progress in developing the kinematic system, it was decided that these two fundamentally-different processing schemes should be treated separately. Since the file-oriented data acquisition and analysis capability was of primary immediate importance, it was given initial attention. The development of the processing software was formulated, however, so that the functional algorithms could be used for either purpose, real-time processing or file-oriented processing. The needs of the file-oriented processing were given higher consideration, implying that at the present development stage, the real-time processing is in general carried out rather inefficiently.

The fast-sampling file-oriented processing is implemented as an automatic multi-program Batch processing stream. The individual programs carry out fundamental step-by-step operations such as data gathering, 3-dimensional point calculation, configurational calculation and so forth. Each program consists of essentially data-storage operations and functional subroutines which carry out some aspect of the overall calculation. A further description of the processing sequence is presented later in this chapter.

The real-time processing, implemented in demonstration form only, utilizes the same subroutines employed above, but they are executed in sequence for each time step. A loop is established which allows sampling to occur after the processing for the previous time step is completed. Although the capability is not configured for practical application, it does give insight into the real-time processing problem, as discussed later in this chapter.

7.2 FUNDAMENTAL STRUCTURE OF THE SOFTWARE PACKAGE

This section is designed to address some of the issues and the features relating to the software implementation of either type of processing, real-time or file-oriented. Three different topics will be covered and they are delineated as follows: 1) subroutine structure, 2) segment file specification and 3) the processing parameter data file.

Modular Subroutine Structure. As introduced, one basic tenet of the software package is the reliance on a functionally-oriented subroutine structure. Each well-delineated operation which must be carried out in the processing stream is formulated in the framework of a subroutine. For illustration, Table 3 gives a description of some of the more important subroutines utilized in the software processing.

To effectively manage the necessary data handling and to transfer programmatic control parameters from subroutine to subroutine, a well-defined "labeled common" data field structure is utilized. In this way, most data arrays and parameter specifications which are needed are defined and internally available to any subroutine. It can be seen that with a

Table 3

PARTIAL SUBROUTINE LIST

Subroutine Name	Description
TKSSM2	Fortran-callable assembly routine for controlling frequency-timed sampling.
TKSTRA	Translates camera data to (X_t, Y_t) coordinate system and applies X-Y scale factor to the data.
TKSSCO	Lens nonlinearity data correction.
TKSPCA	3-dimensional point coordinate calculation.
TKSCCA	Configuration calculation (Maximum of 10 bodies).
TKSCPL	Body coordinate system spatial plot of configuration.
TKSDSV	Result file naming and listing in a user directory.
TKSDSH	User directory search and retireval of listed information.
TKSFLD	Low-pass filter design.
TKSFLP	Data array low-pass filter.
TKSFDP	Linear fit of a data array with data gaps.

structure of this sort, there is a built-in flexibility and efficiency in terms of the replacement, modification, addition or elimination of subroutine tasks.

Segment File Specification. In an experimental situation, regardless of the processing mode, the initial state positional coordinates of the LED points for the given situation must be made available to the software routines. A program is available which carries out the creation of a permanent data file containing a segment-LED specification and the initial state coordinates of the LED points. Thus, entire sets of segment specification files, all with different identifying names, can be created and be permanently available for experimental purposes. Any one of the created segment files can be utilized in its particular experimental situation and accessed through a simple name definition, as further delineated in the next sub-section.

The Processing Parameter Data File. It is readily apparent based on the discussions in previous chapters that there are several calibration parameters as well as control specifications which must be utilized by various subroutines at different stages of the calculation sequence. In order to effectively and automatically carry out this requirement, a processing parameter data file has been defined, and a storing and accessing procedure formulated. A typical printout of the contents of the file is given in Figure 25.

The processing parameter file, as introduced, contains two categories of information: A) calibration parameters and B) control specification parameters. Under the first group, referring to Figure 25, are placed

```
SAMPLING PARAMETERS

LED CHANNELS =  6.          ------------------------ 4
FREQUENCY    = 79.          ------------------------ 5
SEGMENTS     =  2.          ------------------------ 6


CAMERA POSITION DATA

CAMERA 1        RX            RY            RZ
               0.000         1.478         0.000
                AX            AY            AZ
               0.000       -26.565         0.000
                                                  ---- 1
CAMERA 2        RX            RY            RZ
               4.548         1.464         0.000
                AX            AY            AZ
               0.000        26.565         0.000


CAMERA CALIBRATION FACTORS

FOCAL DISTANCE   -- CAMERA 1= 15.50
                    CAMERA 2= 18.00
                                        ---------- 2
XY SCALE FACTORS -- CAMERA 1=  1.00
                    CAMERA 2=   .99


CAMERA LINEARITY FACTORS

CAMERA 1 = 0.0002250
                                  ---------------- 3
CAMERA 2 = 0.0001960


MISCELLANEOUS PARAMETERS

PERCENT VARIATION CUTOFF          = 10.00     -------- 7
SEGMENT FILE NAME ---------------- SEGFL1     -------- 8
3D POINT SMOOTH OPTION (Y-1:N-0) =  1.0       -------- 9
LOWPASS CUTOFF FREQUENCY          = 30.00     --------10
```

Figure 25. Contents of the processing data file.

1) the camera position data, 2) the camera calibration factors, and 3) the camera linearity factors. The second group, also referring to the Figure, consists of the following items; 4) the number of LED channels to be sampled, 5) the frequency of LED sampling, 6) the number of body segments which are to be defined, 7) the distance variation cutoff in percent (bad data elimination), 8) the name of the segment file to be employed for the present situation, 9) the 3-dimensional point filtering option and 10) the desired cutoff frequency for the point filtering.

Three individual computer program sequences must be executed to completely specify the parameter file. Following the discussion of Chapter 4, one program sequence, in the framework of an experimental procedure, determines the camera scale, focal distance and linearity factors, and inserts the results into the parameter file. A second program execution procedure is enlisted to determine the camera position parameters, and again the results are automatically inserted into the parameter file. A third program allows the experimenter to specify and insert the control specification parameters into the file.

The processing parameter file, once it is created, is then permanently available and automatically accessed for all processing needs. It is clear that once an experimental situation has been configured and the parameter file established, any number of experiments can then be easily performed in rapid sequence (3-5 minutes per experimental run). Any changes which are made, whether in terms of calibration or control specification, are immediately stored in the parameter file, thus guaranteeing a completely

relevant parameter file. One final point concerning the file is that real-time processing programs do not respond to a sampling frequency specification (5) or to the 3-dimensional point smoothing specifications (9 & 10) since they are not applicable.

7.3 REAL-TIME PROCESSING

As mentioned in the Introduction, the real-time processing problem was given secondary attention in this thesis. However, because of the subroutine structure, a real-time processing demonstration program could be written which has all the segment-tracking capabilities of the Batch processing stream, except that it operates out of necessity at a lower sampling frequency.

The flowchart for the demonstration program is depicted in Figure 26. It can be seen that the program in its present form operates in a cycling loop whose frequency is dependent on the processing time needed for each data set. The "output" at each time step is a plot of the actual configuration of the defined body coordinate systems in space, as depicted in Figure 27.

The frequency of looping for the program in a single body segment (3 LED) situation has been found to be on the order of 2 Hz. It is readily apparent that this bandwidth is not nearly sufficient for practical real-time experimentation. In Chapter 10, a further discussion of the real-time processing problem and some recommendations for further development will be presented.

As a final note, it should be pointed out that the real-time demonstration program has served a valuable function. It has proven to be a helpful

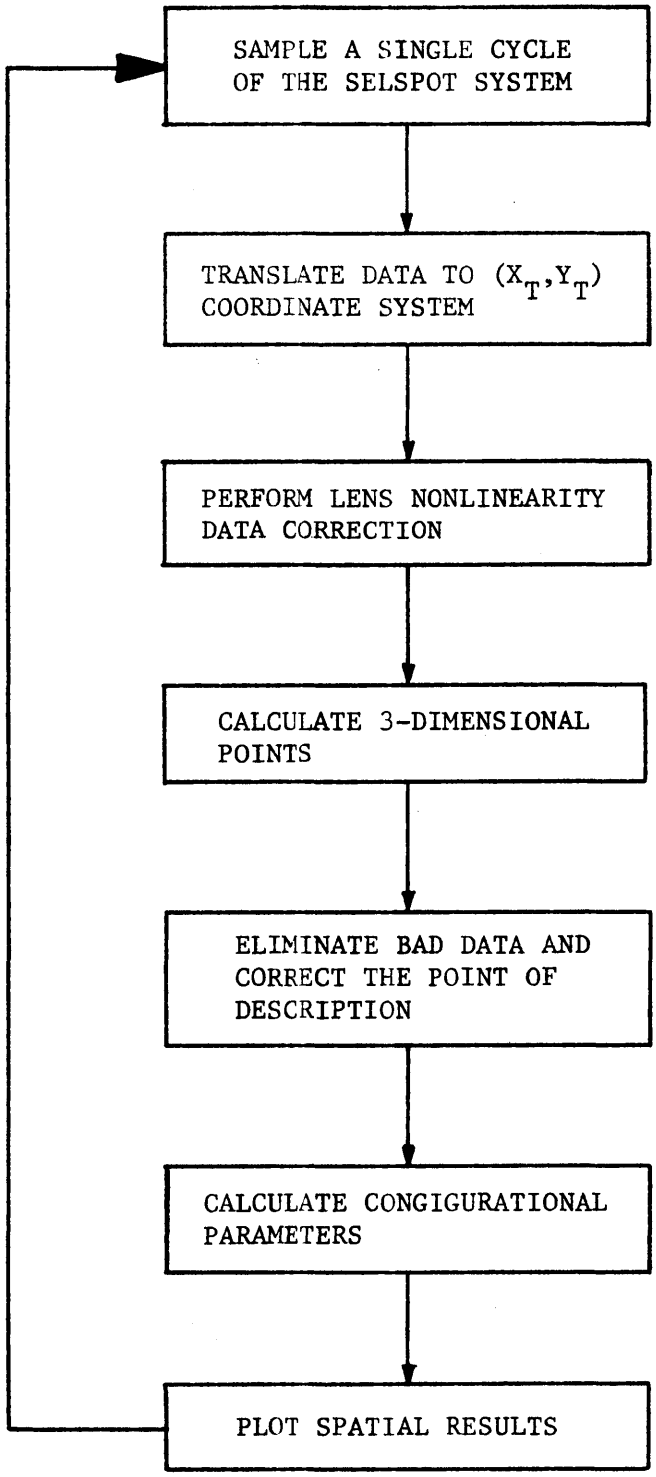

Figure 26. Flowchart for the real-time demonstration program.

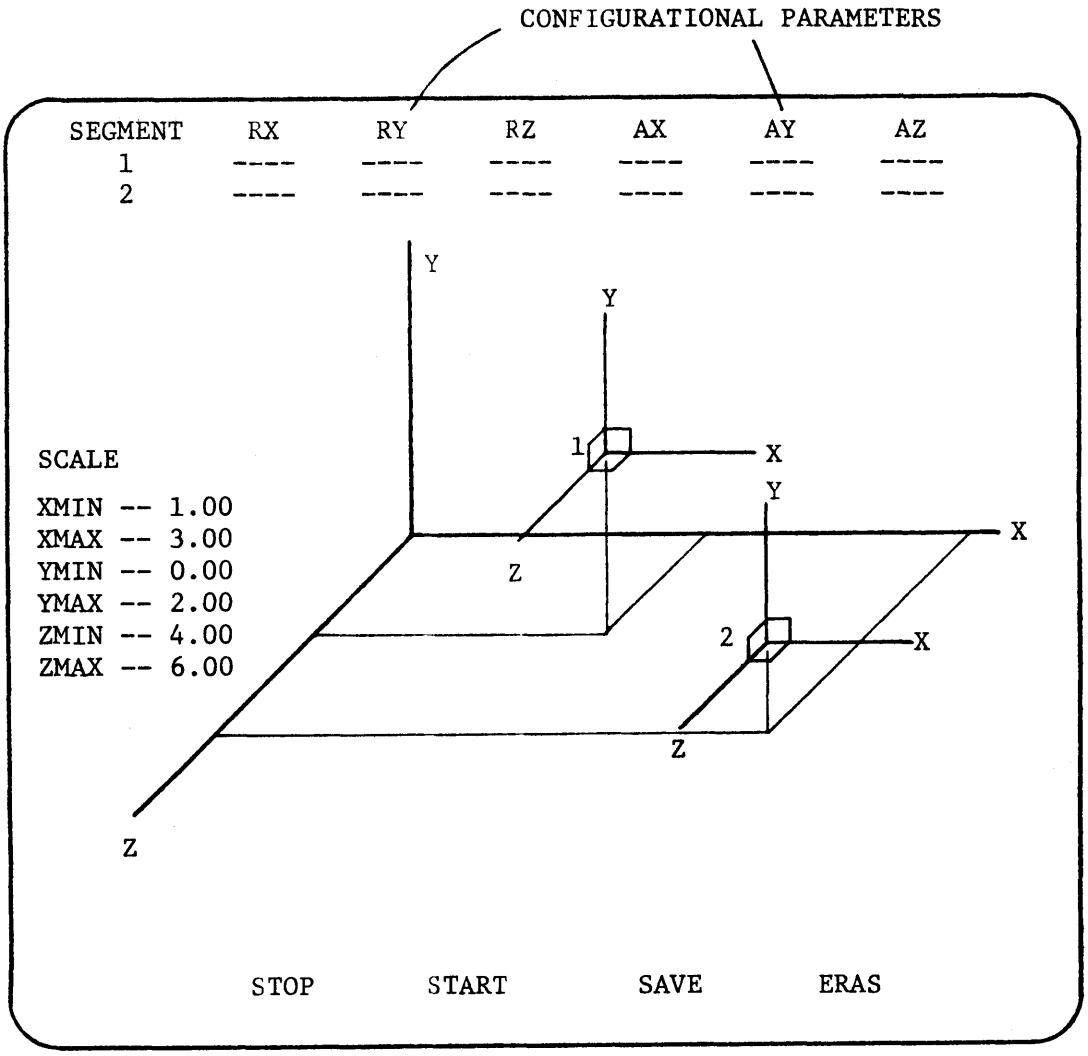

Figure 27. Depiction of the real-time graphics display.

diagnostic tool since it can present immediately a visual rendition of the processing integrity of a particular experimental situation. Thus, a simple real-time check of a laboratory configuration can be easily carried out before experimentation begins to verify that everything is in order.

7.4 FILE-ORIENTED BATCH PROCESSING

As introduced earlier, a fast-sampling file-oriented processing sequence has been implemented in the form of a multi-program Batch processing stream. The data gathering is controlled via start and stop triggers on a control box located in the experimental room. The sampling rate can be any arbitrary frequency which is a discrete cycling less than 315 Hz, the cycling capacity of the Selspot System. After the sampling is stopped by the trigger, the data, which is located in core memory, is then permanently stored and the remainder of the processing sequence carried out automatically.

To allow flexible operation, the functional tasks are divided and carried out in single-program form. The overall flowchart of the Batch stream is depicted in Figure 28. It can be seen that five programs are utilized, and that through the course of the computation sequence, a total of four data files is created. The different data files are temporary storage files and each running of the Batch stream will process the results of a new experiment and thus modify the previous set of data files.

Since the entire purpose of the processing stream is to permanently store the experimental results, the body segment configurational time

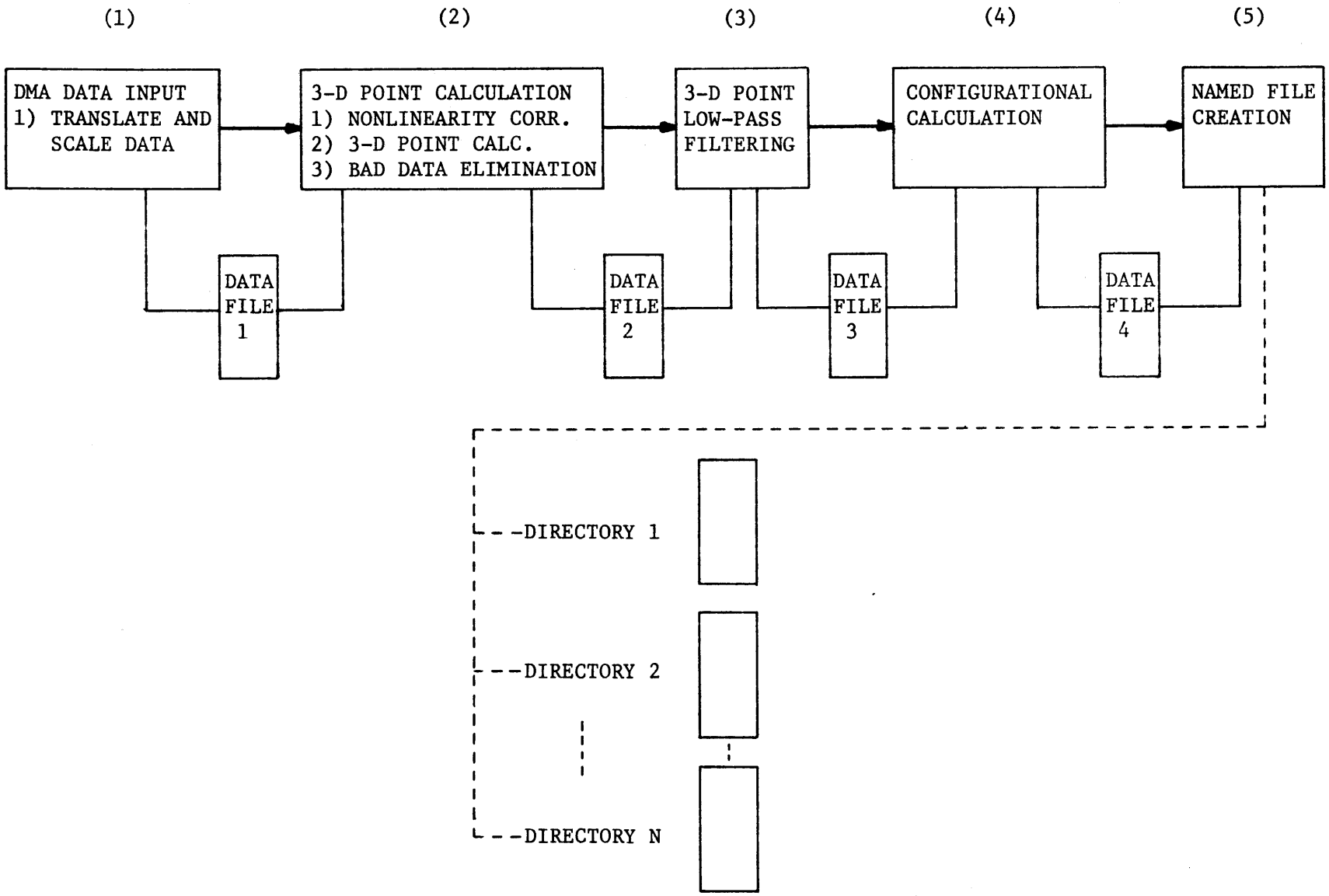

Figure 28. Flowchart for the Batch processing stream.

histories, a user-oriented file creation and tabulation system has been implemented. This operation occurs at the end of the Batch stream and allows the user to create a "result" data file with a designated name, and containing the contents of the present temporary result file. Also, the file name and a one-line description can be entered into a user directory, all of which is carried out by a few keyboard terminal responses. As illustrated in Figure 28, any number of user-named directories can be created and later accessed from the Batch stream. In this way, several experimenters can easily create named result files and maintain independent directory records of their particular files.

Each result data file contains the following information: 1) the 6 positional and orientative parameters and 2) the 9 rotation matrix parameters which describe at each time step the relationship between the body coordinate system and the reference coordinate system for each designated body segment. It is readily apparent that the result data files will be any of a range of sizes depending on the number of time steps and the number of body segments employed in the experiments. As discussed below, there are certain operations such as plotting and filtering which must access the data in a result file. The user directory thus serves another purpose, that of recording the information concerning the data file structure and size needed to access it under the programming rules of FORTRAN. The result file operational programs employ a filename directory-search subroutine which locates the necessary parameters to access the result data file.

At present, three operations can be performed on a named result file in a user directory. First, a spatial replay display of the movement of the defined body coordinate systems can be obtained for the time span of the experiment. The effect can be likened to a "moving picture replay" of the experiment in 3-dimensional graphical space. A second capability is that of obtaining precision graphs (see Figures 38-39) of the time behavior of the configurational parameters for any defined body segment in the result file. The graphics program has several user-oriented features, such as user-specified or automatic scaling, plot labeling, flexible plotting parameter specification and hard-copy output. The third operation which can be carried out, as discussed in Chapter 6, is that of result file low-pass filtering. Any file in a user directory can be accessed, the data filtered as specified, and a new filtered result file created, thus maintaining the original raw result data file. Provision is made for the new file to be listed in the user directory, thus making it possible for a directory to contain several files which are different "versions" of the same experiment. All the above programs are designed such that they can be interactively executed in a straightforward fashion by an experimenter sitting at the PDP 11/40 graphics display and input keyboard.

As a final conclusionary point, it is apparent that many experimenters will desire different types of motion descriptions than the general one calculated in the Batch stream. Further data-reduction programs are clearly required to attain the specific goals of these individual projects. The result file structure enlisted in this thesis and the user directory

tabulation can in most cases be easily employed for such modified result files. Therefore, it would be straightforward to utilize the directory concept, and hence a consistent data file structure, as a sort of "common" starting and ending point. In this way, newly-developed computational capability could be applied by several experimenters if desired, and the advantages of convenient file creation, naming and tabulation can continue to be utilized.

Chapter 8

DEMONSTRATION AND ANALYSIS OF THE TRACK SYSTEM PERFORMANCE

The kinematic-monitoring system, at the present level of development, has now been described in all respects. The overall system has been acronymed the TRACK (Telemetered (infrared information) Real-time Acquisition and Computation of Kinematics) System. This short descriptive acronym has been designated so that the overall system, consisting of the Selspot System, a DMA interface, a PDP 11/40 computer system and a software support package, can be encompassed with a single descriptive statement.

In this chapter, a demonstration and analysis of the measurement performance of the TRACK system is presented. In attempting to set forth a criteria with which to judge the performance, it was concluded that the two measurement qualities, resolution and accuracy, were the most important assessment parameters which could be studied. The relevant output of the TRACK System is the positional and orientative quantities which describe the relationship between the body coordinate systems and the reference coordinate system. Thus, it is desired to determine the resolution and the accuracy in physically-relevant terms for these output results. A quantitative statement of the performance of the TRACK System with respect to these measurement qualities would represent the most concise and relevant information with which to evaluate its capabilities. Following the analysis section is a demonstration of the capability of the system in a laboratory-structured experiment. The TRACK System was employed

to determine the time-dependent configuration at a point on a moving pendulum and the results will be presented in graphical form.

A series of simple and well-structured experimental tests were performed to address the two issues of resolution and accuracy. The experiments were performed in a similar experimental configuration to that which would be employed for human gait experiments (see Figure 35a). The reasons for examining this configuration were two-fold: 1) gait-related experiments are envisioned for the immediate future, and 2) it represents a moderately-difficult measurement situation. Since gait experiments require a reasonably large measurement volume, the cameras were positioned such that a space, no less than approximately 2 meters by 2 meters by 2 meters, was dual-camera detectable. Measurements made within this volume bordered on the range distance limit of the Selspot System for full resolution measurement.

Since the TRACK System performance is not affected by the number of body segments which are defined due to independency of calculation, all the experiments were carried out with a single LED structure. The LED structure which was employed consisted of three LEDs configured in an equilateral triangle formation, with 6 inches (152.4 mm) between each LED. In order to decouple the position and orientation calculation, the body coordinate system was defined such that its origin and the mean point $\underline{Q}$ were synonomous.

Employing this basic setup, experiments were carried out to determine the positional and orientative resolution, and the positional and orientative accuracy of the TRACK System. These tests are the subject of the next two sections.

8.1 ANALYSIS OF THE RESOLUTION OF THE TRACK SYSTEM

The resolution of a system can be defined as the smallest unit of measurement which can be consistently discerned. Thus, a straightforward method to determine the resolution of the TRACK System would be to examine the deviation of the configurational results for a set of calculations involving a stationary LED structure. In this way, the measurement unit which encompasses the deviation is a meaningful representation of the resolution capability of the System. Several expriments were carried out and a typical result is presented.

The LED structure was situated at an arbitrary location within the designated measurement volume, and was pointed in the general direction of the cameras. An approximately-timed 3-second sampling experiment at 157 Hz was performed. This sampling frequency was chosen since it could be a typical sampling frequency for any experiment dealing with low to medium bandwidth experimental phenomenon. In order to provide comparison and to study the effect of pre-configurational and post-configurational filtering, the same experimental data was processed in three different ways: 1) normal processing with no filtering; 2) normal processing and 3-dimensional point prefiltering (39 Hz cutoff); and, 3) same as (2) but, in addition, configurational result low-pass filtering (5 Hz cutoff). The results are depicted in Figures 29-34, each Figure being a composite illustration of the three processing modes for one of the six parameters (P_x, P_y, P_z, θ_1,θ_2,θ_3).

The positional plots indicate clearly the digital nature of the Selspot System since discrete levels still permeate through the LED point-

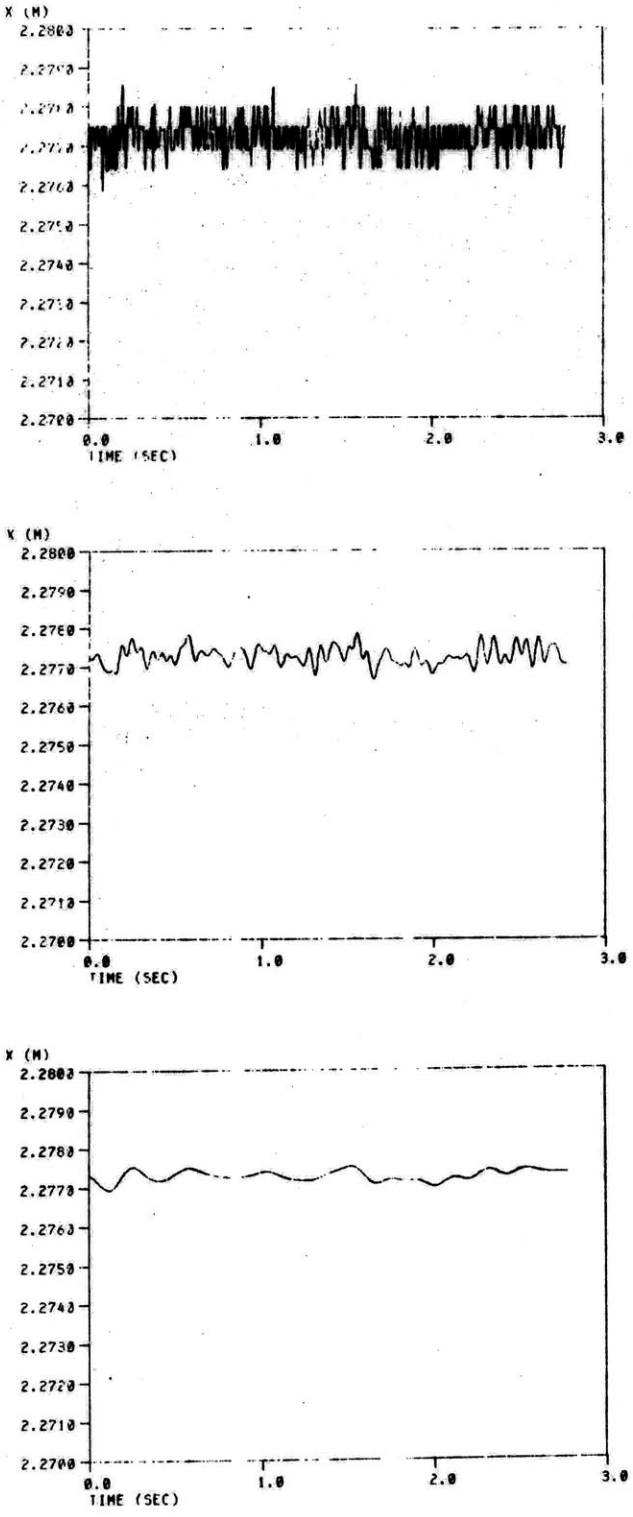

Figure 29. Stationary test of resolution; X-coordinate position (dimensional units: meters vs. seconds).

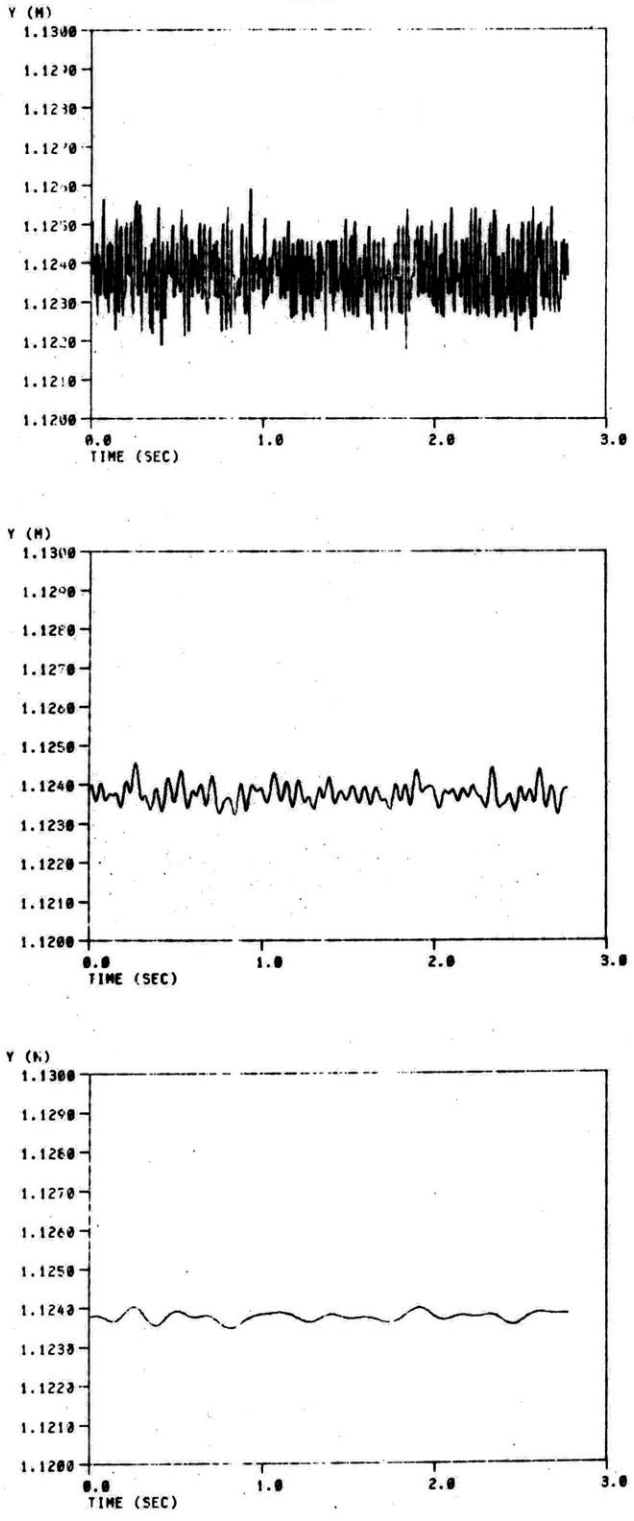

Figure 30. Stationary test of resolution; Y-coordinate position (dimensional units: meters vs. seconds).

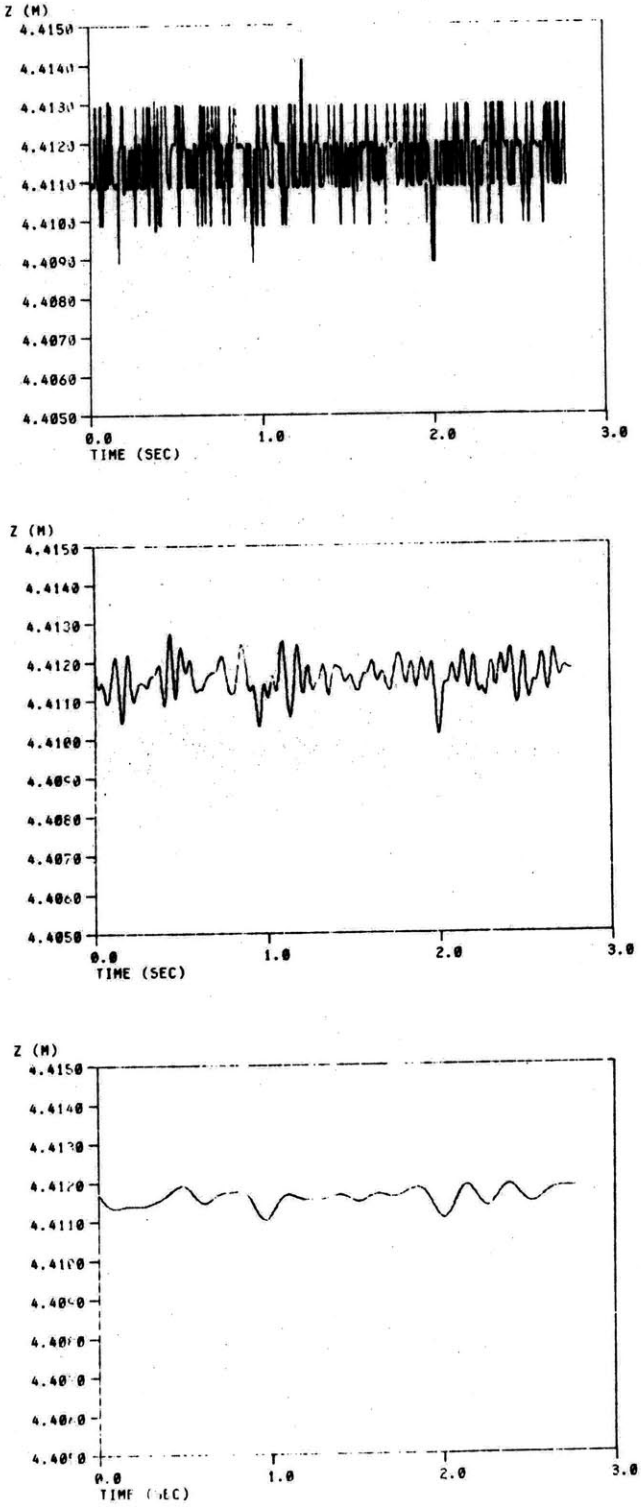

Figure 31. Stationary test of resolution; Z-coordinate position (dimensional units: meters vs. seconds).

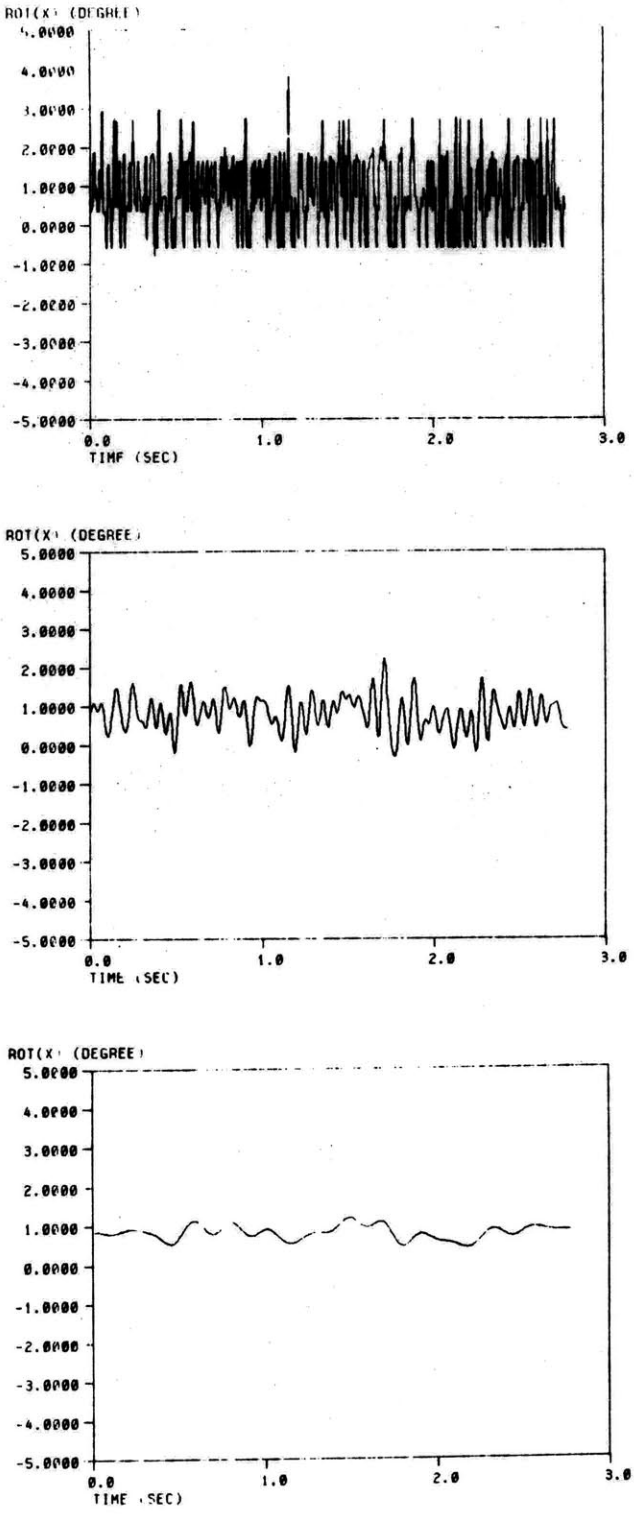

Figure 32. Stationary test of resolution; θ_1-coordinate orientation (θ_1 = Rot(X)).

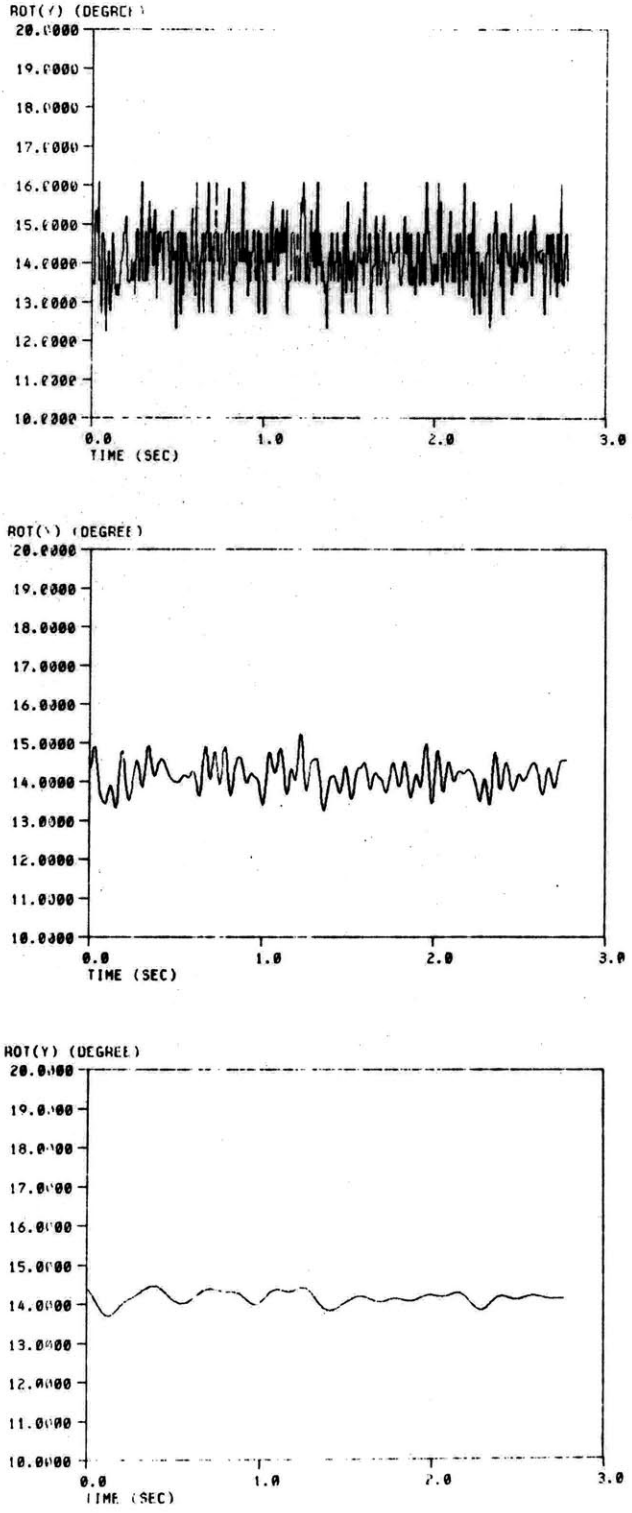

Figure 33. Stationary test of resolution; θ_2-coordinate orientation (θ_2 = Rot(Y)).

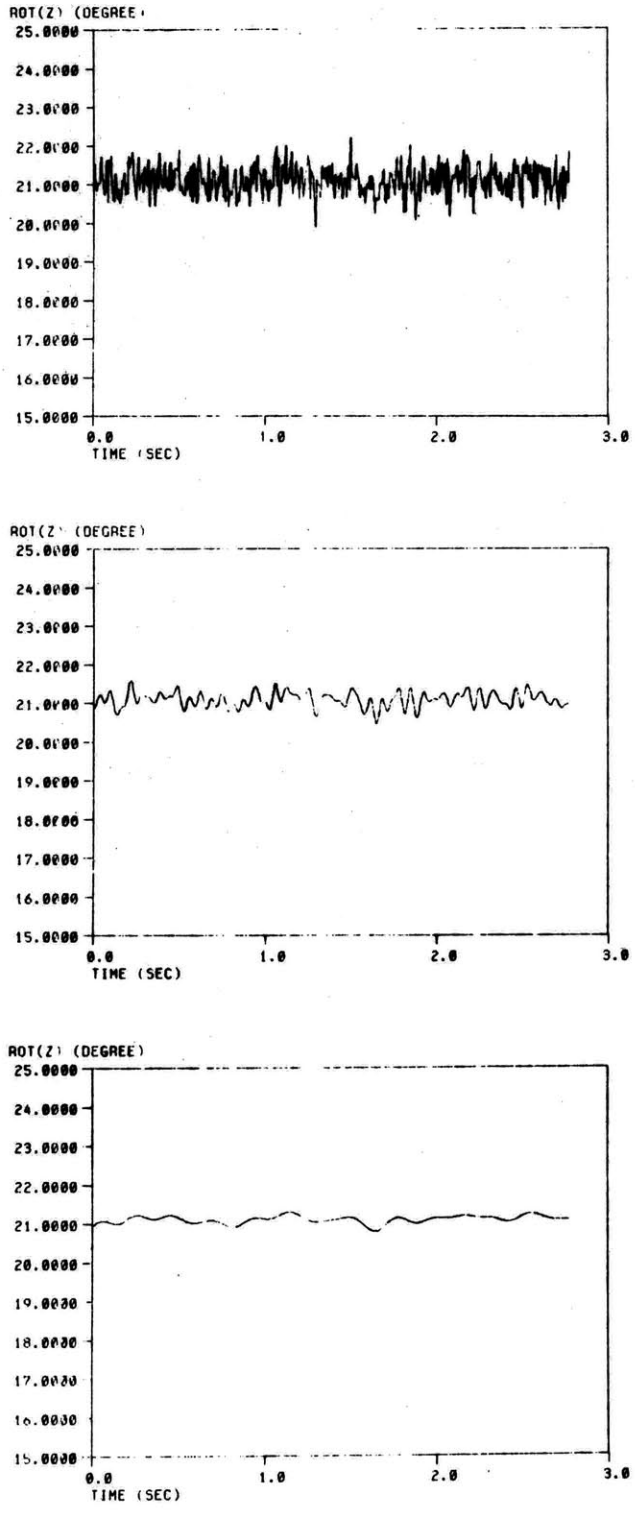

Figure 34. Stationary test of resolution; θ_3-coordinate orientation (θ_3 = Rot(Z)).

dependent results. It is apparent that filtering actually increases the resolution of the TRACK System to a level somewhat finer than the digital resolution which is represented by the Selspot System data. It can be seen that with the employment of smoothing specifications such as might be applied in a gait experiment, the resolution of the TRACK System is approximately 1 millimeter for the positional parameters of the body coordinate system origin and approximately 1 degree for the orientative rotations.

As a final note, it can be observed that the raw result parameters about the Z axis represent the extremes of resolution when compared to their counterparts. The positional resolution appears to be the worst for the Z axis coordinate while the orientative resolution is the best for the Z axis. This observation does lend itself to explanation. From a geometric point of view, it appears that the Z coordinate is subject to the greatest variation given a certain range of camera measurement error, as exhibited in the plots. On the other hand, given the LED structure positioned in a plane which is relatively close to being parallel to the X-Y reference coordinate system plane (see Figure 35a), it is reasonable that a rotation parameter about the Z axis should be the most stable. In this position, small angular movements about the Z axis are more easily detected than small angular movements about the X or Y axis, which is again a geometric realization. It is very encouraging to note, however, that filtering does effectively eliminate the high-frequency result fluctuation in such a way that the final filtered traces are very similar at all coordinate descriptions. Experiments performed at other locations

in the measurement volume had similar types of patterns and the filtering had the same neutralizing effect.

8.2 ANALYSIS OF THE ACCURACY OF THE TRACK SYSTEM

An analysis of the accuracy of the TRACK System output is not as easily carried out as that for resolution since accuracy must be examined in the framework of an absolute reference. It would be desirable, of course, to delineate experimental tests which would quantify in as simple a manner as possible the accuracy for positional and orientative parameters. Two such types of experiments have been performed which do give relevant indications for both parameters, and they are discussed separately in the following two sub-sections.

Position Accuracy Analysis Through Distance Analysis. A reasonable approach to determine positional accuracy might be that of comparing the TRACK System positional coordinates of the body coordinate system to those obtained with an independent system of measurement. With this information, some statement concerning the accuracy could then be formulated. However, the independent quantification of the coordinates is a difficult measurement task. Even if an effective direct measurement procedure could be developed, the precise location of the reference system origin would still remain to be determined. The reference origin, as defined in this thesis, is a fictitious point located at the camera 1 system focal point. It is unclear how such a point could be reliably referenced.

In view of these problems, a completely different approach was explored. It appeared that a simple and relevant assessment of positional accuracy could be obtained through linear distance measurements. In this

way, an error could be determined based on the defined distance measured with the TRACK System and the knowledge of the actual distance. This calculated error should be a valid indication of the positional measurement accuracy of the System since the whole question of accuracy, in this case, appears to center around the question of scale; that is, is the measurement scale of the TRACK System a true reflection of reality.

Such a comparison can be easily carried out employing the bad-data elimination routine discussed in Chapter 6. By utilizing this algorithm, it is possible to obtain a single percentage-error indication of the measurement accuracy which, it can be seen, really indicates the scaling relationship between the measured situation and the real situation. This type of assessment is a superior one because an error criterion based in absolute units would not necessarily indicate the scaling phenomenon and it could be a misleading result.

For the particular LED structure utilized in the experiments, the initial state position coordinates were measured with a vernier caliper to a much better accuracy than the TRACK System is theoretically capable of. An experimental test was then designed employing the LED structure and the distance variation algorithm of the TRACK System.

Contrary to the resolution parameter which is dependent only on the effect of sampling error in the system, the accuracy of the TRACK System will be directly dependent on several factors such as the camera focal distance values, camera nonlinearity effects and camera position parameters. A large error in any of these categories could severely affect the accuracy

of the results. Considering the lens nonlinearity, for instance, it is apparent that its effects are spatially dependent. That is, if no lens nonlinearity corrections were made, then it would be expected that measurements in the region near the lens neutral axes would be more accurate than measurements made elsewhere (see Figure 35a).

Based on the above observation, a straightforward experiment presents itself which will allow 1) an examination of accuracy throughout the measurement volume, 2) a study of the effect of the lens nonlinearity correction algorithm, and 3) an opportunity for relevant comparison of two different sets of measurement information.

A grid plane was defined, as shown in Figure 35b, which is parallel to the X-Y plane of the reference coordinate system and which has as its effective center the point of intersection of the camera neutral axes (camera heights equal). An array of 19 point locations was designated, as shown in the Figure, at regular spatial nodes.

Two experiments were performed, one employing the lens correction algorithm as part of the processing and the other without the algorithm. In each experiment, the percent distance variation for the LED structure was individually monitored at the 19 defined grid locations in the measurement volume. The results of the experiments are summarized in Figure 36. The depicted percent distance variations are the average of the 3 distance errors calculated for the structure (3 LEDs) for 3 continuous samples. It should be observed that the values are illustrated at the actual location in the plane where the particular measurements occurred.

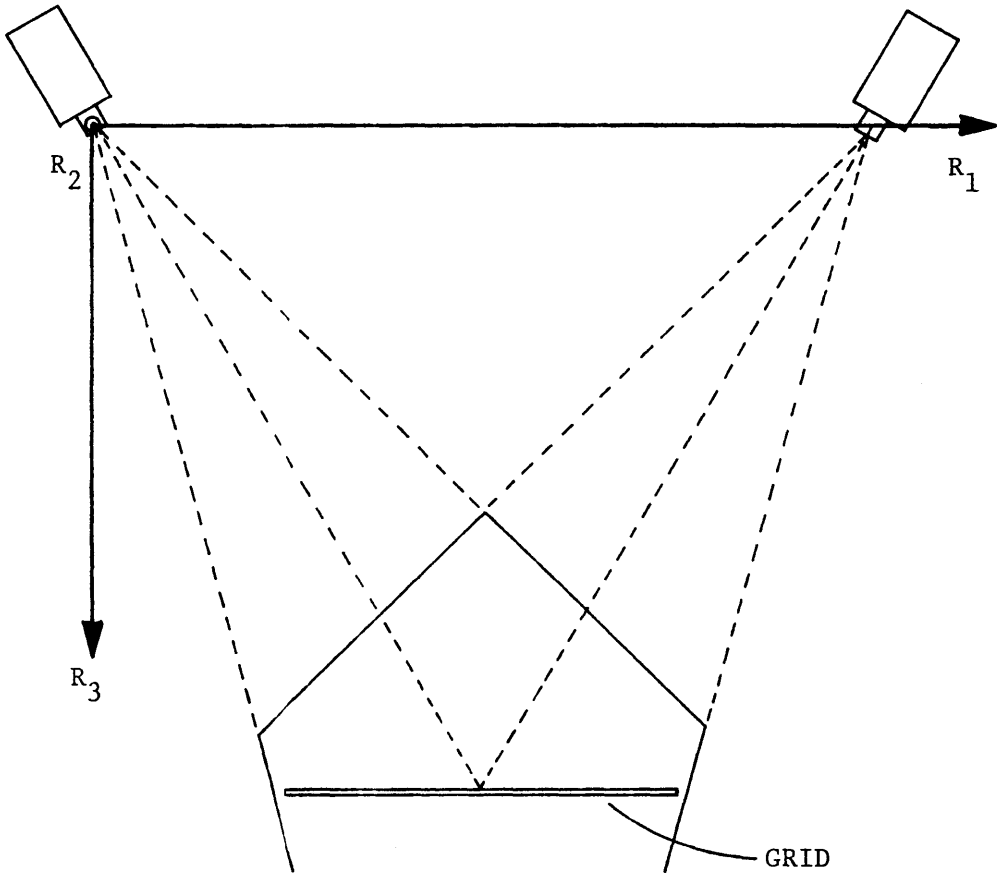

a)

NOTE: GRID
NODE-TO-NODE
DISTANCE = 1 FOOT

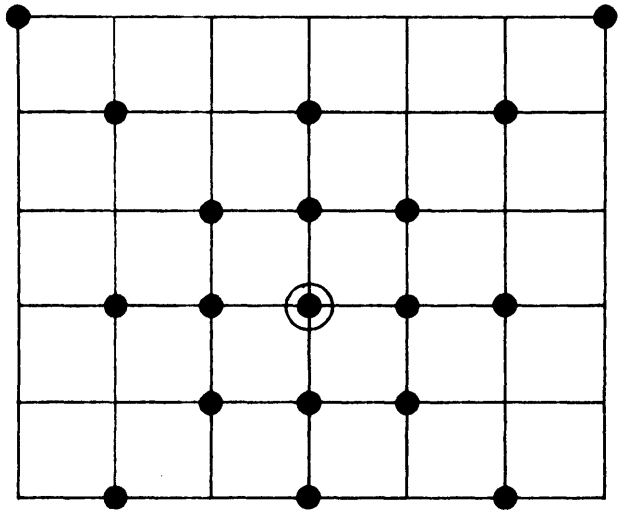

b)

Figure 35. Configuration of the distance accuracy experiment.

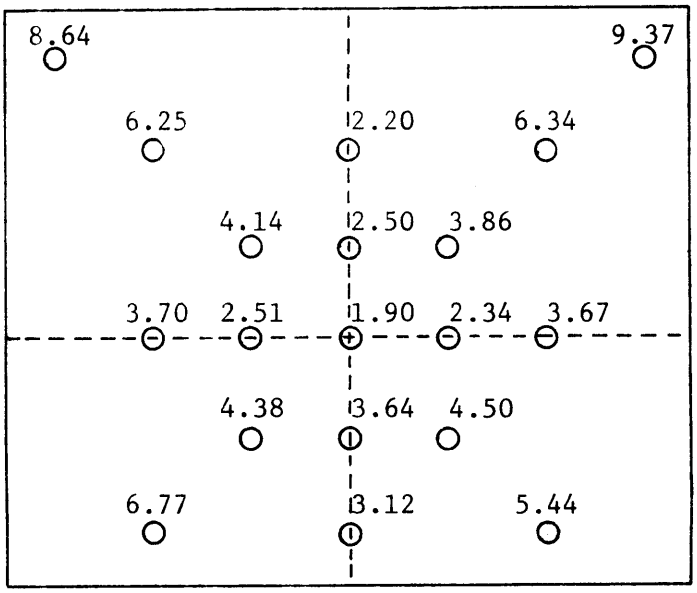

a) Uncorrected

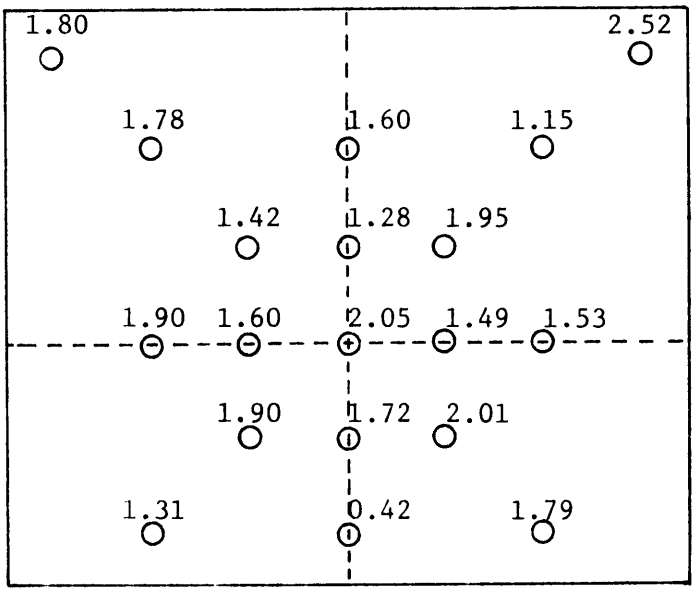

b) With lens nonlinearity correction

Figure 36. Percent distance variation experimental results.

Several observations can be made concerning the results. First, it is evident that there is some variation error in both experiments, but that the error is uniformly lower in the experiment with the non-linearity correction. Secondly, it can be observed that the variation error for the non-corrected experiment increases uniformly with distance from the grid center, reaching a maximum approaching 10%. This result gives further support for the nonlinearity conceptual model employed in Chapter 4 and is vivid illustration of the need for the algorithm. Finally, it can be seen that the variation error for the corrected experiment is consistently between 1% and 2%, with the average of the samples being 1.64%.

The results of the nonlinearity-corrected experiment are fundamentally encouraging for they appear to indicate that the TRACK System, on a percentage basis, reflects reality in a respectable fashion. On the other hand, the implication of the percent distance error result is that any distance or position measurement, large or small, is subject to approximately a $\pm$ 2% error. For large distances, this represents an appreciable error in absolute units, and some unrelated experiments have tended to bear out this observation. However, further experimentation is needed to determine the validity and the implication of the scaling error premise. Some final remarks concerning the results are presented in the "Conclusions" section of this Chapter.

Analysis of Orientative Accuracy. In order to study orientative accuracy in the most straightforward manner, an experiment was conceived which allowed the evaluation of pure rotation increments about a single

axis. The LED structure was attached to the metal rim of a bicycle wheel, and was situated within the measurement volume in a plane parallel to the X-Y plane of the reference coordinate system. The wheel was free to rotate, and the resulting orientative change was measured as a pure rotation about the Z-axis. Thus, a fixed rotation of the bicycle wheel could be directly monitored as a pure Z-axis orientative parameter result. The selection of this particular type of physical arrangement also allowed a complete 360° orientative analysis.

The bicycle wheel was precisely rotated by increments of 10° through the 360° range, with approximately 10 samples being taken at each position. To more effectively depict the results, they were translated a few degrees so as to be synonomous with a 0-360° scale. The mean and the standard deviation of the absolute parameters at each increment was determined, and the results are given in Table 4. They can be seen to indicate a consistent rendition of the rotation throughout the entire 360° range. Rarely is the accuracy error of the mean more than $\pm$.5 degrees, and it can be seen that the standard deviation of the samples is also consistently below .5 degrees.

A valid description of the orientative accuracy in percentage terms can be approximately specified by $\pm$ 1 degree error/360 degrees = $\pm$ .3%. Since orientative accuracy is a more pattern-oriented characteristic than spatially-oriented one, it is readily apparent that it is not as dependent on calibration parameter errors as is positional accuracy. An error in any of the calibration parameters will have a minimal effect on

Table 4

ORIENTATIVE ACCURACY RESULTS

ABSOLUTE MEAN (DEGREES)	STANDARD DEVIATION (DEGREES)	ANGULAR INCREMENT (DEGREES)
10.154	.225	10.154
19.848	.248	9.694
29.534	.163	9.686
39.382	.312	9.848
49.655	.296	10.273
59.952	.320	10.297
70.133	.370	10.181
79.690	.183	9.568
89.845	.446	10.155
99.958	.404	10.113
110.173	.369	10.215
119.918	.248	9.745
130.085	.241	10.167
141.552	.280	11.467
150.491	.498	8.939
159.983	.341	9.492
169.458	.227	9.475
180.229	.277	10.771
189.567	.184	9.338
200.554	.344	10.987
210.326	.269	9.772
219.654	.281	9.328
229.507	.106	9.853
239.602	.283	10.095
250.124	.333	10.522
259.758	.298	9.634
269.905	.239	10.147
280.293	.167	10.388
290.060	.305	9.767
299.926	.241	9.866
309.897	.334	9.971
320.229	.193	10.332
330.244	.320	10.015
340.260	.357	10.016
350.277	.424	10.017

the orientative accuracy since the local pattern integrity is essentially maintained, and thus the integrity of the accuracy.

8.3 CONCLUSIONS

The TRACK System's performance, although judged by admittedly small numbers of well-structured experimental tests, appears to be at a level commensurate with optimistic expectations based on the precision of the hardware system.

The positional resolution of the TRACK System, by taking advantage of digital filtering, can attain better discernment than the hardware limits of the Selspot System itself. The resolution and accuracy of orientative parameters appear to approach theoretical limits, considering the geometry of the LED structure and the measurement error in the LED points. A simple thought experiment can illustrate the basis of this observation. In the orientative calculation, the distance from each LED to the mean point Q of description is approximately 90 millimeters. Considering a single LED, a 1 millimeter positional error at that distance could be perceived as a maximum angular error of (1mm/90mm)(57.3) = .64 degrees. Although the actual situation is certainly more complicated than this simple geometric calculation, it does indicate the probable order of magnitude resolution and accuracy which can be theoretically expected in the face of measurement error. As a final note, it can be seen that the implication of the above exercise is that the orientative resolution and accuracy is directly dependent on the size of the LED structure.

The positional accuracy, as interpreted through the distance variation parameter, defies clear interpretation and evaluation. Of primary concern

is the lack of a suitable basis with which to judge the nature of the percentage error. It is evident that the accuracy of the calibration parameters is of direct importance and relevance since they determine the scaling nature of the TRACK System and hence, the positional accuracy. The key to understanding the kind of positional accuracy which can be achieved with the TRACK System rests with a better knowledge of the effects of the calibration parameters. Only when there is evidence concerning their nature and their accuracy can a judgment be made as to the acceptability of the present positional accuracy and the possibility or feasibility of improved performance.

8.4 DEMONSTRATION OF THE TRACKING CAPABILITY

As a final statement of the performance and capability of the TRACK System, the results of an experiment employing a two degree-of-freedom swinging pendulum will be presented. The experiment was configured, as shown in Figure 37, such that all six configurational parameters would be involved in describing the motion patterns of the pendulum.

The experiment consisted of a 10-second sampling phase as the pendulum underwent free swinging. Because of the long sampling duration desired, the sampling frequency was set at a somewhat low frequency, 39 Hz. The experiment was prefiltered at 7 Hz and post-filtered at 2 Hz. The positional time traces of the body coordinate system are reproduced in Figure 38 and the orientative time traces are given in Figure 39. Due to damping in the pendulum system, the motion patterns slowly decayed, as monitored by the TRACK System. It should be pointed out that as a result

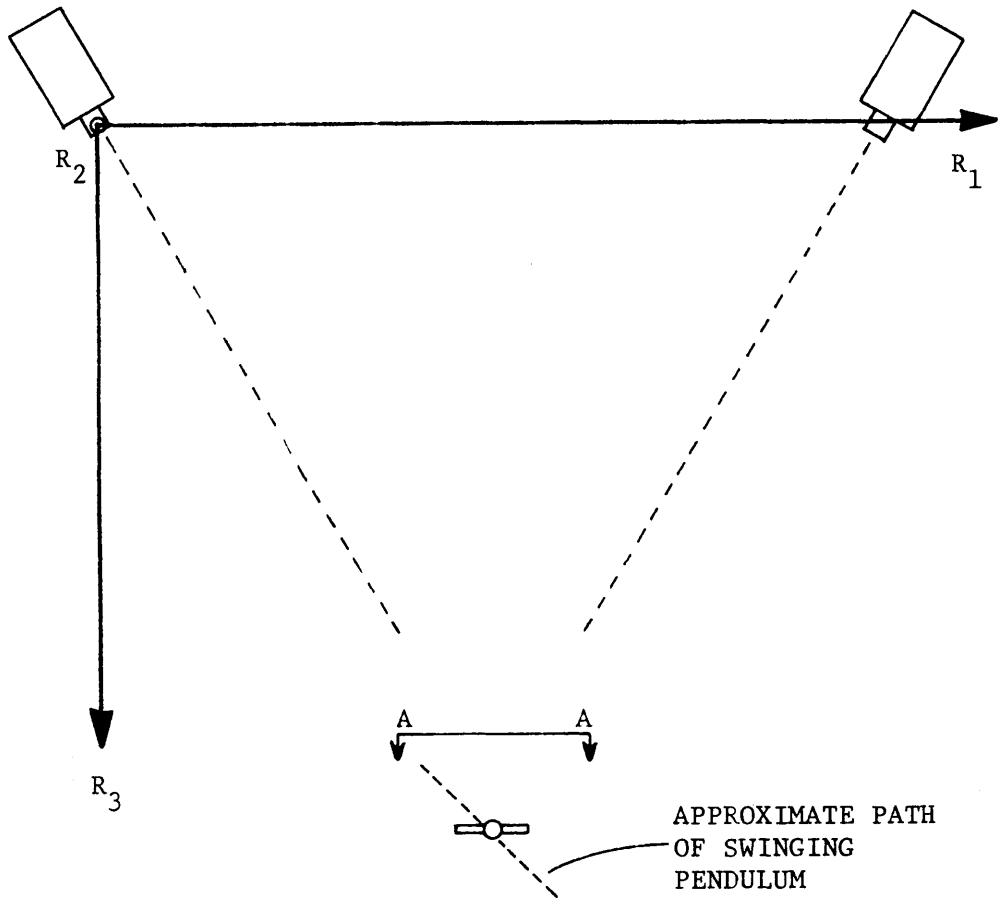

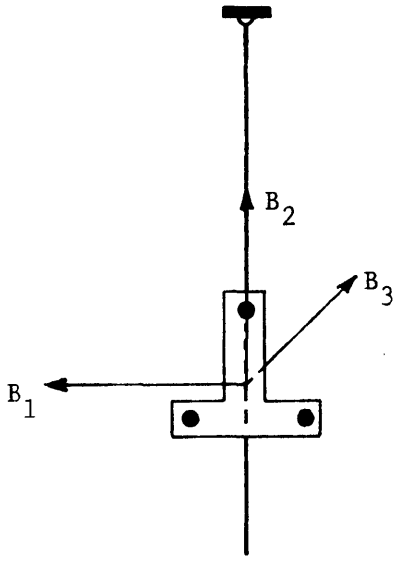

SECTION A-A

Figure 37. Arrangement of the swinging pendulum demonstration.

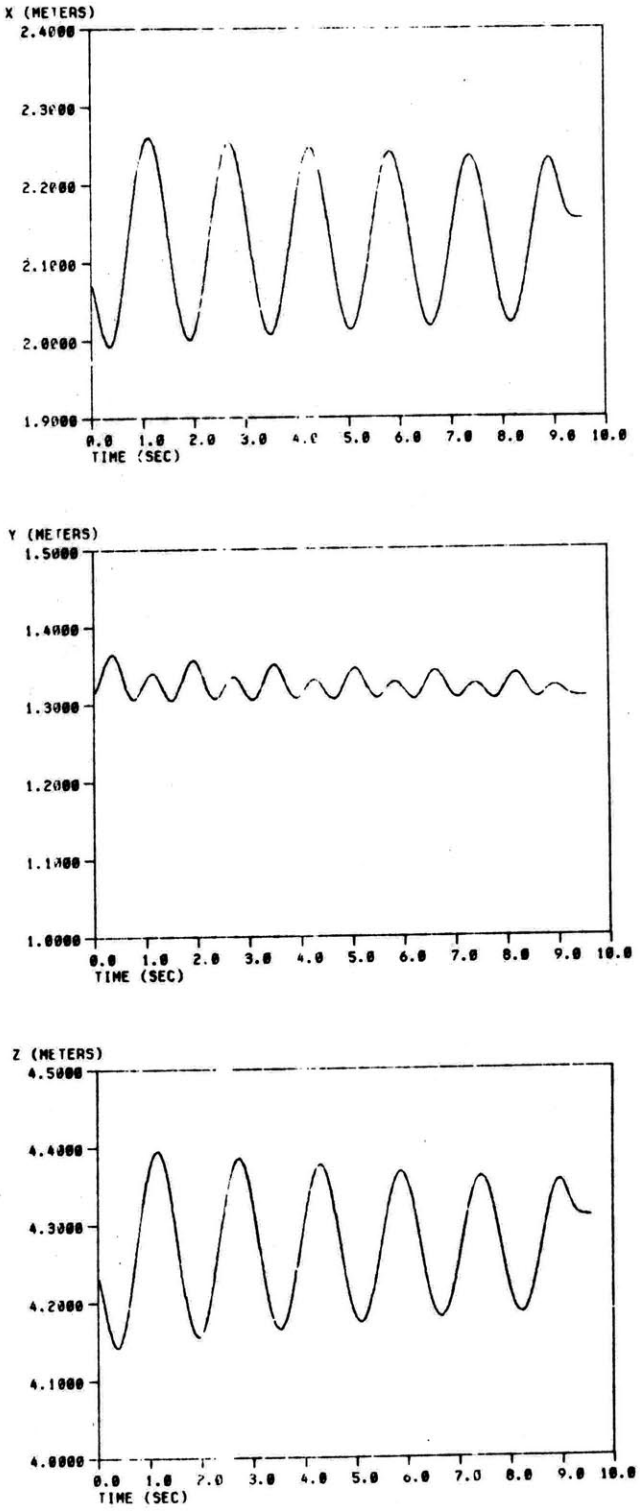

Figure 38. Positional traces of the swinging pendulum--body coordinate system $\underline{B}$ with respect to reference $\underline{R}$ ($X=B_1$, $Y=B_2$, $Z=B_3$).

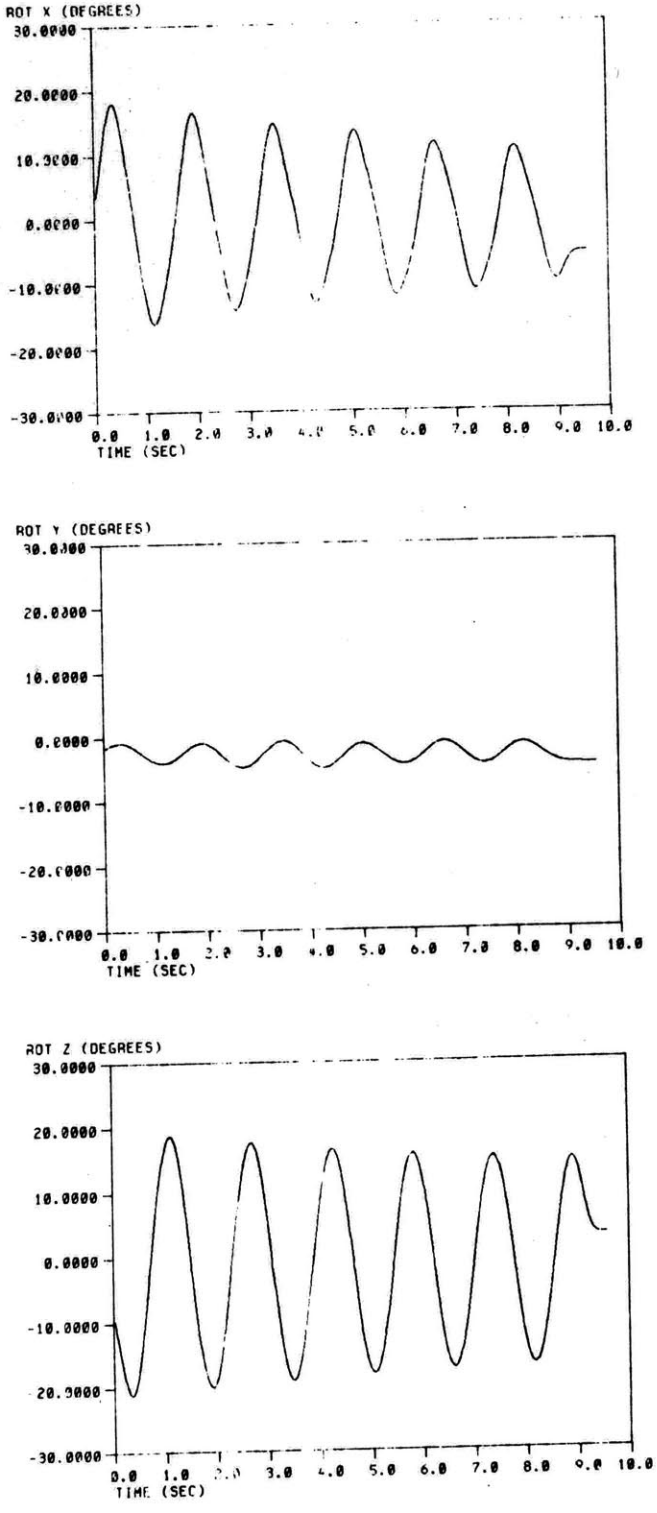

Figure 39. Orientative traces of the swinging pendulum--body coordinate system $\underline{B}$ with respect to reference $\underline{R}$ (ROT X=θ_1, ROT Y=θ_2, ROT Z=θ_3).

of the LED structure attachment, the actual point of configurational description in this case was not "exactly on" the pendulum, which accounts for the unequal displacement extremes in the Y direction.

Chapter 9

THE LARGE-VOLUME TRACKING PROBLEM - A PRELIMINARY DESIGN SOLUTION

In view of the discussion in Chapter 1 concerning the proposed blind-mobility aid research, it is evident that the utilizable measurement volume of the TRACK System in its present form is not sufficient for this application. The present usable volume is on the order of 10-12 cubic meters whereas the desired volume is on the order of 400 cubic meters (10m by 20m by 2m). The approach for meeting this desired tracking capability poses a severe design challenge.

A thorough examination of this problem is not within the scope of this thesis. However, an attempt will be made in this chapter to introduce and conceptualize the problem, and to propose a design solution which appears to hold practical promise. The original problem statement of Chapter 1 was an ambitious one, and the problem to be addressed here is one of the central issues in the progression towards the final goal.

9.1 OVERVIEW OF THE PROBLEM

In basic terms, the problem to be addressed is that of increasing the effective 2-camera measurement volume of the TRACK System. An approach will be undertaken which attempts to meet this goal while still employing the TRACK System as presently configured, and with moderate capital investment.

The obvious and most effective way to increase the measurement volume is to actively move the camera in a sort of tracking fashion. In

this way, there is an effective dynamic measurement volume which is always encompassing the mobile human subject. This straightforward approach, however carries with it some important ramifications. It can be seen that it is now necessary to determine in real-time the transformational relationships between the camera coordinate systems and the reference coordinate system. Although the TRACK System is not presently configured to handle complete 3-dimensional angular and positional coordinate system disparity, it would be a straightforward addition so as to allow complete freedom in terms of the design of the tracking technique. It is readily apparent that there would be many practical problems associated with accurately measuring the 12 transformational parameters in real-time if they were all employed. In addition, the computational time involved in carrying out camera data transformations (trigonometric calculations) may be prohibitively long in view of the computations which are already required, the overall cycling bandwidth which is desired, and the amount of processing capability which can reasonably be brought to bear on the problem.

It is evident that any design for moving the cameras in a tracking fashion, in order to be practical, must minimize the measurement problems and the computational overhead. Two designs will be presented which reasonably approach the problem in fundamentally different manners and which are cognizant of the above discussion, with one having then been selected for further discussion.

The two designs are depicted in schematic form in Figure 40. Each design is a single degree-of-fashion tracking system, the main difference

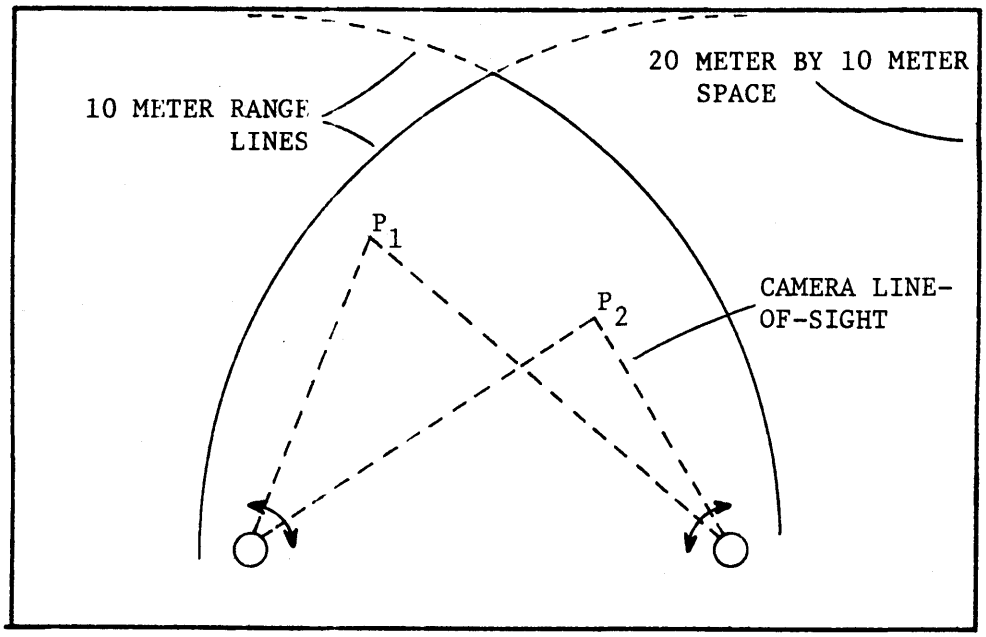

a) Rotary tracker

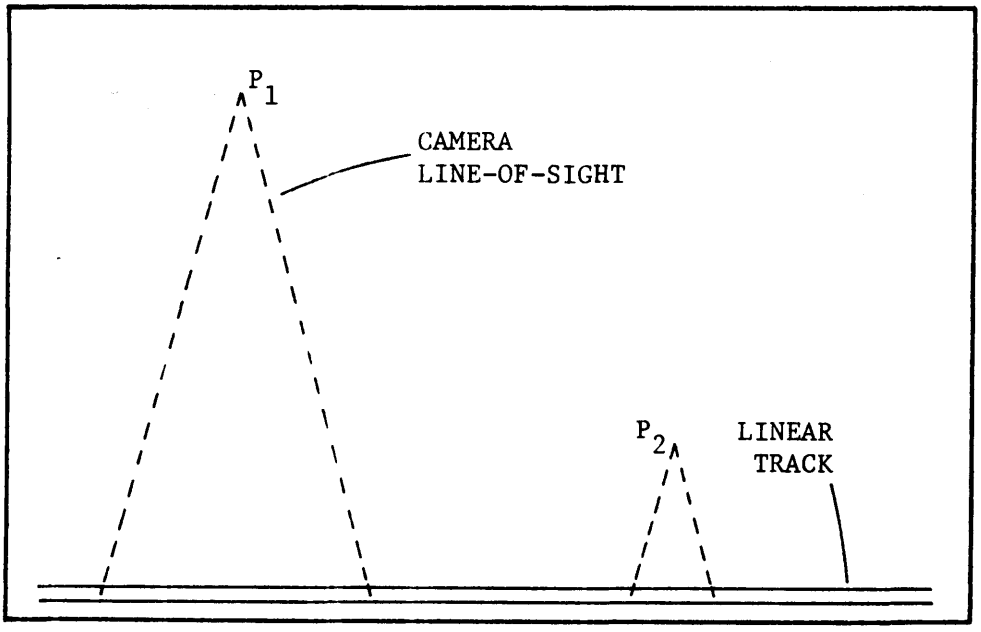

b) Translational tracker

Figure 40. Two approaches to the large-volume tracking problem.

being the degree of freedom which is employed. In Part a), the cameras are mounted on tripods with rotary actuators which can control rotation about the vertical tripod axis. Each actuator operates independently and responds to a control signal which attempts to maintain the LED image points in the view of each camera. A rotary encoding device is located on the moving axis to measure the angle of rotation in real-time. In part b), the tracking degree of freedom is a linear one. Each camera is mounted on an independently-controlled camera mobilizer which translates in a precise fashion on a linear track, and can measure its movement. The control problem is similar in this case, except that the control compensation is manifest as a linear movement of the camera mobilizer.

The linear mobilizer has been chosen for further discussion since it appears to hold the greatest promise of effectively meeting the design goal. The rotary tracker, although simpler in terms of mechanical design and system components, has associated with it several undesirable characteristics which diminish its attractiveness. There are four distinct problems: 1) range of volume, 2) cost of encoding components, 3) computational overhead, and 4) geometric implications.

As a result of the limited range of detection (approximately 10 Meters) of the LEDs, the actual measurement volume of the rotating camera design would be limited to the overlapping volume within 10 meters of each camera (see Figure 40). This situation clearly represents a severe and undesirable concession in terms of measurement ability.

In terms of the encoding components, it is readily apparent that very accurate angular measurements must be made since a small angular error can be manifest as a sizeable linear distance at a large operating range. To match the resolution of the TRACK System (1mm) at 5 Meters, for instance, an encoder capable of resolving .01° (36,000 units) is required. Reliable measurements at this order of resolution or higher would require expensive, high-precision components.

The computational overhead in this case centers around a real-time dynamic axis-transformation which must be carried out for each data point. Although clearly an improvement over the general case (3-axis transformation), it nonetheless represents further time-consuming trigonometric calculations to be executed in an already computation-laden situation.

Finally, the geometric considerations concerning LED viewability and 3-dimensional point calculation, which were discussed in Chapter 6, are completely violated in most parts of the measurement volume. This implies that calculations may be compounded in their inaccuracy at some locations, and problems of viewability may be manifest at others. To maintain measurement reliability, this kind of situation must be avoided.

The linear mobilizer approach represents an advantage in all of these areas. It can be seen that the total measurement volume is determined only by the length of the track and the detection distance. Although the width of the volume rectangle may be somewhat less than desired, the length dimension is unrestricted.

Since the mobilizers move in a linear fashion, the other problems discussed are minimized. As presented in the next section, low-cost

encoders can be employed for the linear tracking since there is a one-to-one measurement correspondence. In addition, there are no dynamic transformations to be carried out since there are no rotary degrees of freedom. It can be appreciated that only an initial set of planar rotation factors need be found, and later applied to the data. Therefore, in the real-time processing loop, only a few multiplication operations need be performed to transform the data, as opposed to the lengthy trigonometric operations in the previous case. Further, it can be seen that once the desired geometric configuration of the cameras on the mobilizers has been set, this relationship remains intact for all the ensuing measurement possibilities, representing a very important advantage.

The linear mobilizers, although conceptually elegant, do clearly present a challenging design problem. Precise vibration-free movement is a requirement as well as linear measurement capability over large distances. In spite of these types of difficulties, it is the opinion of the author that it represents a straightforward and effective approach to the problem, and a further discussion of the design is presented.

9.2 A DESIGN SOLUTION -- TWO INDEPENDENTLY TRANSLATING CAMERA MOBILIZERS

There are several practical mechanical design problems which must be overcome in order to implement the mobilizer approach. A design approach aimed at resolving some of the major ones is presented in this section. The major design issues can be delineated as the following: 1) a precision-translating set of camera mobilizers is required; 2) a power system for moving the cameras is required and 3) a linear distance measurement system is needed over the tracking distance.

A further definition of the actual measurement needs is in order. It is a requirement, as shown in Figure 41, that a stationary global coordinate system be established in the laboratory room, particularly in the case of blind mobility-aid simulation experiments. It can be seen that with proper location of the global coordinate system, the only difference between the stationary-camera situation and the present one is the fact that there are now two positional coordinates which must be measured, and that the real-time values must be dynamically placed into the computer core locations which represent the two parameters in the 3-dimensional point calculation.

A preliminary conceptual design of a camera mobilizer which confronts the above-mentioned issues is given in Figure 42. A precision-moving mechanism can be afforded by a triangular-based support table guided via three linear bearings on a precision dual-shaft linear track. Several manufacturers market these types of movement components and have developed straightforward techniques for constructing large-distance precision track-ways at moderate cost. Each mobilizer is independently powered by a direct-drive electric motor and wheel arrangement. A survey has been carried out, and drive components are commercially available which can meet the performance specifications entailed with such a configuration. In this way, the power system can be of compact design and possess a minimum of undesirable dynamics (backlash, slip, etc.). In addition, the camera mobilizer can effectively translate over large distances if required since the entire system is self-contained, and independent of any particular track configuration.

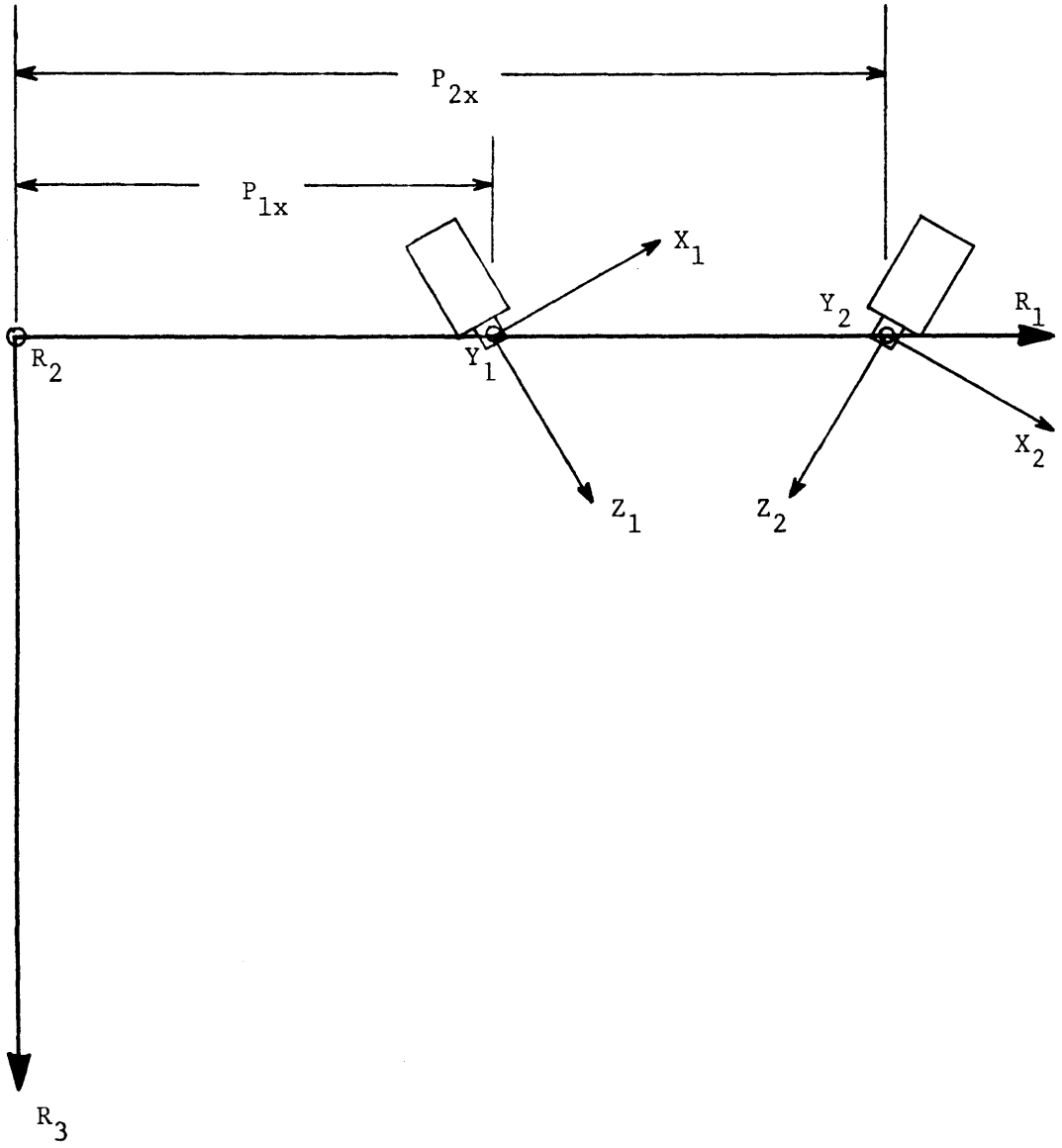

Figure 41. Coordinate system placement for single-dimension real-time measurement.

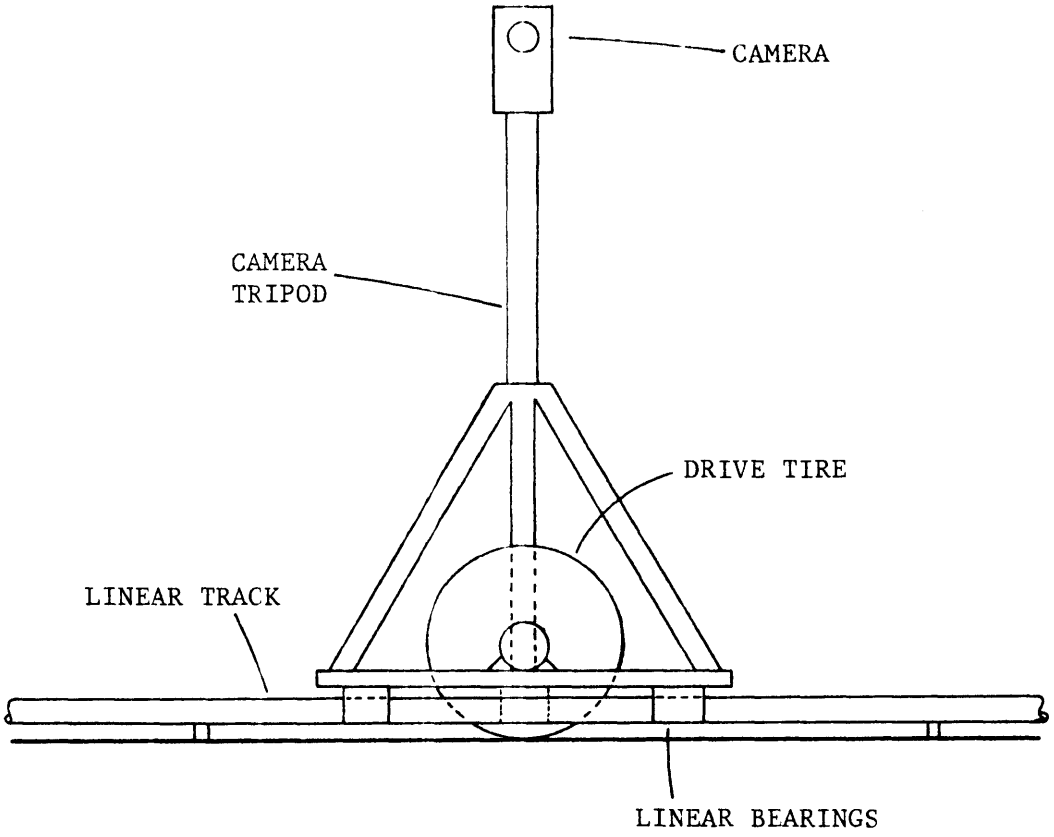

a) Front view

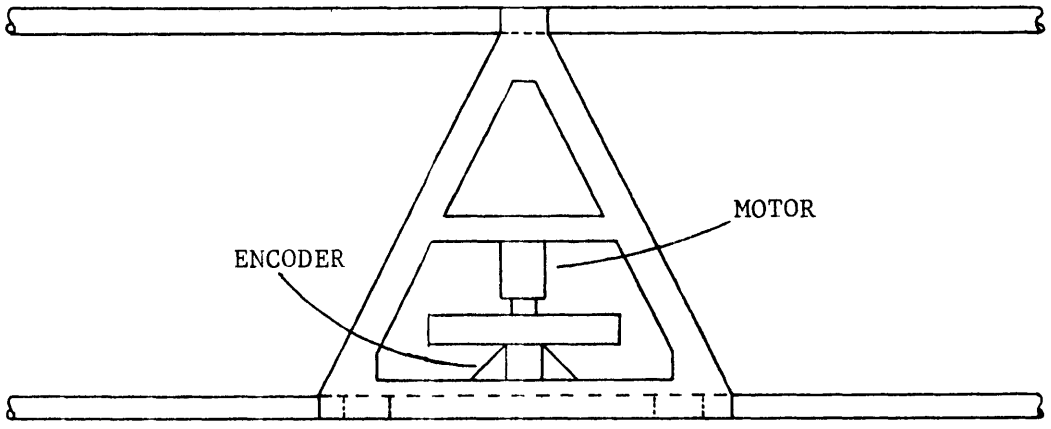

b) Top view

Figure 42. Sketch of a camera mobilizer design.

In view of the earlier discussion concerning the measurement situation and in line with the concept of a self-contained mobilizer system, the problem is addressed employing a measurement system consisting of two basic components. They are: 1) an angular encoder mounted on each mobilizer drive wheel, and 2) a set of absolute position markers attached to the track. Each angular encoder, after suitable conversion, represents an efficient self-contained method of precisely measuring the linear translation, and it can be seen that the length of the track is an unimportant issue in this case also since the wheel rotation measurement is not spatially dependent.

It is apparent that the encoding system has no inherent absolute reference to the global coordinate system since a typical encoding device can measure only the discrete changes caused by a movement. Also, any occurrence of slippage or creep in the system between the wheel-riding surface and the measurement device will introduce errors. To address these problems, the second component of the measurement system, an absolute position indication system, comes into play. With proper design, it could consist of simple components, such as opaque markers and a photoelectric-related emitter and detector. A limited number of the markers could be precisely and permanently attached to the track, and the sensor mounted on each camera mobilizer. Through proper arrangement of the components, the movement of a mobilizer past a marker could be precisely detected by a temporary blockage of light between the emitter and the detector.

Through the synthesis of a suitable start-up procedure, knowledge of the translational direction (from the encoding device) and sensor-related arithmetic logic, the encoding device data could be given absolute significance as well as be examined and corrected for errors. The configuration of the system could be such that the positional information would be updated in the main processor, the PDP 11/40, in real-time such that each iteration of the 3-dimensional calculation always utilized the most current information (see Figure 43).

9.3 THE TRACKING AND CONTROL PROBLEM

During an experiment, it is required that the LEDs being employed always remain in view of both cameras. A reliable technique is needed to formulate a control signal which is indicative of the need for camera movement, and a suitable controller designed to command the correct motor movement. In considering a technique to formulate a control signal, it is clear that the LED camera data represents the most readily available and direct means of forming an error indicator. In view of the possible unreliability of attempting to track a single LED, it is proposed that an average (X-data) of all the detected LEDs for a particular camera be found. This would be a more reliable indication of the location of the LEDs, and an error signal could then be formulated for each mobilizer based on the difference between the average and the Y_T-axis of each camera.

At first examination, it would seem that a reasonable way to calculate the error signal would be through the real-time execution of a small algorithm in the main processor, the PDP 11/40. The incoming

data could be processed, an error signal calculated and then output to a mobilizer controller. This approach is not recommended for two reasons. The first disadvantage relates to that of computer overhead. As discussed previously, any further computations which can be avoided by the main processing system through logistic means should be investigated. In this case, it would be desirable for a small microprocessor or an advanced logic system to carry out this same function without encumbering the main system. The second reason centers around the question of independency. It would be advantageous for the real-time control of the camera mobilizers to be maintained as an independent process apart from the main processor. In this way, a fairly simple inner-loop function can be carried out independent of higher-level more complicated functions with lower system reliability. In addition, the computer structure and the experimental protocol can be simpler in view of the independence of this control operation.

The control algorithm itself can take on a straightforward design since the control problem is not of an extraordinary nature. However, since the setting of the camera angle does affect the nature of the control signal, and because different experimental situations may require unique dynamic response characteristics, it is recommended that a computer-based controller be implemented to provide flexibility.

In summary, two important real-time functions have been described, 1) the measurement of positional information and 2) the control of the movements of the camera mobilizers. An overall block-diagram schematic

of their implementation is given in Figure 43. It can be seen that they are also independent functions and it is suggested that they be treated as such. However, since they both require some arithmetic processing, a shared computational processor with dual real-time responsibilities is envisioned.

The presentation of a preliminary design for a large-volume tracking was presented for two reasons: 1) to illustrate a design approach which appears to hold practical potential and 2) to illustrate the integrity of the present TRACK System design. The present system as configured can be expanded to this new capability with minimal change in its processing algorithms and overall procedures.

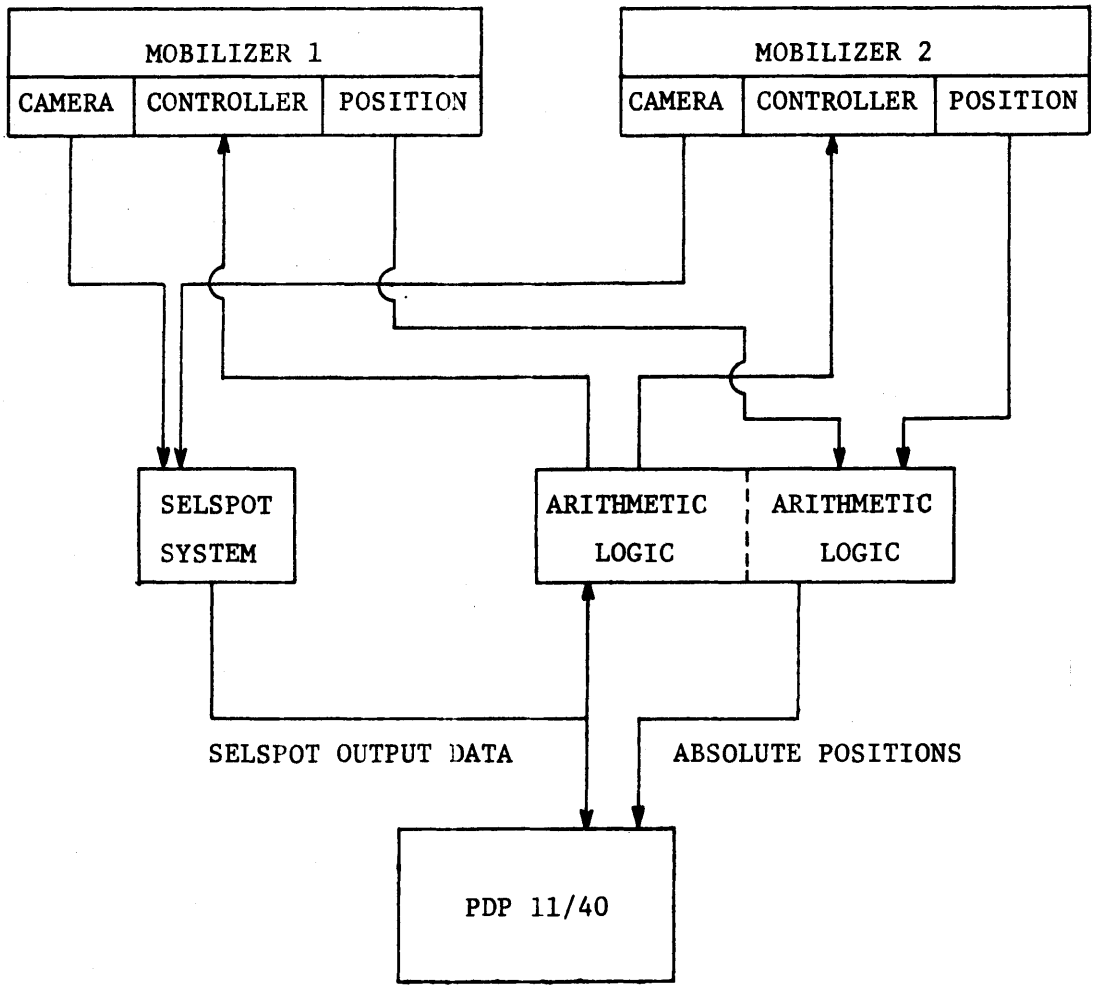

Figure 43. Information pathways for the moving camera situation.

Chapter 10

CONCLUSIONS AND RECOMMENDATIONS FOR FURTHER DEVELOPMENT

In Chapter 1, a conceptual problem statement was set forth. In response to that statement, a system design was conceived and a first stage of its implementation was achieved, as presented in this thesis. The TRACK System, the acronymn for the overall software-hardware design solution, is able to accurately track the 3-dimensional motion patterns of up to 10 body segments at arbitrarily-defined points of description. The ability to track in real-time has been demonstrated, although not presently at a level of bandwidth to have direct experimental application. The large-volume tracking problem has been examined in a preliminary design, and it has been shown that it could be implemented with only minor changes to the present form of the TRACK System. In view of the development to date and the scenario for further development, the overall conceptual design is concluded to be a fundamentally sound means of approaching the problem statement.

Concerning the issues of further TRACK System development, the discussion will follow the lines of the present state of the system, real-time processing and large-volume tracking. The main issues relating to the TRACK System in its present stage of development center around the calibration of the system. The overall calibration sequence can be somewhat unwieldy if frequent changes of camera settings and camera positions are necessary. The focal distance calibration, a case in point,

must be repeated whenever a focus setting is changed. This is unfortunate given the unimportant nature of the focusing process. A reasonable elimination of this problem could be a course of action such that the camera focusing is permanently fixed at a certain setting, or allowed only a few discrete settings. In this way, a single set of focal distance determinations could be made, and the correct one utilized for the particular setting which, it is assumed, can be precisely found and rigidly fixed. The camera lens correction is another problem which deserves further attention. This problem is a lens-related issue, and the procurement of a suitable linear set of lenses should be investigated. Although the correction in software appears to work reasonably well, it is a solution which should be permanently employed only as a last resort. Finally, if camera positions must be frequently changed, the calibration procedure enlisted in this thesis may prove to be time-consuming. In such an experimental situation, procedures which could streamline the process should be developed.

If system calibration is examined from a wholistic perspective, it can be appreciated that the overall effectiveness of the process is not known at this time. Positional accuracy is directly dependent on the calibration, and the limit of improving this parameter, if at all, can be determined only by further knowledge of the nature and the performance of the calibration procedure. In addition, mechanisms are needed to diagnose the credibility of each calibration step, and to pinpoint a changing situation which would invalidate a calibration parameter. Minor changes in focus setting, system gain factors and camera positions could

all nullify the precision of a calibration. With the availability of diagnostic algorithms, the calibration process could attain and maintain its highest practical level, and concomitantly, positional accuracy could then maintain its practical limit.

It has been discussed that a real-time processing demonstration program has been developed, but which lacks the necessary processing bandwidth. In Chapter 7, it was explained that real-time processing was given secondary consideration in view of the immediate need for file-oriented fast-sampling capability. Thus, some of the computational algorithms utilized by the TRACK System are quite inefficient from a real-time point of view. It is therefore recommended that a new level of TRACK System development be undertaken in which real-time processing is the primary concern. A minimal amount of redevelopment of the existing routines will greatly increase the efficiency and the speed of the processing. At the same time, further investigation is needed into the overall real-time processing problem in the framework of its applications. In projects such as the mobility-aid simulation, specific system design requirements need to be formulated. Preliminarily, it appears that further processing capability is required to effectively perform this kind of experiment, and such requirements should be further delineated so that the TRACK System can be appropriately and effectively developed to operate within such a framework.

It is apparent that the large-volume tracking problem is closely associated with the above discussion. However, based on the design

introduced in the previous chapter, it can proceed in an independent fashion, which is a desirability. Although a preliminary prototype design of a camera mobilizer could be implemented and tested using the main processor, the PDP 11/40, it is recommmended that the overall implementation be carried out independent of the main processing structure so as to keep it from becoming unnecessarily complex. In this way, the overall system structure will be more straightforward and the system performance more reliable.

Appendix I

DERIVATION OF THE SCHUT ORIENTATION EQUATION FROM THE RODRIGUES FORMULAS

Let $\underline{R}$ be a vector before rotation about some axis whose unit direction vector is $\hat{\underline{\lambda}}$, and let $\underline{R}'$ be that same vector after rotation through an angle θ. From Lenox (1976),

$$\underline{\rho} = \hat{\underline{\lambda}} \tan \frac{\theta}{2}$$

where $\underline{\rho}$ = the Rodrigues vector.

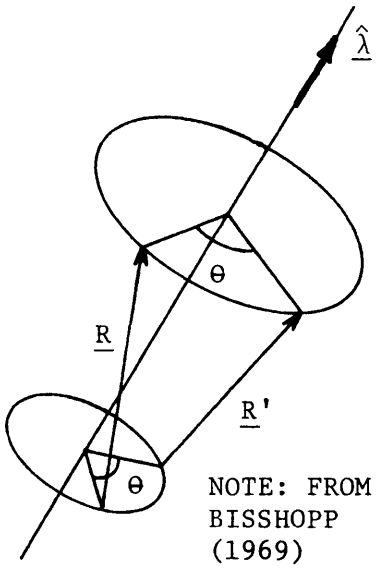

NOTE: FROM BISSHOPP (1969)

It is desired to find the rotation matrix, $\underline{T}$, in terms of the Rodrigues vector components. From Bisshopp (1969), the vectorial form of the rotation tensor can be written

$$\underline{R}' = \underline{R} \cos\theta + \hat{\underline{\lambda}}(\underline{\lambda} \cdot \underline{R})(1 - \cos\theta) + \hat{\underline{\lambda}} \times \underline{R} \sin\theta$$

Let $\underline{R} = \hat{\underline{P}} = \hat{X}i + \hat{Y}j + \hat{Z}k$

$\underline{R}' = \underline{P} = Xi + Yj + Zk$

$\underline{\lambda} = \lambda_1 i + \lambda_2 j + \lambda_3 k$

The coordinates of $\underline{R}'$ are linear combinations of the coordinates of $\underline{R}$. Therefore, from Bisshopp (1969),

$$\underline{P} = \underline{T}\hat{\underline{P}}$$

where

$$\underline{T} = [t_{ij}] = \left[\lambda_i\lambda_j(1 - \cos\theta) + \delta_{ij}\cos\theta - \varepsilon_{ijk}\lambda_k \sin\theta\right]$$

where ε_{ijk} is the alternating tensor. Expanding,

$$\underline{T} = \begin{bmatrix} \lambda_1^2(1-\cos\theta)+\cos\theta & \lambda_1\lambda_2(1-\cos\theta)-\lambda_3\sin\theta & \lambda_1\lambda_3(1-\cos\theta)+\lambda\sin\theta \\ \lambda_1\lambda_2(1-\cos\theta)+\lambda_3\sin\theta & \lambda_2^2(1-\cos\theta)+\cos\theta & \lambda_2\lambda_3(1-\cos\theta)-\lambda_1\sin\theta \\ \lambda_1\lambda_3(1-\cos\theta)-\lambda_2\sin\theta & \lambda_2\lambda_3(1-\cos\theta)+\ {}_1\sin\theta & \lambda_3^2(1-\cos\theta)+\cos\theta \end{bmatrix}$$

An expression for $\sin\theta$ and $\cos\theta$ in terms of the Rodrigues components is needed.

$$\underline{\rho} = \underline{\lambda} \tan\frac{\theta}{2}$$

$$\tan\frac{\theta}{2} = \frac{\underline{\rho}}{\underline{\lambda}}\sqrt{\frac{1 - \cos\theta}{1 + \cos\theta}}$$

$$\underline{\rho}^2 + \underline{\rho}^2\cos\theta = \underline{\lambda}^2 - \underline{\lambda}^2\cos\theta$$

Therefore, $\cos\theta = \dfrac{\underline{\lambda}^2 - \underline{\rho}^2}{\underline{\rho}^2 + \underline{\lambda}^2}$ and $\sin\theta = \dfrac{2\underline{\rho}^2}{\underline{\rho}^2 + \underline{\lambda}^2}$.

$$\underline{T} = \begin{bmatrix} t_{11} & t_{12} & t_{13} \\ t_{21} & t_{22} & t_{23} \\ t_{31} & t_{32} & t_{33} \end{bmatrix}$$

$$t_{11} = \lambda_1^2(1 - \cos\theta) + \cos\theta$$

$$= \lambda_1^2 \left(1 - \frac{(\underline{\lambda}^2 - \underline{\rho}^2)}{(\underline{\rho}^2 + \underline{\lambda}^2)}\right) + \frac{\underline{\lambda}^2 - \underline{\rho}^2}{\underline{\rho}^2 + \underline{\lambda}^2}$$

$$= \frac{\underline{\rho}^2 \left(2\rho_1^2 + 1 - |\underline{\rho}|^2\right)}{\underline{\rho}^2 \left(|\underline{\rho}|^2 + 1\right)}$$

$$= \frac{1 + \rho_1^2 - \rho_2^2 - \rho_3^2}{1 + \rho_1^2 + \rho_2^2 + \rho_3^2}$$

It can be seen from inspection that the following is true:

$$t_{22} = \frac{1 + \rho_2^2 - \rho_1^2 - \rho_3^2}{1 + \rho_1^2 + \rho_2^2 + \rho_3^2}$$

$$t_{33} = \frac{1 + \rho_3^2 - \rho_1^2 - \rho_2^2}{1 + \rho_1^2 + \rho_2^2 + \rho_3^2}$$

An off-diagonal term is examined:

$$t_{21} = \lambda_1\lambda_2(1 - \cos\theta) + \lambda_3 \sin\theta$$

$$= \lambda_1\lambda_2 \left(1 - \frac{(\underline{\lambda}^2 - \underline{\rho}^2)}{(\underline{\rho}^2 + \underline{\lambda}^2)}\right) + \lambda_3 \frac{2\underline{\rho}^2}{(\underline{\rho}^2 + \underline{\lambda}^2)}$$

$$= \frac{2(\rho_1\rho_2 + \rho_3)}{\underline{\rho}^2\left(|\underline{\rho}|^2 + 1\right)}$$

$$t_{21} = \frac{2(\rho_1\rho_2 + \rho_3)}{1 + \rho_1^2 + \rho_2^2 + \rho_3^2}$$

It can be seen that this pattern will be reflected in a special way for the other off-diagonal terms. Therefore,

$$t_{12} = \frac{2(\rho_1\rho_2 - \rho_3)}{1 + \rho_1^2 + \rho_2^2 + \rho_3^2}$$

$$t_{31} = \frac{2(\rho_1\rho_3 - \rho_2)}{1 + \rho_1^2 + \rho_2^2 + \rho_3^2} \qquad t_{13} = \frac{2(\rho_1\rho_3 + \rho_2)}{1 + \rho_1^2 + \rho_2^2 + \rho_3^2}$$

$$t_{32} = \frac{2(\rho_2\rho_3 + \rho_1)}{1 + \rho_1^2 + \rho_2^2 + \rho_3^2} \qquad t_{23} = \frac{2(\rho_2\rho_3 - \rho_1)}{1 + \rho_1^2 + \rho_2^2 + \rho_3^2}$$

Finally,

$$\underline{T} = \frac{\begin{bmatrix} 1+\rho_1^2-\rho_2^2-\rho_3^2 & 2(\rho_1\rho_2-\rho_3) & 2(\rho_1\rho_3+\rho_2) \\ 2(\rho_1\rho_2+\rho_3) & 1+\rho_2^2-\rho_1^2-\rho_3^2 & 2(\rho_2\rho_3-\rho_1) \\ 2(\rho_1\rho_3-\rho_2) & 2(\rho_2\rho_3+\rho_1) & 1+\rho_3^2-\rho_1^2-\rho_2^2 \end{bmatrix}}{1 + \rho_1^2 + \rho_2^2 + \rho_3^2}$$

The transformation matrix employed in Chapter 4 has been found.

BIBLIOGRAPHY

Baecker, R.M. (1964), "Computer Simulation of Mobility Aids--A Feasibility Study," S.M. Thesis, Massachusetts Institute of Technology.

Beer, F.P., Johnston, E.R. Jr. (1972), Vector Mechanics for Engineers: Statics and Dynamics, McGraw-Hill, New York.

Bisshopp, K.E. (1969), "Rodrigues Formula and the Screw Axis," J. Eng. Ind., Trans. ASME 91(1).

Cheng, I.S., Koozekanani, S.H., and Fatehi, M.T. (1975), "A Simple Computer-Television Interface System for Gait Analysis," IEEE Trans. on Biomed. Engr., BME-22(3).

Cuscino, G. (1976), "Design and Implementation of an Ultrasound Head Position-Detection System," S.B. Thesis, Massachusetts Institute of Technology.

Duda, R. and Hart, P. (1973), Pattern Classification and Scene Analysis, Wiley & Sons, New York.

Hirzebruck, F. and Scharlau, W. (1971), "Einführung in die Funktionalanalysis," Bibliographisches Institut AG, Mannheim.

Ingels, N.B., Rush, S.K., and Thompson, N.P., "Analytic Stop Motion Stereo Photogrammetry," Rev. Sci. Instr. 40(3).

Kettelkamp, D.B., Johnson, R.J., Smitt, G.L., Chao, E.Y.S., and Walker, M. (1970), "An Electrogoniometric Study of Knee Motion in Normal Gait," J. Bone and Joint Surg. 52-A(4).

Landsman, E. (1966), "Mobility-Aid Simulation Studies," Sc.D. Thesis, Massachusetts Institute of Technology.

Leithold, L. (1968), The Calculus with Analytical Geometry, Harper & Row.

Lenox, J.B. (1976), Six Degrees of Freedom Human Eyeball Movement Analysis Involving Stereometric Techniques," Ph.D. Thesis, Stanford Univ.

Panjabi, M.M. (1971), "Theoretical Treatment of Vibrations in Single and Multiple Body Suspension Systems Based on Matrix Methods," Report No. LIC-24, Division of Machine Elements, Chalmers University of Technology, Gothenburg.

Mann, R.W. (1974), "Technology and Human Rehabilitation: Prostheses for Sensory Rehabilitation and/or Sensory Substitution," Adv. in Biomedical Engineering, Vol. 4, Academic Press.

Rinsky, A.H. (1966), "Inertial System for Straight Line Guidance of the Blind," S.M. Thesis, Massachusetts Institute of Technology.

Roth, B. (1969), "Discussion: "Rodrigues Formula and the Screw Matrix," J. Eng. Ind., Trans. ASME 91(1).

Schut, G.H. (1960/61), "On Exact Linear Equations for the Computation of the Rotational Elements of Absolute Orientation," Photogrammetria 17(1).

Stearns, S.D., Digital Signal Analysis, Hayden Book Co., Inc.

Stoutemyer, D.R. (1965), "Systems Study and Design of a Blind Mobility Aid Simulator," S.M. Thesis, Massachusetts Institute of Technology.

Thompson, E.H. (1958/59), "An Exact Linear Solution of the Problem of Absolute Orientation," Photogrammetria 15(4).

Winter, D.A., Greenlaw, R.K., and Hobson, D.A. (1972), "Television Computer Analysis of Kinematics of Human Gait," Computer & Biomedical Res. 5.